الجمهورية الجزائرية الديمقراطية الشعبية

People's Democratic Republic of Algeria

وزارة التعليم العالي والبحث العلمي

Ministry of Higher Education and Scientific Research

جامعة 20 أوت 1955-سكيكدة

University of 20 August 1955-Skikda

كلية التكنولوجيا

Faculty of Technology

Department: Civil Engineering

Reference N°: **D012124019D**

Doctoral Thesis

3rd Cycle Doctoral (D-LMD)

by

Hisham Suleiman

Speciality: Structures and Soil

Analysis and Control of Non-Classically Damped Structures

Committee in charge:

First and Last Name	Grade	Institution of Affiliation	Designation
Mr. Salah Bouziane	Professor	University of 20 August 1955-Skikda	President
Mr. Hamid Afra	Professor	National Delegation of Disaster Risk Reduction	Supervisor
Mr. Hamoudi Bouzerd	Professor	University of 20 August 1955-Skikda	Co-Supervisor
Mr. Ramdane Bahar	Professor	University of Science and Technology Houari Boumediene	Examiner
Mr. Abdelghani Seghir	Professor	University Abderrahmane Mira of Béjaïa	Examiner
Mr. Mohamed Saleh Nouaouria	Professor	University of Guelma	Examiner
Mr. Kamel Fillali	MCA	University of 20 August 1955-Skikda	Examiner

Skikda University, FT-2024

الجمهورية الجزائرية الديمقراطية الشعبية

République Algérienne Démocratique et Populaire

وزارة التعليم العالي والبحث العلمي

Ministère de l'Enseignement Supérieur et de la Recherche Scientifique

جامعة 20 أوت 1955-سكيكدة

Université du 20 Août 1955-Skikda

كلية التكنولوجيا

Faculté De Technologie

Département: Génie Civil

Réf N°: **D012124019D**

Thèse du Doctorat

3éme Cycle Doctorat (D-LMD)

Par

Hisham Suleiman

Option: Structures et Sol

Analyse et Contrôle des Structures à Amortissement Non Classique

Jury de Soutenance:

Prenom et Nom	Grade	Affiliation	Qualité
Mr. Salah Bouziane	Professeur	Université du 20 Août 1955-Skikda	Président
Mr. Hamid Afra	Professeur	Délégation Nationale aux Risques Majeurs (DNRM)	Rapporteur
Mr. Hamoudi Bouzerd	Professeur	Université du 20 Août 1955-Skikda	Co-Encadrant
Mr. Ramdane Bahar	Professeur	Université des Sciences et de la Technologie Houari Boumediene	Examinateur
Mr. Abdelghani Seghir	Professeur	Université Abderrahmane-Mira de Béjaïa	Examinateur
Mr. Mohamed Saleh Nouaouria	Professeur	Université de Guelma	Examinateur
Mr. Kamel Fillali	MCA	Université du 20 Août 1955-Skikda	Examinateur

Université de Skikda, FT-2024

Acknowledgement

I sincerely thank Allah for granting me the health, strength, and patience needed to complete this endeavour.

Special thanks are extended to **Prof. Hamid Afra**, my supervisor, for generously sharing his knowledge and experience and providing invaluable guidance and encouragement throughout this PhD thesis. I also extend my gratitude to **Prof. Hamoudi Bouzerd**, my thesis co-supervisor, for his insightful advice, intensive interest, and the wealth of knowledge and research experience he imparted to me during this work.

I am indebted to the committee members for their interest in my work and agreeing to serve as examiners. I would like to thank my lifelong best friends and fellow PhD colleagues at the University of Skikda for their unwavering support.

My gratitude extends to the teachers in the Civil Engineering Departments at both Skikda and Biskra universities, as well as my fellow PhD students and friends. A special acknowledgement goes to **Dr. Mahdi Abdeddaim** from the University of Biskra for his steadfast support and guidance, helping me overcome challenges encountered throughout my academic journey.

I am also deeply grateful to the LGCH Laboratory at the University of Guelma for accepting me as a researcher, and the LARGHYDE Laboratory at the University of Biskra for hosting me. I am genuinely thankful for the kindness and support extended to me during my time in these esteemed laboratories.

Dedication

To my father and mother, the pillars of my strength and the architects of my dreams, your boundless love and encouragement have been the guiding lights throughout my academic journey. From the earliest days of my studies to the culmination of this significant achievement, your unwavering belief in me has fuelled my determination. My brothers and sisters, your collective support and understanding have been invaluable to me. I am proud of you, my sweet-hearted family. Each of you has contributed to the tapestry of my success, and I am grateful for the love and unity that defines us.

I express my appreciation to the Algerian professors and colleagues who have been part of this shared academic and social experience. Your guidance, mentorship, and amity have enriched my academic pursuits.

To my dearest friends from (Palestine, Yamen and Jordan), your friendship has been a source of pleasure and endurance, your fellowship has made the journey all the more meaningful.

Finally, I dedicate this achievement to my homeland, Palestine, and the brave city of Gaza. May peace prevail and may the aspirations of freedom seekers be realised. I extend my prayers to all the souls of Palestinian martyrs, and I hope for a brighter future for our beloved Palestine.

With gratitude,

Hisham Suleiman

ABSTRACT

This thesis explores the dynamic analysis of complex civil engineering structures, focusing on accurately modelling their responses to external forces. Solving the equation of motion directly for these systems often demands extreme computational time. Another option is to decouple these systems into modal form by solving the quadratic eigenvalue problem for them. Forced diagonalization or lightly damping assumptions are often used for this purpose. However, this technique has limited applicability for lightly damping scenarios. These challenges need more adaptable solutions. The exact state-space method stands out for its analytical accuracy in decoupling. It addresses the quadratic eigenvalue problem without simplifying the physical phenomenon. However, this method doubles the problem size, increasing computational demands. In response to these limitations, this research advances the field by examining approximation decoupling techniques that maintain the system's physical meaning while minimizing computational efforts. These techniques aim to improve the modelling efficiency of complex civil engineering structures and ensure the clarity of their dynamic behaviour interpretations. Two innovative methods introduced in our published papers are central to the thesis. The first proposed method, "Exploring Decoupling Techniques for Linear Structures with Non-Classical Damping," looks at a system with four degrees of freedom (4-DOF) and shows that it works well in three different damping situations. This method evaluates the efficacy of lightly non-classical damping against Adhikari's method, underscoring the importance of choosing a method based on the damping matrix's characteristics. It also introduces a new subspace technique that merges the advantages of previous methods for enhanced results. The second proposed method, "An Extension to Adhikari Iterative Method," builds upon existing frameworks by incorporating spectral localization and the self-adjoint theorem. This improves stability and precision in identifying complex eigenvalues. This advancement facilitates a novel approach for calculating the frequency response function (FRF), showcasing significant progress in the field. By integrating these methods, this thesis addresses computational and applicability challenges in modelling complex civil engineering structures and paves the way for further developments in structural dynamics analysis.

Keywords: Non-classical damping; Complex modes; Quadratic eigenvalue problem; Self-adjoint eigenvalue problem; Spectrum theory; Viscous damping; Modal analysis, Complex structures.

ملخـــــص

تستكشف هذه الأطروحة التحليل الديناميكي لهياكل الهندسة المدنية المركبة، مع التركيز على نمذجة استجاباتها للتحريضات الخارجية بدقة. حل معادلة الحركة مباشرةً لهذه الأنظمة غالبًا ما يتطلب وقتًا حسابيًا كبيرًا. هناك طريقة أخرى تتمثل في فصل هذه الأنظمة في شكل أنماط من خلال حل مشكلة القيمة الذاتية التربيعية لها. وغالبًا ما تُستخدم افتراضات التأقطر القسري "التخميد الخفيف" لهذا الغرض. ومع ذلك، فإن هذه التقنية لها قابلية تطبيق محدودة لسيناريوهات التخميد الخفيف. تستلزم هذه التحديات حلولاً أكثر قابلية للتكيف. تبرز طريقة فضاء الحالة (State–space) لدقتها التحليلية في فصل هذه الانظمة. فهي تعالج مشكلة القيمة الذاتية التربيعية دون تبسيط الظواهر الفيزيائية. ومع ذلك، تضاعف هذه الطريقة من حجم المشكلة، مما يزيد من المتطلبات الحسابية ومن المحتمل أن يؤدي إلى تشويش المعنى الفيزيائي من خلال دمج مصفوفات ذات طبيعة متنوعة. واستجابةً لهذه القيود، يعمل هذا البحث على تطوير هذا المجال من خلال دراسة تقنيات الفصل التقريبي التي تحافظ على الأصالة الفيزيائية للأنظمة مع تقليل الجهود الحسابية. تهدف هذه التقنيات إلى تحسين كفاءة نمذجة هياكل الهندسة المدنية المركبة وضمان وضوح تفسيرات سلوكها الديناميكي. هناك طريقتان مبتكرتان تم تقديمهما في أوراقنا البحثية المنشورة وهما محوريتان في الأطروحة. الأولى بعنوان "استكشاف تقنيات الفصل في الهياكل الخطية ذات التخميد غير الكلاسيكي"، وتطبق على نظام رباعي درجات الحرية (4–DOF) وتوضح فعاليتها عبر ثلاثة سيناريوهات للتخميد. تقيّم هذه الطريقة فعالية التخميد غير الكلاسيكي الخفيف مقابل طريقة Adhikari، مما يؤكد أهمية اختيار طريقة تعتمد على خصائص مصفوفة التخميد. كما أنها تقدم أيضًا تقنية فضاء فرعي جديدة تدمج مزايا الطرق السابقة للحصول على نتائج محسّنة. تعتمد الطريقة الثانية، "امتداد لطريقة Adhikari التكرارية"، على الأطر الحالية من خلال دمج التوطين الطيفي ونظرية الترافق–الذاتية. يعمل ذلك على تحسين الاستقرار والدقة في تحديد القيم الذاتية المركبة. يسهّل هذا التقدم نهجًا جديدًا لحساب دالة الاستجابة الترددية(FRF) ، مما يُظهر تقدمًا كبيرًا في هذا المجال من خلال دمج هذه الأساليب. تعالج هذه الأطروحة التحديات الحسابية والتطبيقية في نمذجة هياكل الهندسة المدنية المركبة، وتمهد الطريق لمزيد من التطورات في التحليل الديناميكي للمنشآت.

الكلمات المفتاحية: التخميد غير التقليدي؛ الأنماط المركبة؛ مشكلة القيم الذاتية التربيعية؛ مشكلة القيم الذاتية ذاتية–الترافقية؛ نظرية الطيف؛ التخميد اللزج؛ التحليل النمطي؛ الهياكل المركبة.

Table of Contents

CHAPTER 3: A COMPARATIVE EVALUATION OF DECOUPLING TECHNIQUES FOR NON-CLASSICAL LINEAR DAMPED STRUCTURES

CHAPTER 4: ADVANCING EIGENANALYSIS IN LINEAR NON-CLASSICALLY DAMPED SYSTEMS: A NEW EXTENDED VERSION OF THE ADHIKARI ITERATIVE METHOD

List of Figures

List of Tables

NOMENCLATURE

Symbols

A	*State-space characteristic matrices*
atan2	*2-argument arctangent function*
B	*State-space characteristic matrices*
$\mathbb{C}$	*Complex coordinate space notation*
C	*Damping matrix [N-sec/m]*
$\tilde{\mathrm{C}}$	*Modal damping matrix [N-sec/m]*
$\hat{\mathrm{C}}$	*Identified damping matrix [N-sec/m]*
C_R	*The reduced damping matrix [N-sec/m]*
c	*Damping scalar [N-sec/m]*
C_l	*Parameter regards Adhikari's method*
D	*The dynamic stiffness matrix*
F	*Vector of forcing load*
F_d	*Represents the damping force*
$\mathrm{g}(t)$	*State-space input vector*
H	*FRF response function*
I	*Identity matrix*
K	*Stiffness matrix [N/m]*
$\tilde{\mathrm{K}}$	*Modal stiffness matrix [N/m]*
$\hat{\mathrm{K}}$	*Identified stiffness matrix [N/m]*
K_R	*Reduced stiffness matrix [N/m]*
k	*Stiffness scalar [N/m]*
MAC	*Modal assurance criterion [-]*
m	*Mass scalar [kg]*
M	*Mass matrix [kg]*
$\tilde{\mathrm{M}}$	*Modal mass matrix [kg]*
M_R	*The reduced mass matrix [Kg]*
N	*Number of modes*

NOMENCLATURE

N_c	*The number of modes to compute*
$\mathcal{O}$	*Big O notation*
O	*Null matrix*
Q	*Damping quality factor [-]*
$\mathrm{q}(t)$	*Vector of modal displacement*
$\dot{\mathrm{q}}(t)$	*Vector of modal velocity*
$\ddot{\mathrm{q}}(t)$	*Vector of modal acceleration*
R	*Complex eigensolutions residual matrix*
R_j	*Reduced subspace vector*
p	*Perturbation parameter regarding Lazaro's method*
$\mathbb{R}$	*Real coordinate space notation*
u(t)	*State vector*
X	*FRF Input vector*
Z_j	*State space complex eigenvector*

Greek Letters

Λ	*Spectrum of complex eigenvalues [rad/sec]*
Ω	*Matrix of circular frequencies [rad/sec]*
Ψ	*Complex eigenvectors matrix*
α_j	*A decoupling parameter regarding Lazaro's method.*
ψ_j	*Complex eigenvector*
δ	*Kronecker delta function*
$\mathcal{E}$	*Absolute relative error [%]*
η_j	*Vector regarding Adhikari's method*
λ_j	*Complex eigenvalue [rad/sec]*
ν	*Vector regard Adhikari method*
ω	*Undamped eigenvalue [rad/sec]*
$\bar{\omega}$	*Excitation frequency [rad/sec]*
ω_d	*Damped eigenvalue [rad/sec]*

NOMENCLATURE

ϕ_j	*Undamped modal vector*
Φ	*Undamped modal matrix*
ζ	*Modal damping ratio [%]*
γ	*Perturbation parameter*
ϵ	*Error of Adhikari's method*
$\epsilon_{Tol.}$	*Error tolerance*

Abbreviations

AM	*Adhikari method*
EAM	*Extended Adhikari method*
EVP	*Eigenvalue problem*
FRF	*Frequency response functions*
HD	*High damped case*
LD	*Light damped case*
MDOF	*Multi-degrees-of-freedom*
QEVP	*Quadratic eigenvalue problem*

Superscripts

$(\bullet)^*$	*Conjugation operator*
$(\bullet)^H$	*Hermitian operator*
$(\bullet)^T$	*Transpose conjugation operator*

GENERAL INTRODUCTION

Modern engineering structures, characterised by features like intelligent materials, supplementary damping sources, and diverse damping mechanisms, pose challenges to accurate representation using traditional methods like forced diagonalisation. The Rayleigh damping assumption encounters mode coupling issues in damped systems, leading to a loss of orthogonality between damped modes.

Commonly used state-space method provides exact solution, its adoption comes with challenges. Doubling the size of matrices introduces computational complexity, and using sub-matrices with different characteristics may compromise the physical meaning of the solved system.

Addressing these issues is crucial for advancing the accuracy and efficiency of analytical methods in the dynamic analysis of complex engineering structures. This research explores innovative approaches to navigate these challenges, contributing to a more accurate and applicable framework for dynamic analysis in advanced engineering systems.

This thesis explores the current state of the art in representing and analysing complex civil industrial engineering structures, (such as frames or bridges with vibrated machines, encompassing intelligent materials, supplementary damping sources, and diverse damping mechanisms). A comprehensive discussion will be presented, evaluating the strengths and limitations of different available methods. Subsequently, the focus will shift towards the critical need for enhanced approaches to approximate complex eigensolutions in these systems.

In the latter part of this thesis, we will introduce and delve into two novel methods designed to tackle the complexities associated with non-classically linear damped systems. These methods aim to provide more accurate and efficient solutions by leveraging innovative techniques to decouple and analyse the challenging dynamics of such structures. Exploring these new methodologies seeks to contribute valuable insights to the field.

This thesis is highlighted by two publications: In the first paper, we present our pioneering research, *"Exploring Decoupling Techniques For Linear Structures With Non-Classical Damping: A Numerical Study And Evaluation,"* recently published in Periodico di Mineralogia [1]. Our study addresses the challenges of decoupling non-classical linear damped systems in structural dynamics, aiming to replace the state-space technique with more cost-effective alternatives. Two main methods were investigated: the diagonal approximation, a technique based on undamped eigenanalysis with lightly non-classical damping, and the Adhikari first-order iterative method, leveraging Galerkin's method and the Neumann series for approximating complex eigensolutions. Hence, diagonal element dominance metrics were employed to evaluate these methods across various non-classical linear damped systems. Additionally, we propose a new

subspace technique that combines the strengths of both approaches to enhance their effectiveness. This comprehensive study strives to usher in a new era of structural dynamics analysis, promising improved efficiency and precision in design processes across diverse engineering applications.

The second paper entitled, *"An Extension to Adhikari Iterative Method: A Novel Approach for Obtaining Complex Eigensolutions in Linear Non-Classically Damped Systems Structures"* recently published in Structures journal [2], which introduces a novel extension to the Adhikari iterative method, addressing its limitations in analysing linear, non-classically damped systems with high and indefinite damping mechanisms. By incorporating the self-adjoint theorem and spectral localisation, the extension significantly improves the decoupling of these systems, enhancing the accurate determination of complex eigenvalues. The study demonstrates the efficacy of this extension through a comprehensive analysis of dynamic characteristics, introducing a new methodology for computing frequency response functions and showcasing notable improvements in approximating complex eigensolutions.

This thesis is organised into four chapters as follows:

Chapter 1 explores advanced damping mechanisms in complex civil engineering structures, crucial for enhancing their resilience and sustainability. This is an in-depth analysis of the present techniques, materials, and technologies in the field, emphasising their contributions to improving structural safety and performance under dynamic situations. Exploring is crucial for creating inventive solutions to tackle the changing issues in civil engineering. The chapter explores several damping mechanisms, providing a detailed comparison and contrast to contribute to scholarly discussions. The chapter also summarises typical complex engineering constructions, ranging from regulated systems to those incorporating cutting-edge materials. Furthermore, it proposes avenues for future research to connect scholarly progress with real-world applications.

Chapter 2 explores the challenges and techniques of decoupling linear structural systems with non-classical damping, the modal coupling and the limitations of Rayleigh damping assumptions, an essential aspect of complex structural dynamics. We primarily concentrate on addressing intricate quadratic eigenvalue problems (QEVP). The techniques constitute a breakthrough in numerical approaches to structural dynamics, essential for enhancing the design and robustness of structures under dynamic stresses. This chapter provides a comprehensive framework for comprehending the state-space method, also referred to as the exact analytical method, and approximation strategies for addressing the QEVP. This chapter concludes with a fresh examination of the frequency response function (FRF) and parametric dynamical validation techniques to confirm the effectiveness of the presented methodologies.

Chapter 3 presents the results of our first paper, "Exploring Decoupling Techniques For Linear Structures With Non-Classical Damping: A Numerical Study And Evaluation," which addresses innovative and cost-effective computation methods for decoupling non-classical linear damped systems in structural dynamics. Non-classical damping impacts linear system modal decoupling,

and this chapter uses two diagonality dominance indices to determine its non-classicality. A comparison of the weakly non-classical damping method and Adhikari's method on a 4-DOF frame system with different external damping characteristics shows the necessity of choosing the process based on the damping matrix's diagonal dominance. According to the study, the lightly non-classical damping method performs best with dominant diagonal elements. In contrast, Adhikari's algorithm performs better with non-diagonal dominance, which affects damping loss factor estimations and FRF predictions.

Chapter 4 presents the results of our second paper, "An Extension to Adhikari Iterative Method: A Novel Approach for Obtaining Complex Eigensolutions in Linear Non-Classically Damped Systems Structures," This chapter's results show that our suggested extended version of the Adhikari approach emphasises the developments in decoupling non-classically linear damping systems. By incorporating spectral localisation and the self-adjoint theorem, this enhancement renders the approach more reliable and precise when determining complex eigenvalues. Consistent convergence rates and complex eigenvalues, reminiscent of the original Adhikari approach, prove the method's effectiveness. In addition, it shows how a new method for determining responses from Frequency Response Functions (FRFs) can be applied to the analysis of dynamic systems. The significance and potential of these methodologies are demonstrated by their practical implementation on three non-classically damped system models, which bodes well for future exploration and application in diverse scientific and technical sectors.

CHAPTER 1: Complex civil engineering structures

1.1. Introduction

This chapter delves into the state-of-the-art damping mechanisms in complex civil engineering structures, an essential key for ensuring their resilience and sustainability. It is a comprehensive review of the field's current methodologies, materials, and technologies, highlighting their roles in enhancing structural safety and performance under dynamic conditions. This exploration is critical for developing innovative solutions that address the evolving challenges in civil engineering. The chapter delves into several damping strategies, comparing and contrasting them in detail, adding to the scholarly exchanges. It also overviews the common complex engineering structures, from controlled systems to those using innovative materials. Moreover, it suggests directions for future studies, aiming to link academic advances with practical use.

1.2. Damping mechanisms

Any vibrating structure cannot continue vibrating in the body. After a while, it will cease. Every structure has some degree of damping or energy loss. The dynamic system analysis should, however, consider damping when applicable since it is a desired property of the structure. An issue in dynamic analysis is the incorporation of damping, the origin of which is not fully understood. Several experimental studies spanning years have been conducted to interpret the phenomena of damping and the factors impacting the damping process [3]. This section is dedicated to the exploration of four significant damping mechanisms: viscous damping, hysteretic damping, structural damping, and friction damping. These mechanisms play a crucial role in complex civil and industrial engineering applications. It is worth noting that while there are other damping mechanisms such as radiation damping, fluid damping, and electromagnetic damping, etc., they are not included in this chapter. Our primary goal here is to differentiate, compare, and establish connections between the characteristics of the aforementioned four damping mechanisms, further information about the models of damping can be found in [4-6].

Tables 1.1 - 1.2 serve as a condensed overview of the principal attributes of these four damping mechanisms. Tables 1.1 specifically outlines the physical representation of each mechanism, its corresponding mathematical model, force-displacement characteristics, and a

standard time response behaviour. The dissipation of energy per cycle caused by the various damping forces is determined using the following formula [7]:

$$D_i = 4\int_0^{\pi/2\omega} F_d \dot{q} dt \tag{1.1}$$

Table 1.1 Properties of Viscous, Hysteretic, Structural, and Friction damping [8]

Damping mechanism	Physical representation	Model	Force-displacement	Time response
Viscous	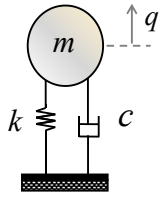	$F_d = c\dot{q}$	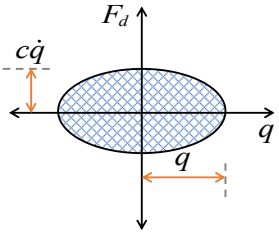	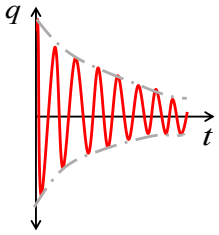
Hysteretic	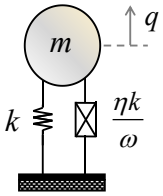	$F_d = \frac{\eta k}{\omega}\dot{q}$	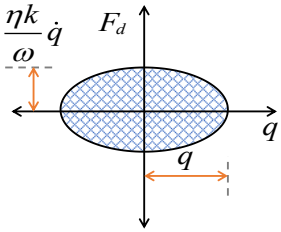	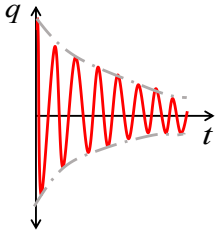
Structural	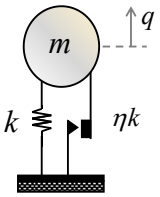	$F_d = \eta k \mid q \mid sgn(\dot{q})$	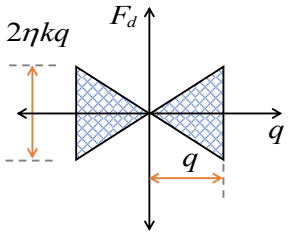	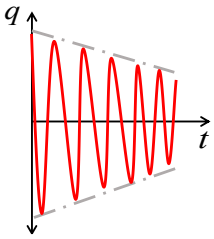
Friction	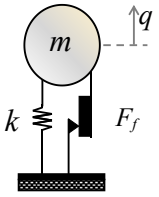	$F_d = F_f sgn(\dot{q})$	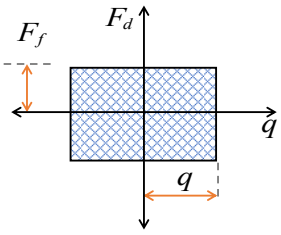	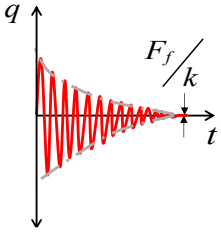

Here, the symbol F_d represents the damping force as specified in the third column of Table 1.1. To derive the equivalent viscous damping coefficient for any damping mechanism, the energy

dissipated by the ith mechanism is equated with that of the viscous damping mechanism D_v. Consequently, the equivalent damping ratio of the ith mechanism is computed in the subsequent manner :

$$\zeta_i = \frac{c_i}{2\sqrt{km}} \tag{1.2}$$

Eq. (1.2) Based on $\zeta_i = c_i / c_c$ Assumes Critical Damping Coefficient $c_c = 2\sqrt{km}$ for a single degree-of-freedom (SDOF) vibration system.

Table 1.2 Energy dissipation and damping ratios in different damping mechanisms [8]

Damping mechanism	Energy dissipation (D)	Equivalent damping coefficient (c)	Equivalent damping ratio (ζ)
Viscous	$\pi c\omega q^2$	c	$\frac{c}{2\sqrt{km}}$
Hysteretic	$\pi k\eta q^2$	$\frac{k\eta}{\omega}$	$\frac{\eta}{2}$
Structural	$2k\eta q^2$	$\frac{2k\eta}{\pi\omega}$	$\frac{\eta}{\pi}$
Friction	$4F_f q$	$\frac{4F_f}{\pi\omega q}$	$\frac{2}{\pi}(\frac{F_f}{kq})$
Viscoelastic	$\pi k\eta q^2$	$\frac{k\eta}{\omega}$	$\frac{\eta}{2}$

1.3. Overview of complex engineering structures

Complex and highly sophisticated structures showcase the prototype of engineering creativity in structural engineering. Found as integral components in various industries such as aerospace, civil engineering, and manufacturing. These diverse structures, ranging from towering skyscrapers to expansive bridges and intricate machinery, exemplify thorough planning, precision, and applying advanced engineering principles.

The relationship between complex engineering structures and damping complexity is primarily related to the need for managing and controlling vibrations, oscillations, and dynamic responses within these structures [9]. Damping is a crucial aspect of structural design and is essential for ensuring the safety, stability, and functionality of complex engineering systems. Moreover, it is worth noting that in complex engineering structures, damping can manifest with

spatial variations, leading to the transportation of vibrational energy across the structure toward locations where it can be dissipated [10].

Understanding the complex dynamics of energy dissipation is pivotal to ensuring the structural integrity and stability of these complex engineering structures [11]. The complexity of these structures also needs the use of advanced structural analysis techniques, such as Multiphysics modelling, finite element method (FEM) analysis, and smoothed particle hydrodynamics (SPH) analysis [12]. These analytical tools enable engineers to capture and understand comprehend the intricate interplay of structural elements and energy dynamics, ensuring that the design and construction of these structures account for the spatial variations in damping effects. This comprehensive approach allows engineers to effectively address the challenges posed by large-scale architectural projects.

1.4. Examples of complex civil engineering structures

In civil engineering, addressing specific challenges and ensuring enhanced performance in complex structures often requires advanced mechanisms and materials. Hao et al. [13] explore the evolution of civil engineering structure design, transitioning from strength-based to resilience-based approaches. This evolution underscores the increasing importance of safety, performance, and resilience. Simultaneously, the authors recognise the imperative to consider sustainability, durability, and smart lifecycle management. Introducing the concept of (sustainable, durable, multi-hazard resistant, resilient, and smart) for the next generation of civil engineering structures. It critically reviews and discusses these aspects, offering research directions to achieve these goals. Despite acknowledging its limited scope.

The following subsections explore diverse categories of complex civil engineering structures, encompassing topics such as vibration-controlled structures, with particular emphasis on passive control systems, structures with innovative materials, structures with vibrating machines, bridges.

1.4.1. Passive energy dissipation system

Buildings or structures designed with specific damping systems to mitigate the effects of vibrations caused by factors such as wind, seismic activities, human activities or industrial activities. This can include vibration-controlled skyscrapers in earthquake-prone areas [14]. Structural control systems are generally classified as passive, active, semi-active, and hybrid. Passive control is an overall and grown strategy because it does not rely on extra energy input [15]. Figure 1.1 presents a comprehensive depiction of these controlling systems. In this thesis, the focus revolves around linearly damped systems. Specifically, this subsection will focus on the passive energy dissipation systems, shedding light on their significance and implications within the context of the discussed linearly damped systems.

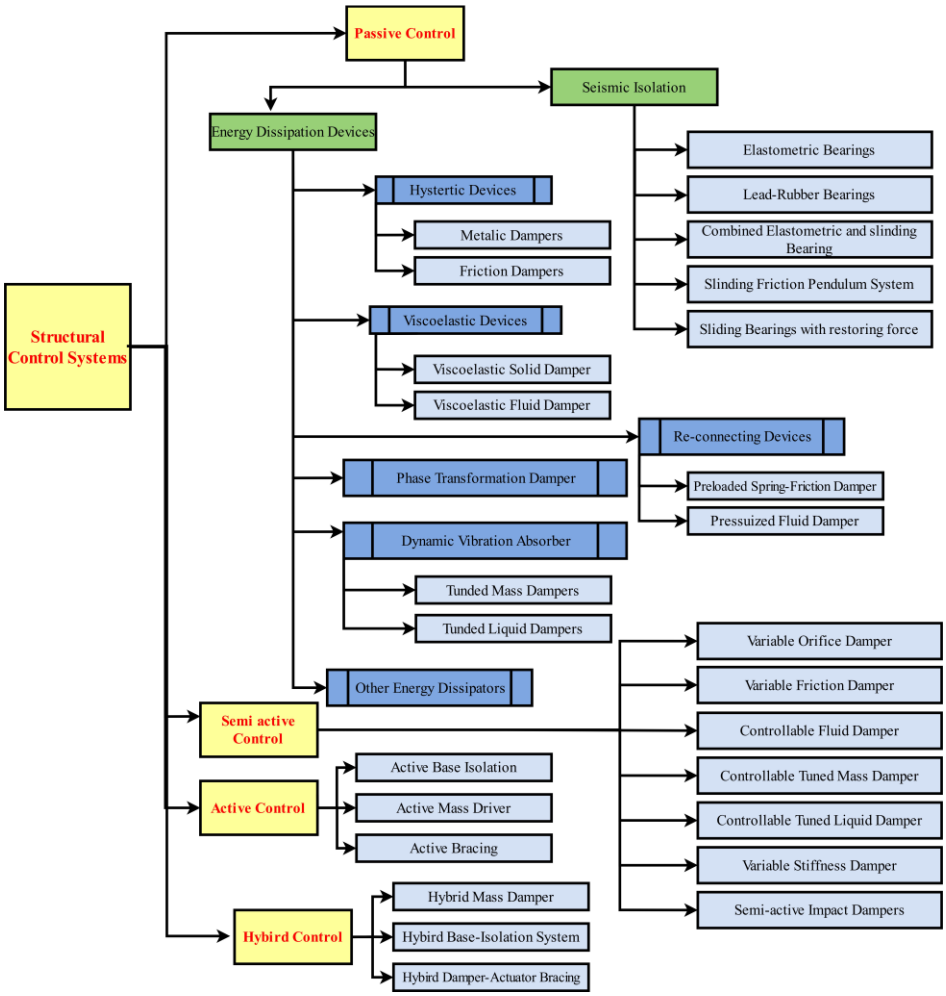

Figure 1.1 Different vibration controlling systems [16]

During an earthquake, structures typically have inherent damping, leading to the dissipation of a portion of the input seismic energy. However, a significant amount of energy is absorbed by the structure, resulting in various deformations and potential collapse [17]. Passive dissipation systems absorb or redirect a portion of the input energy, thereby decreasing the energy that needs dissipation in the primary structure [18]. Typically, these devices are not the primary load-bearing structure, but their motion or deformation results from the structural deformation or vibration. Consequently, these devices can effectively dissipate the energy of the structure. This approach leads to a reduction in dynamic responses and damage to the primary structure [19]. Notably, these systems do not rely on external power or measurements of structural response. The intelligence of structures equipped with such systems lies in their ability to generate a heightened damping force as the structural response increases. However, it's important to note that passive systems have a limited control capacity [20]. The various types of passive systems encompass metallic dampers, friction dampers, viscoelastic dampers, phase transformation dampers, tuned mass dampers, and liquid-tuned mass dampers, briefly discussed in the following subsections.

1.4.1.1. Metallic dampers

Metallic dampers represent a highly efficient means of dissipating energy imparted to a structure during an earthquake, primarily through the inelastic deformation of metallic substances [21]. According to [22], the concept of incorporating individual metallic hysteretic dampers within a structure to absorb a significant portion of seismic energy originated from the conceptual and experimental efforts of Kelly et al. [23]. These metallic dampers function as hysteresis devices designed by the yielding behaviour of metals. The typical force-displacement loops characteristic of hysteretic energy dissipation systems are illustrated in Figure 1.2 [21].

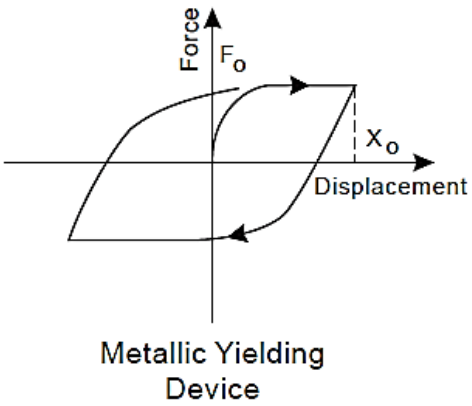

Figure 1.2 Force-displacement loops of hysteretic energy dissipation of metallic dampers [21]

Metallic yield devices generally exhibit stable hysteretic behaviour, low-cycle fatigue, long-term reliability, and a degree of insensitivity to environmental temperature. However, their capacity to absorb energy is limited during initial elastic behaviour, with significant energy dissipation occurring only after experiencing substantial inelastic deformation. Furthermore, the nonlinear nature of metallic yield dampers introduces complexities, as they provide damping and increase structural strength. This nonlinear behaviour needs an iterative design process, adding to the analysis challenges [20].

In Figure 1.3, the seismic response of the X-ADAS damper during an earthquake is depicted, highlighting its effectiveness in stabilizing the structure against seismic forces. Figure 1.4 illustrates the behaviour of the T-ADAS damper during an earthquake, offering insight into its role in minimizing structural oscillations.

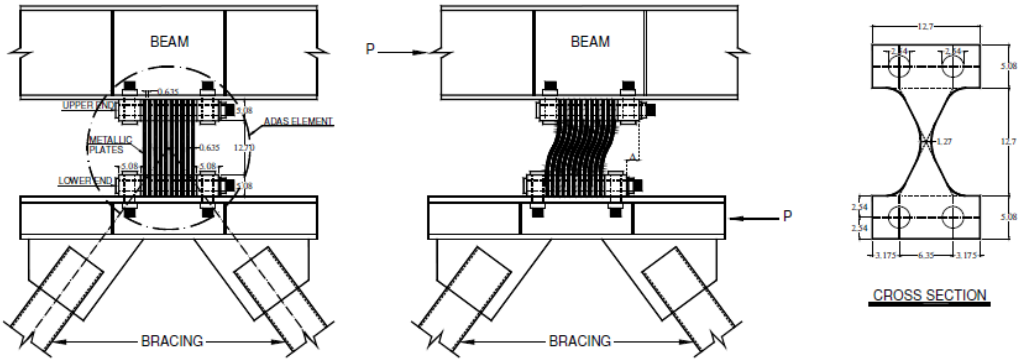

Figure 1.3 The behaviour of X-ADAS damper during earthquake [24]

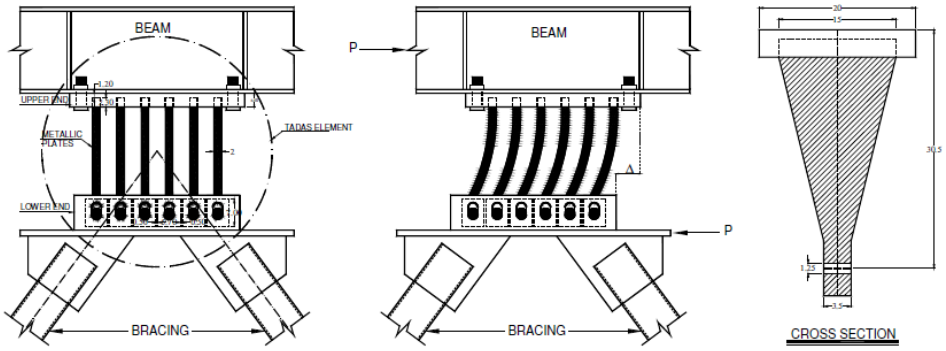

Figure 1.4 The behaviour of T-ADAS damper during earthquake [24]

Figure 1.5 visually outlines the installation of metallic dampers within a structure, highlighting their strategic placement to optimize seismic energy absorption and force dissipation. Figure 1.6 presents a photograph of the X-ADAS damper, allowing a detailed examination of its design and key features. In Figure 1.7, a close-up image is presented, revealing the physical attributes of the T-ADAS damper and providing valuable insights into its appropriateness for seismic applications.

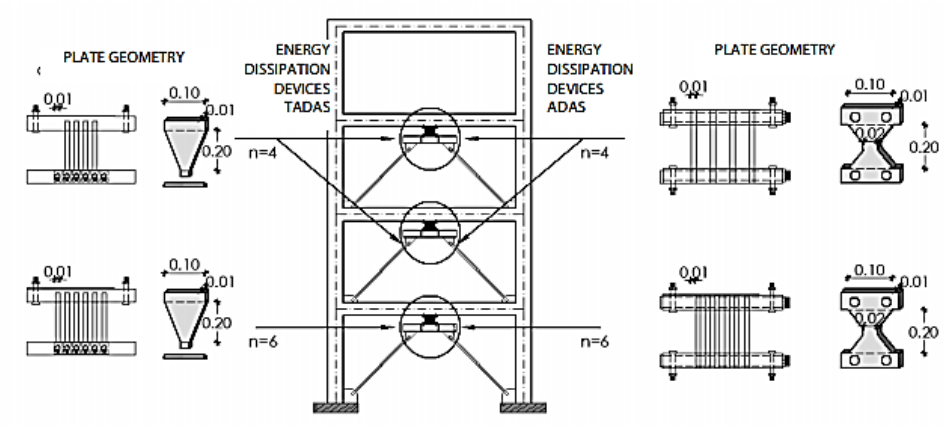

Figure 1.5 Installation of metallic dampers in structure [25]

Figure 1.6 Photo of X-ADAS damper [26]

Figure 1.7 Photograph featuring the T-ADAS damper [27]

In their comprehensive review paper, Javanmardi et al. [28] delve into the discussion of metallic dampers, shedding light on recent developments and advancements in this domain. Their work's intricate details and novel insights explain the evolving landscape of metallic dampers in structural engineering. Figure 1.8 within the paper visually encapsulates these dampers' most recent and innovative shapes, providing a visual reference to complement the insightful discussion presented in their review.

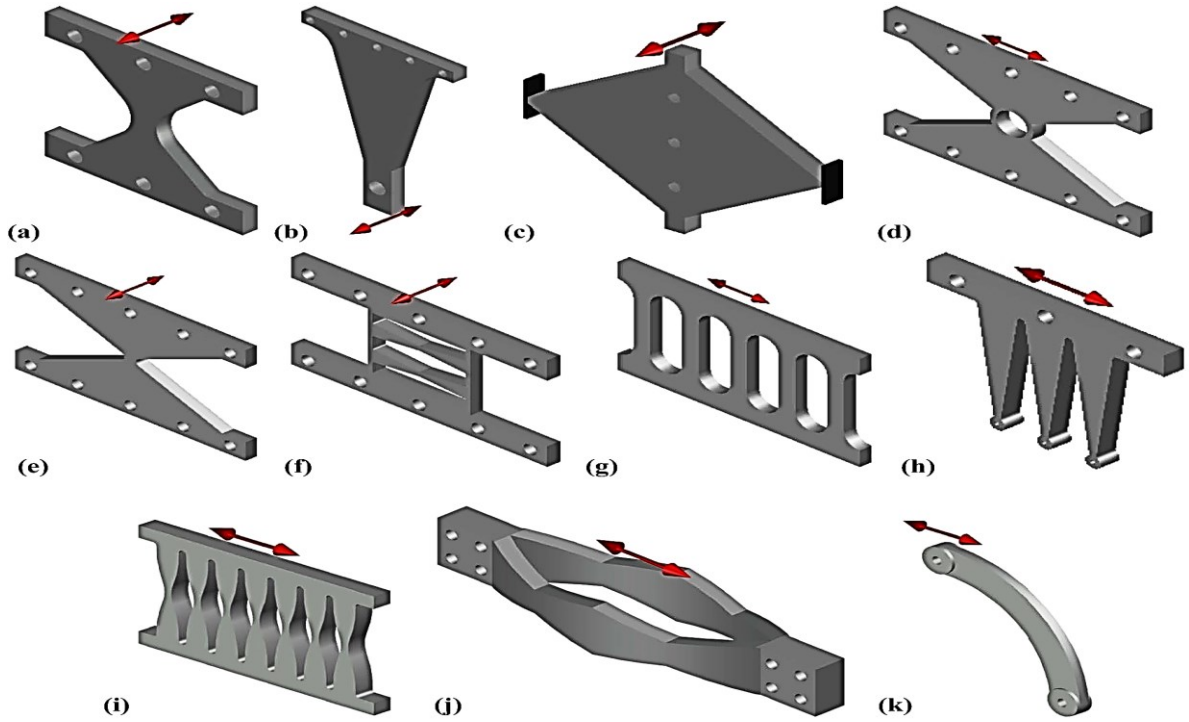

Figure 1.8 Different section of metallic dampers, (a) ADAS, (b) TADAS, (c) rhombic, (d) single round-hole, (e) X-shaped, (f) double X-shaped, (g) slit, (h) comb-teeth, (i) parabolic, (j) pre-bent strips and (k) curved steel dampers [28]

1.4.1.2. Viscoelastic dampers

Viscoelastic (VE) dampers leverage the high damping characteristics of viscoelastic materials such as rubber, polymers, and glassy substances to dissipate energy through shear deformation [20]. This category of VE dampers encompasses both viscoelastic solid dampers and viscoelastic fluid dampers, with the latter incorporating devices based on fluid deformation and orifice mechanisms [21]. Figure 1.9 illustrates typical force-displacement responses obtained for these dampers under constant amplitude, displacement-controlled cyclic conditions. VE dampers generally exhibit a combination of damping and stiffness. A noteworthy case is a purely viscous damper, where force and displacement are 90 degrees out-of-phase [21]. The response of these dampers is frequency-dependent and confined to the linear range. As energy dissipation occurs even with infinitesimal deformation, viscoelastic devices hold potential applications for wind and seismic protection [21].

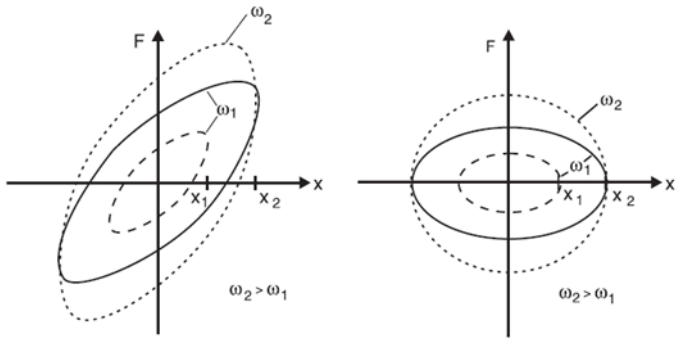

Figure 1.9 Force-displacement loop of solid and fluid viscoelastic dampers [21]

1.4.1.2.1. Viscoelastic Solid dampers

In civil engineering structural applications, viscoelastic solid materials, typically copolymers or glassy substances, are employed to dissipate energy through shear deformation. A common implementation is the viscoelastic (VE) damper, composed by viscoelastic layers bonded with steel plates. When integrated into a structure, this damper undergoes shear deformation and facilitates energy dissipation when structural vibrations induce relative motion between the outer steel flanges and the plate centre [22].

The energy dissipation process is triggered by various sources, ranging from severe earthquakes to smaller excitations like wind, traffic, or mild earthquakes. However, the drawback

of the VE solid damper is its dependency on frequency and temperature. Hence, it poses challenges in the design process since the properties of VE materials are typically expressed through shear storage modulus and shear loss modulus [20]. In this context, Shu et al. [29] conducted a comprehensive review of VE-solid dampers for structural control against earthquakes and dynamic loads. The study systematically covers various VE-solid damper types, offering a comparative analysis of their efficiency and advantages. The paper also compiles analytical models for simulating VEM mechanical behaviour. Addressing complexities in VEM compounds and uncertainties in material selection for civil applications, the study concludes by identifying challenges and proposing improvements for future research. Figure 1.10 provides additional details about this damper.

Figure 1.10 Common practical applications and devices associated with VE-solid dampers (a) Yonge Building; (b) Columbia Centre; (c) Two Union Square; (d) Technologies application of VE-solid damper in Japan; (e) typical VE-solid dampers [29]

1.4.1.2.2.Viscoelastic fluid dampers

The viscoelastic (VE) fluid damper, traditionally used in the military and aerospace sector, has found application in civil engineering for structural purposes. The swift integration of viscous fluid dampers into civil engineering is attributed to their extensive and successful history in military applications [22]. The classical dashpot directly inspires a common and straightforward design approach for fluid VE dampers. In this configuration, dissipation occurs as mechanical energy is converted to heat when a piston deforms a thick fluid. These devices can also be incorporated into superstructures, presenting an alternative and more efficient design known as the viscous damping wall (VDW). The VDW design involves a steel plate constrained to move within its plane within a narrow rectangular steel container filled with a viscous fluid [21].

Viscous fluid dampers behave linearly but are temperature and frequency-dependent. High-strength seals are required to prevent viscous fluid from leaking. Cost remains relatively low while effectiveness is high. Thus, viscous fluid damper holds promises for civil engineering structure application [20]. Figure.1.11. representing the different types of VE fluid dampers.

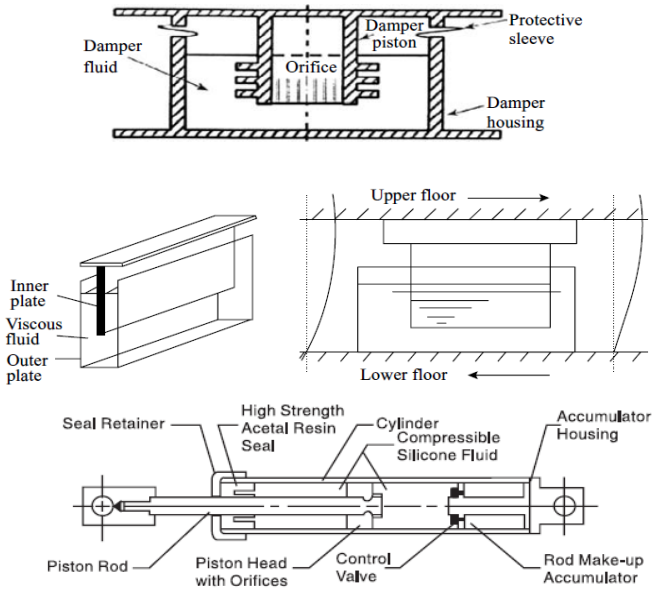

Figure 1.11 Different types of viscoelastic fluid damper: (1) Cylindrical pot fluid, (2) fluid wall damper, and (3) orifice fluid damper [20]

1.4.1.3. Phase transformation dampers

Phase transformation dampers are energy dissipation devices. In recent years, new techniques for controlling the seismic response of structures using smart materials have been developed; superplastic properties characterize this material and can produce large control forces despite its slow response time. Phase transformation dampers serve as energy dissipation devices, and recent advances in seismic response control techniques involve using smart materials. These materials, exemplified by superplastic properties, can generate substantial control forces despite their slow response time. One such smart material is shape memory alloy (SMA), characterized by the unique capability to recover its original shape after undergoing significant strain, up to 10%, either through heating (shape memory effect) or stress removal (pseudo-elastic effect).

SMAs possess notable properties, including pseudo-elasticity, substantial ductility, excellent corrosion resistance, and fatigue resistance, making them attractive for structural vibration control. Figure 1.12 illustrates the stress-strain response of SMA. However, it is important to note that SMAs are highly sensitive to earthquake excitation, leading to changes in stiffness and consequently altering the structure's first natural frequency towards the dominant earthquake frequency. As a result, the design of SMA dampers requires meticulous study [30]. Figure 1.13 provides additional details about SMA dampers.

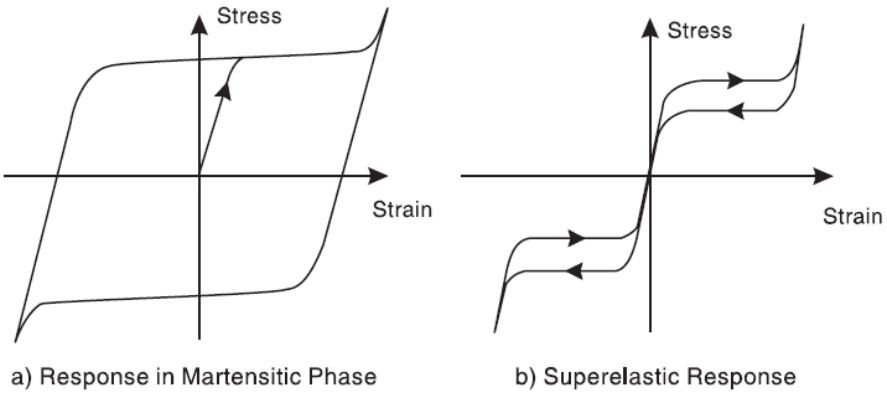

Figure 1.12 Stress-strain response of shape memory alloy [21]

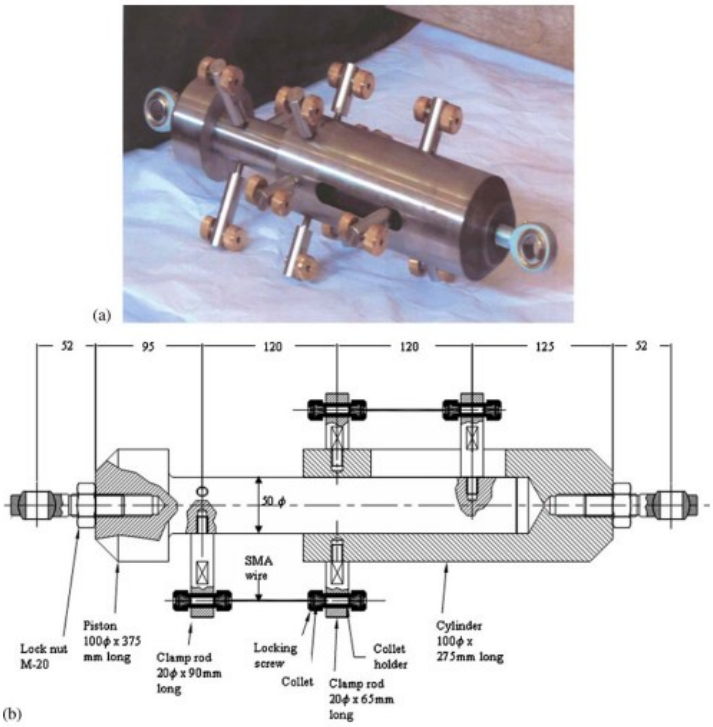

Figure 1.13 Details about SMA damper [30]

1.4.1.4. Tuned mass dampers

The tuned mass damper (TMD) is a passive energy-absorbing device comprising a mass, a spring, and a viscous damper attached to a vibrating system to mitigate undesirable vibrations [31]. The damper's frequency is specifically tuned to a structural frequency, ensuring resonance out of phase with the structural motion. Energy dissipation occurs through the damper inertia force acting on the structure [21, 32]. Vibration absorber systems like Tuned Mass Dampers (TMD) find widespread use in controlling vibrations in mechanical systems. A TMD consists of a mass attached to a building structure, oscillating at the same frequency as the structure but with a phase shift. Typically connected to the building through a spring-dashpot system, the dashpot dissipates energy as relative motion develops between the mass and the structure [33]. The TMD effect can be likened to altering the damping ratio of the structure to a large value. TMDs effectively reduce peak responses or resonant components for lightly damped structures with a dominant mode. Due to this effectiveness, TMDs are increasingly employed in wind-sensitive structures to minimize excessive building motion and ensure occupant comfort [20].

However, passive TMDs face limitations. Firstly, they are effective only for one mode, making them less suitable for seismic response control. Secondly, they are sensitive to mistuning. Thirdly, they occupy a relatively large space [20]. Figures 1.14 and 1.15 illustrate the mechanical model of TMD and its installation on structures.

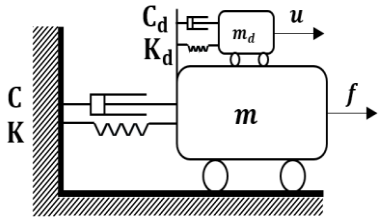

Figure 1.14 Mechanical model of building-TMD [34]

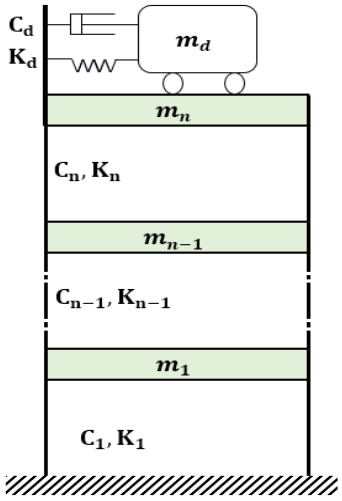

Figure 1.15 The installation of a tuned mass damper on a structure [20]

1.4.1.5. Tuned liquid damper

Another form of dynamic absorber used for reducing structural vibrations is the Tuned Liquid Damper (TLD). In a TLD, a liquid, typically water, is the moving mass, and gravity generates the restoring force. Structural vibrations shake the TLD, causing movement of the liquid inside the container. The turbulence in the liquid flow and the friction between the liquid and the container converts the dynamic energy of the fluid flow into heat, effectively absorbing structural vibration energy. Importantly, the TLD and its mechanism remain relatively uncomplicated [20]. The response of the TLD system is generally highly nonlinear, attributed to factors such as liquid

sloshing or the presence of orifices. Due to this intrinsic nonlinearity, much of the research on characterizing the response of tuned liquid dampers relies on physical experiments [21]. Favourable properties of TLD compared to TMD are because of no mechanical friction, smooth movement in small vibration is possible, no complex mechanisms, thereby reasonable in cost and maintenance, can be applied easily to two horizontal vibrations with a single TLD and can be compact and portable, if large numbers are used. According to [35], and based on the energy dissipation method of each TLD, TLDs are classified into five main groups: (a) tuned sloshing damper (TSD), (b) tuned liquid column damper (TLCD), (c) combined TSD-TLCD system, (d) compliant liquid damper (CLD), and (e) liquid damper with a submerged tuned oscillator (LDSTO), Figure 1.16 represents the previously mentioned TLD types.

Recently, Fu et al. [15] conducted a comparative study on the vibration control performance of particle dampers (PDs) and tuned liquid dampers (TLDs) using the up-to-date substructure shake table testing (SSTT) method. They employed three model-based integration algorithms in SSTT, ensuring unconditional stability. The experimental procedures were detailed for the SSTT methods, and a single-degree-of-freedom (SDOF) structure system with PDs/TLDs was constructed and verified, Figure 1.17 represent the methodology provided by the authors to conduct the experiment.

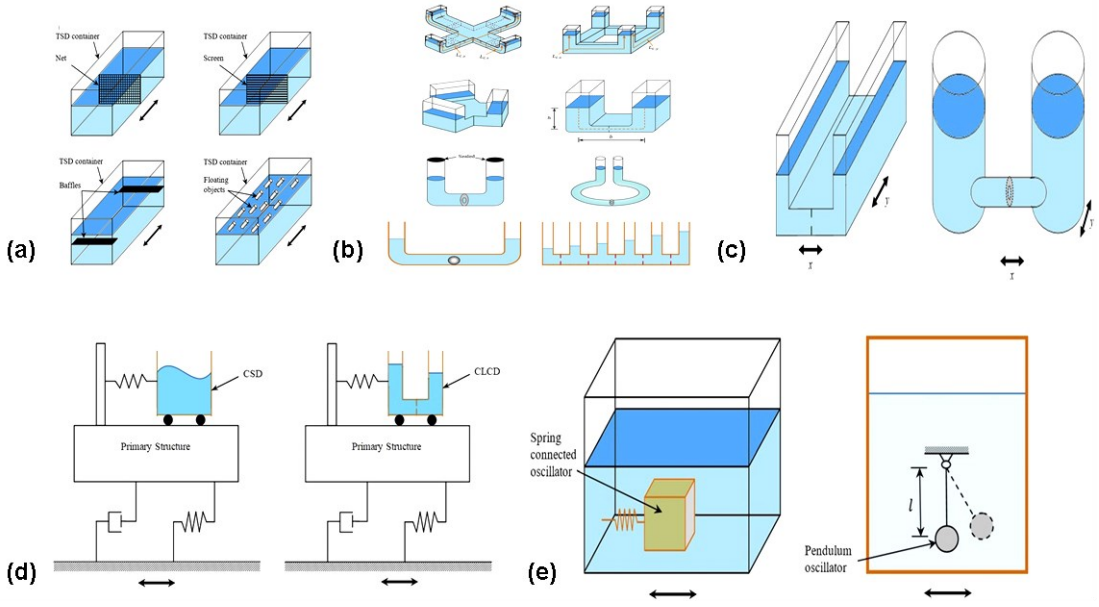

Figure 1.16 Types of TLD; (a) TSD damper, (b) TLCD damper, (c) combined TSD-TLCD system, (d) CLD, and (e) LDSTO damper [35]

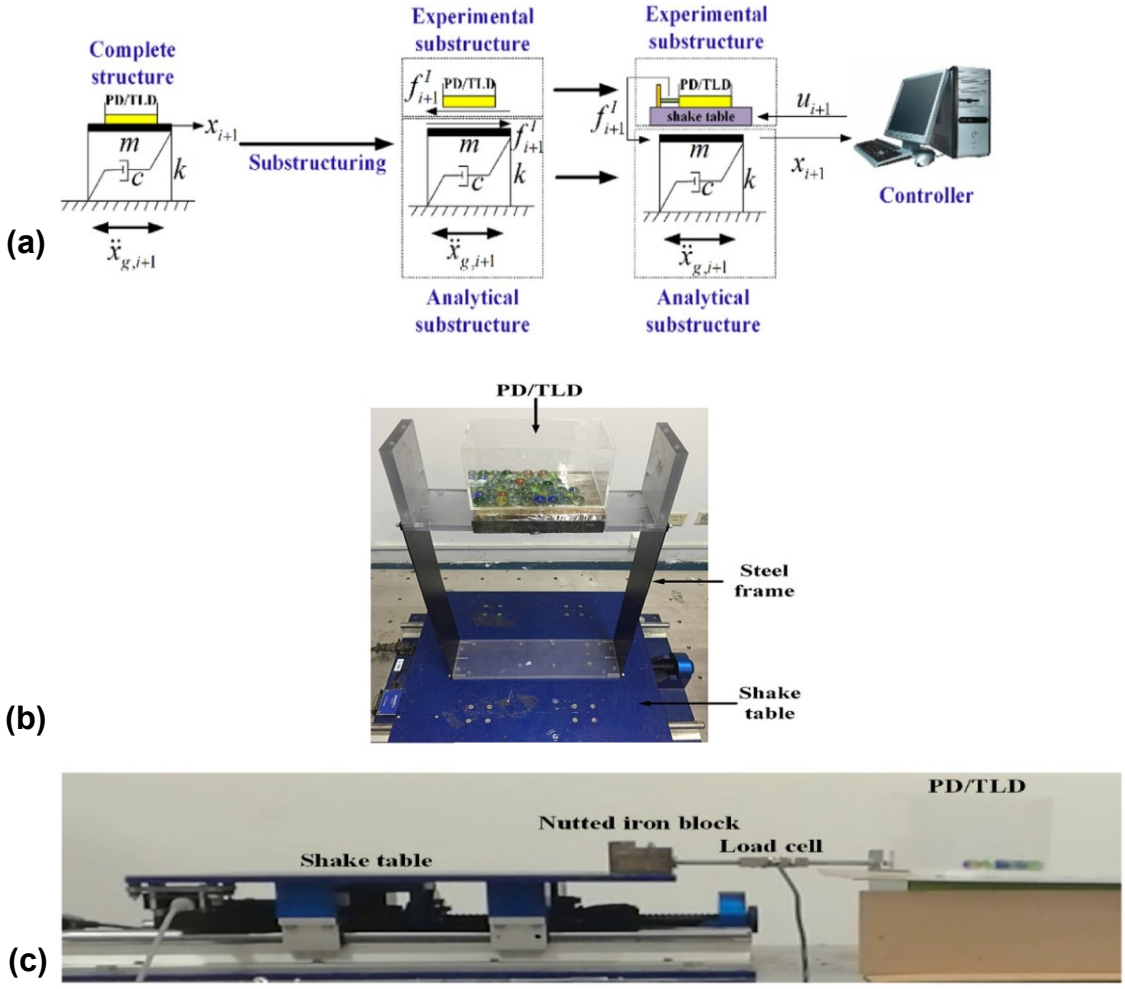

Figure 1.17 Methodology for PD/ TLD shaking test: (a) Conceptual view of the system, (b) Complete structure shake table test. And (c) the structural shake table test [15]

1.4.2. Structures with innovative materials:

Innovative materials, such as Shape Memory Alloys (SMA), can deform and regain their original shape when subjected to an external stimulus, typically involving temperature changes. The SAM includes metallic alloys, with Nitinol (Nickel and Titanium) widely used for its favourable properties. Besides Nitinol, other metal alloys like Copper-Zinc-Aluminium (Cu-Zn-Al), Copper-Aluminium-Nickel (Cu-Al-Ni), and Iron-Manganese-Silicon (Fe-Mn-Si).

However, using SAM is revolutionizing the construction of reinforced concrete buildings by providing enhanced damping properties, effectively mitigating the impact of vibrations caused by seismic events or other forces. These advanced materials offer a proactive approach to structural resilience, ensuring the longevity and safety of buildings in dynamic environments. In this context, Zafar and Andrawes [36] address plastic deformation in seismic steel-reinforced concrete structures by proposing a novel solution: fibre-reinforced polymer (FRP) embedded with super-elastic shape memory alloy (SMA) fibres (See Figure.1.18). This composite enhances concrete structures' seismic resilience through its combined ductility and pseudo-elasticity. Comparative analysis with traditional steel-reinforced frames highlights SMA–FRP's superior energy dissipation and reduced residual drifts. The study underscores SMA–FRP's re-centring capability, mitigating residual drift accumulation, especially in aftershock scenarios. Recently, Hojatirad and Naderpour [37] introduced the use of shape memory alloys (SMAs) and carbon fibre reinforced polymer (CFRP) in reinforced concrete structures to assess their seismic behaviour. They model cases with SMA placement at designated points in three RC frames of different heights. Incremental dynamic analysis (IDA) and fragility evaluation reveal that reinforcing the frames with SMA and CFRP increases ductility, reduces the probability of seismic damage, and enhances resistance to collapse.

Additional information regarding the properties and various types of these innovative materials and their applications in diverse engineering fields is available in reference [38].

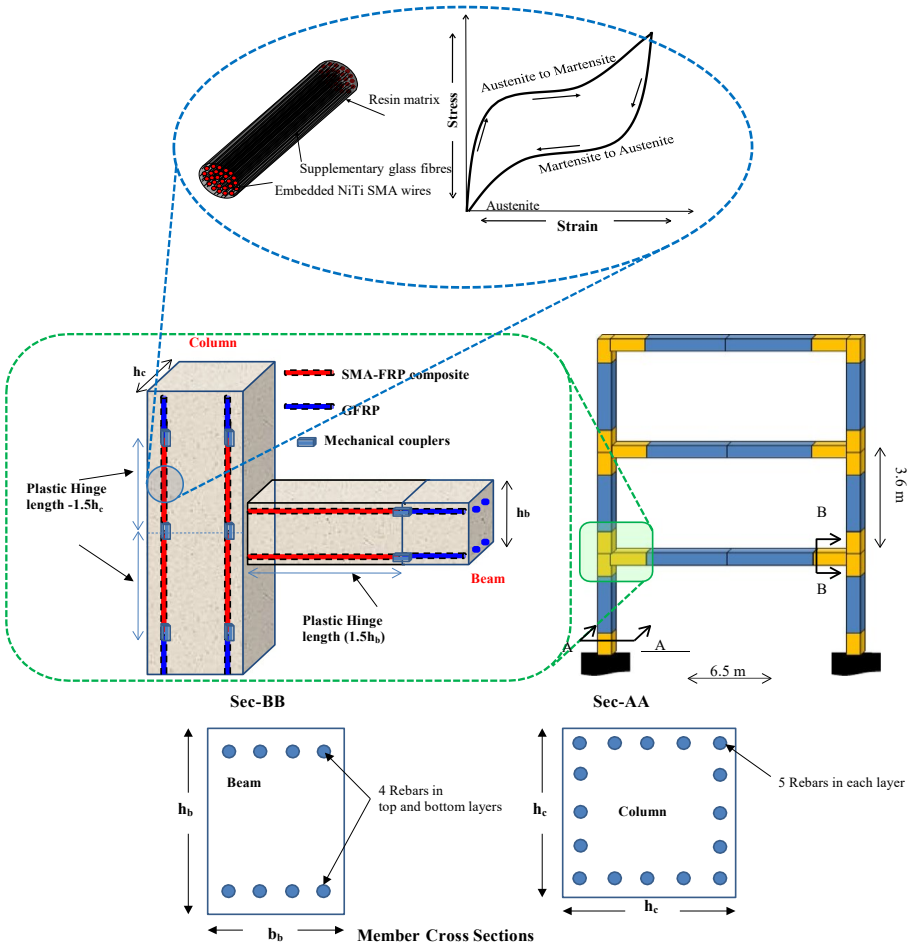

Figure 1.18 Example of a frame system contains innovated SMA materials [36]

1.4.3. Structures with vibrating machines:

Effectively addressing intense vibrations in highly vibrating machines requires strategically applying a floating raft isolation system tailored to their unique structural dynamics. Implementing the mechanical impedance method for analysing acceleration transfer ratios within these systems and incorporating advanced damping technology ensures efficient vibration energy dissipation without compromising isolation capabilities. This integrated approach in structural engineering optimizes overall system performance in dynamic environments. Figure 1.18 depicts a model of a floating raft isolation system as referenced in [39]. In the same context, Lei et al. [40] introduced a composite vibration control method for heavy compressor sets, combining a double-decked floating raft isolation system and particle dampers (Figure 1.19-1.21) to provide three different examples regarding this raft isolation system.

Through the mechanical impedance method, they designed three isolating schemes and optimized particle damper installation using anti-resonance methods and co-simulation. Experimental validation identified the third scheme, integrated with particle damping technology, as the most effective in controlling compressor set vibrations.

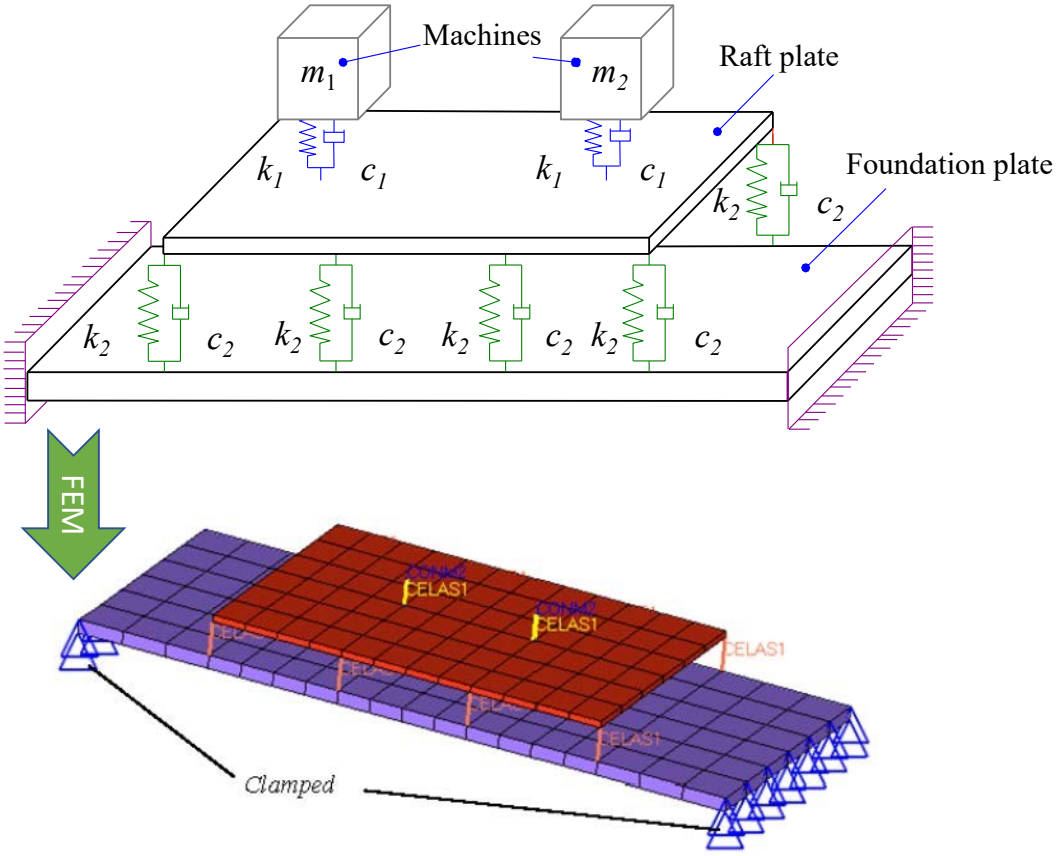

Figure 1.19 Example of Floating Raft Isolation System with Composite Materials [39]

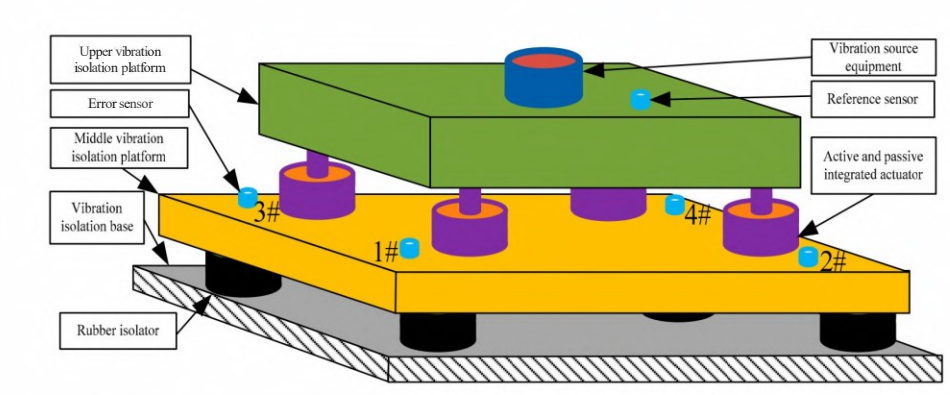

Figure 1.20 Example of Floating Raft Isolation System with controlled dampers [41]

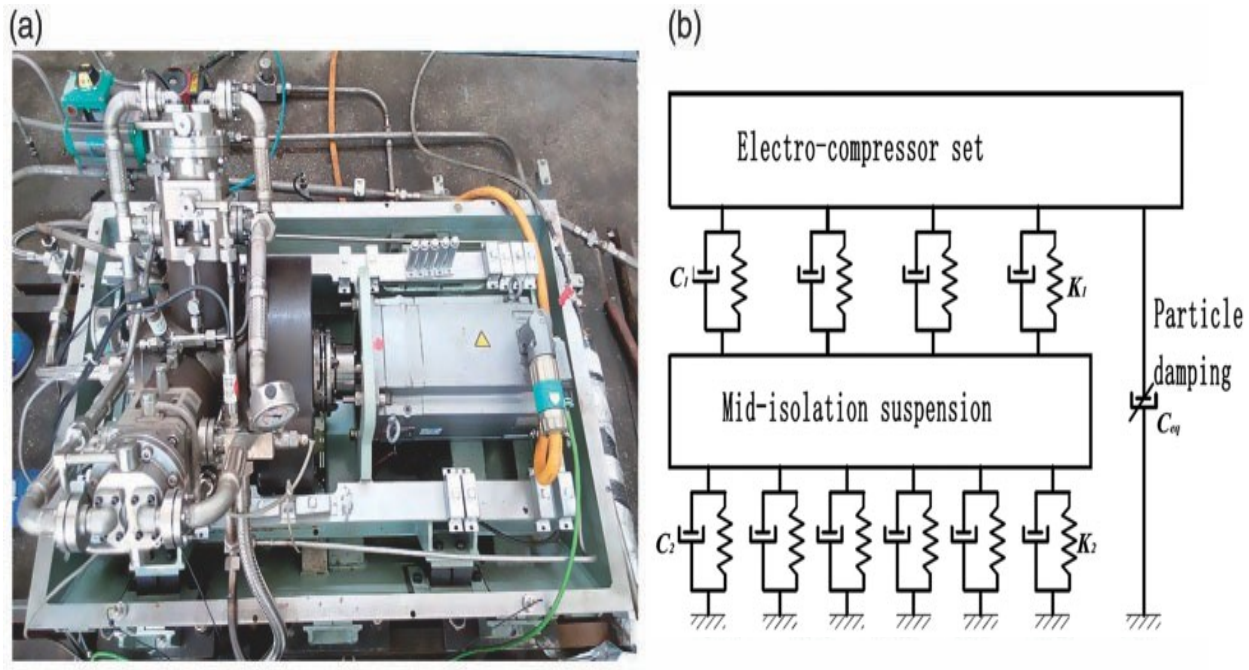

Figure 1.21 Experimental example of the double-decked floating raft isolation system with a particle damper: (a) visual depiction, (b) schematic diagram [40]

1.4.4. Bridges:

Dynamic traffic loads, structural irregularities, seismic considerations, shock loads, resonance risks, and wind dynamic loads intricately shape the structural design of bridges (see Figure 1.22). Hence, to protect against potential failures or degradation stemming from these challenges, bridges are equipped with dampers, absorbers, isolations, and tendon cables. The dynamical analysis of these bridges with the added devices is crucial, with particular emphasis on damping, as it plays a key role in integrating these devices effectively. Additionally, the soil characteristics at bridge sites are crucial for ensuring foundation stability, needing a specialised soil-structure-interaction (SSI) dynamical analysis. For more in-depth information on the SSI of bridges and the dynamical analysis of base-isolated bridges, please refer to [42, 43].

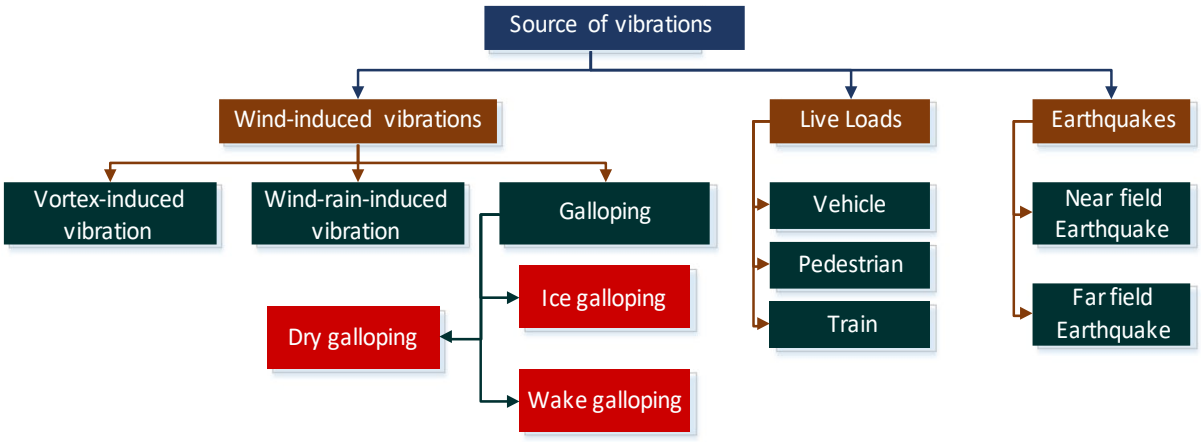

Figure 1.22 The various dynamic loads acting on bridges [44]

These bridges have the potential to integrate damping devices, as showcased in Figure 1.23, or incorporate smart innovative materials, as highlighted in Figure 1.24.

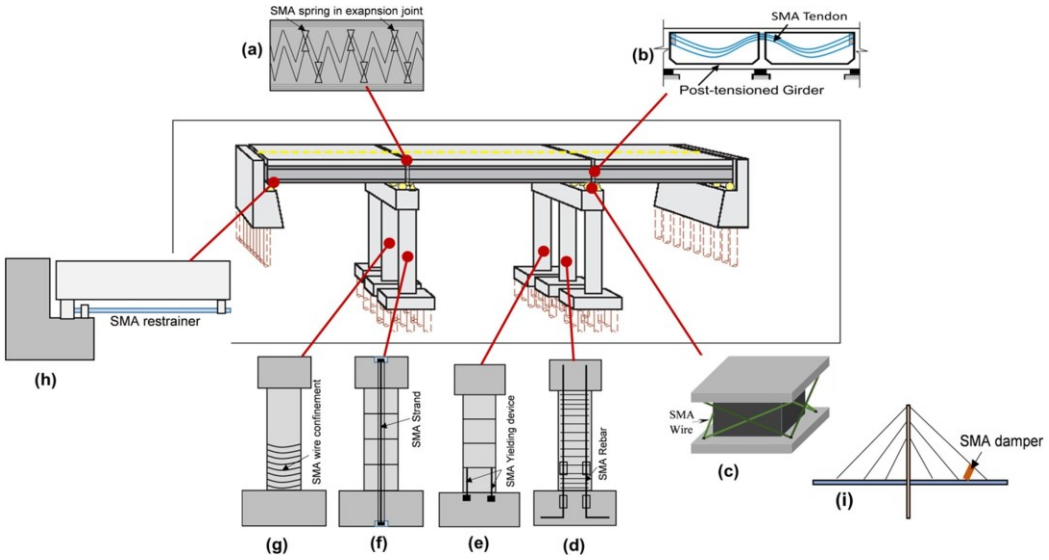

Figure 1.23 Implements of SMA smart materials to bridges [45]

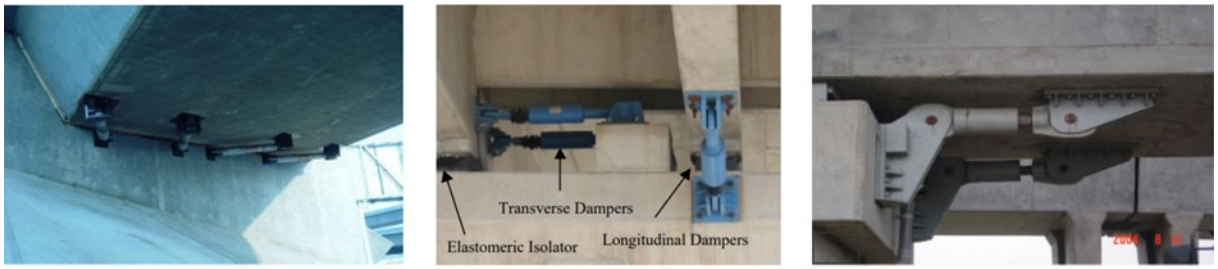

Figure 1.24 Instances of applying fluid viscous dampers in bridges, featuring (a) the 91/I5 Anaheim overcrossing in California, (b) the approach viaduct of the Greek Rion-Antirion bridge, and (c) the Yen-Chou bridge in Taiwan [37-39]

Wen et al. [46] have recently introduced a resilient cable-stage bridge design incorporating both viscous and metallic dampers, as depicted in Figure 1.25.

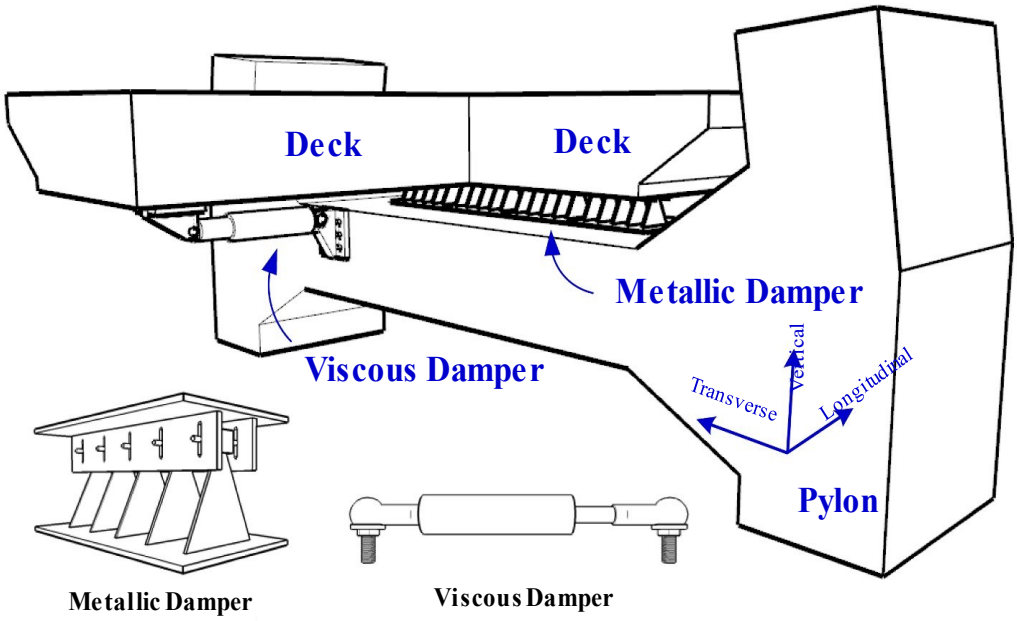

Figure 1.25 A joint part of a cable-stage bridge design incorporating metallic and viscous passive dampers [46]

1.5. Conclusion

This chapter thoroughly analysed different damping strategies, particularly within complex civil engineering structures. It concentrated on linear damping, detailing the careful examination required for passive damping techniques and the incorporation of enhancing devices. Our extensive review covered systems that use innovative smart materials, examined the integration with structures equipped with vibrating machinery, and concluded with an in-depth look at complex bridge designs.

CHAPTER 2: Decoupling linear damped systems

2.1. Introduction

This chapter discusses in depth the difficulties and methods used to decouple linear structural systems with non-classical damping, which is a crucial issue in the field of complex structural dynamics. Our work is mainly focused on the solving of complex quadratic eigenvalue problems (QEVP). At the forefront of this investigation, we introduce innovative methodologies specifically tailored to decouple and understand the specific interactions within these systems. These methodologies represent a significant advances in numerical approaches to structural dynamics, in addition to being a crucial step towards improving the design and resilience of structures under dynamic loads. This chapter gives a complete framework for understanding the state-space method, known as the exact analytical method for this problem, and approximation techniques for handling the QEVP. At the end of this chapter, there is a new analysis of the frequency response function (FRF) and methods for parametric dynamical verification that can be used to make sure the proposed methods are efficient.

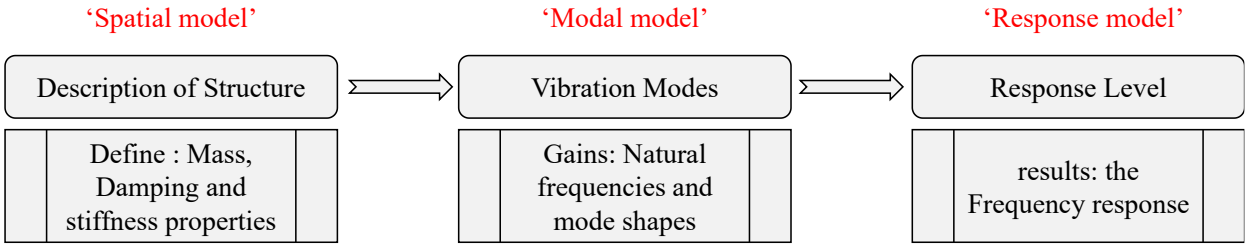

Figure 2.1 Theoretical path of vibration analysis

The dynamical systems' vibrations analysis follows a structured approach detailed in Figure 2.1, encompassing three phases for a thorough vibration analysis. Initially, it involves characterizing the system's physical attributes, such as mass, stiffness, and damping, in the spatial model phase. Then, an analytical modal analysis transforms this into a modal model, highlighting the system's vibration modes, including natural frequencies, mode shapes, and damping factors. The next phase examines the system's response to excitation, focusing on a response model derived from standardized sinusoidal forces applied across a frequency range, resulting in a set of frequency response functions (FRF). This systematic process is crucial for deeply understanding complex systems' dynamic and vibrational behaviours [47].

2.2. Decoupling linear dynamical systems

Gripping energy dissipation mechanisms in vibrating systems is a complicated aspect of structural dynamics. Various damping models have been proposed and examined using analytical and experimental methods to represent observed outcomes accurately. Rayleigh's viscous damping model [48], commonly used, illustrates energy dissipation in structural dynamics. In this model, dissipative forces are directly proportional to the velocities of the system's degrees of freedom (DOF). The model creates the damping matrix by combining the mass and stiffness matrices linearly. The matrix-vector representation of the equation of motion for a linear dynamical system with N-degrees-of-freedom, considering viscous damping and external forcing, is as follows:

$$\mathrm{M}\ddot{\mathrm{q}}(t) + \mathrm{C}\dot{\mathrm{q}}(t) + \mathrm{K}\mathrm{q}(t) = \mathrm{F}(t) \tag{2.1}$$

Let $\mathrm{M,C,K} \in \mathbb{R}^{N\times N}$ represent the mass, damping, and stiffness matrices, respectively, with $\mathrm{q}(t) \in \mathbb{R}^{N}$ being the column vector containing the degrees of freedom. M is assumed to be a positive definite symmetric matrix, while both K and C are positive semidefinite symmetric matrices.

The phenomena of coordinate coupling in linear dynamical systems with viscous damping has historically been regarded as an undesirable aspect in analysing such systems, both in practical applications and theoretical investigations. Therefore, decoupling dynamical systems has been a topic of significant interest among scholars throughout history and continues to earn attention in recent studies. The eigensolutions referred to here are the solutions to the quadratic eigenvalue problem (QEVP). It is worth noting that the QEVPs, known by various names such as quadratic matrix polynomials, nonlinear eigenvalue problems, quadratic pencils, and matrix pencils, are all terms used interchangeably to denote a variety of similar problems [49]. In structural dynamics, the QEVP arises when examining solutions of the form $\mathrm{F(t)=0}$, $\mathrm{q}(t) = \psi e^{\lambda t}$ in the free motion equations described by Eq. (2.1). Therefore, we derive the eigenvalues and eigenvectors of this QEVP problem by solving Eq. (2.2):

$$\left(\lambda_j^2\mathrm{M} + \lambda_j\mathrm{C} + \mathrm{K}\right)\psi_j \equiv \mathrm{D}(\lambda)\psi = 0 \tag{2.2}$$

The dynamic stiffness matrix, represented by $\mathrm{D}(\lambda) \in \mathbb{C}^{N\times N}$, is associated with the system's behaviour and is influenced by the eigenvalue parameter λ. Considering that the matrices M, C,

and K are real. Hence, the complex eigenvalues of this system are calculated by solving the 2*N* characteristic polynomial equation in Eq. (2.3):

$$\det\left[\lambda^2\mathrm{M}+\lambda\,\mathrm{C}+\mathrm{K}\right]=0 \tag{2.3}$$

In their work, Tisseur and Meerbergen [50] introduced a valuable tool to aid in the process of decoupling the (QEVP) presented in Eq. (2.2) back into its original form. This tool is a summary table designed for linear damped systems, enabling the prediction of eigenvalue and eigenvector characteristics. By consulting Table 2.1, one can assess the properties of the eigensolutions and subsequently determine the appropriate decoupling procedure.

Table 2.1 The matrix characteristics of QEVPs examined in linear damped systems, accompanied by their respective spectral properties [50]

Matrix properties	**Eigenvalue properties**	**Eigenvector properties**
M non-singular	2*N* finite eigenvalues	
M singular	Finite and infinite eigenvalues	
M, C, K real	Eigenvalues are real or come in pairs (λ,λ^*)	If ψ is a right eigenvector of λ then ψ^* is a left eigenvector of λ^*
M, C, K Hermitian	Eigenvalues are real or come in pairs (λ,λ^*)	If ψ is a right eigenvector of λ then ψ^* is a left eigenvector of λ^*
M Hermitian positive definite, C, K Hermitian positive semi-definite	$\mathrm{Re}(\lambda)\leq 0$	
M, C symmetric positive definite, K symmetric positive semi-definite	λs are real and negative, gap between *N* largest and *N* smallest eigenvalues	*N* linearly distinct eigenvectors associated with the *N* largest (*N* smallest) eigenvalues
M, K Hermitian, M positive-definite, C = − C^H	Eigenvalues are purely imaginary or come in $(\lambda,-\lambda^*)$	If ψ is a right eigenvector of λ then ψ^* is a left eigenvector of $-\lambda^*$
M, K real symmetric and positive-definite, C = − C^T	Eigenvalues are purely imaginary	

By consulting Table 2.1 and acknowledging that C dictates a purely dissipative nature without leading to overdamped conditions, it is established that all eigenvalues consist of *N* pairs of complex conjugates. With the assumption of unique eigenvalues, they are expressed as (λ_j, λ_j^*), along with their corresponding complex eigenvectors (ψ_j, ψ_j^*). Note that $(\bullet)^*$ signifies the complex conjugate operation.

2.2.1. Classical modal analysis

It is widely recognized that systems following the form depicted in Equation (2.1) can decouple through a congruence transformation applied within the *N*-dimensional configuration space. This transformation leverages the eigenvectors of the undamped system, as demonstrated in previous references [51-53]. The importance of analysing undamped eigenvalue problems in the study of structural dynamics arises from their utility in uncovering the inherent frequencies and modes of vibration in *N*-DOF linear mechanical systems, whether discrete or discretised models. When ignoring damping characteristics, the motion equation that characterises the systems' free vibrations can be described as follows:

$$\mathrm{M}\ddot{\mathrm{q}}(t) + \mathrm{K}\mathrm{q}(t) = 0 \tag{2.4}$$

Addressing the eigenvalue issue for the undamped system, as outlined in Eq. (1.4), requires adopting a solution approach where $\mathrm{q}(t) = \phi \mathrm{e}^{\omega \mathrm{t}}$. This method identifies *N* unique eigenvalues, represented by $(\omega_j \in \mathbb{R})$, and their associated eigenvectors $(\phi_j \in \mathbb{R}^N)$. The representation of each discrete mode in this system is described below:

$$\mathrm{K}\phi_j = \omega_j^2 \mathrm{M}\phi_j, \qquad \forall j = 1, 2, \ldots, N \tag{2.5}$$

The variable ω_j signifies the inherent natural frequency of the undamped system. The corresponding eigenvector ϕ_j within this system can be used to obtain the generalized form of the system matrices, demonstrated as follows:

$$\phi_k^T \mathrm{M}\phi_j = \delta_{kj}, \qquad \phi_k^T \mathrm{K}\phi_j = \omega_j^2 \delta_{kj}, \qquad \forall k, j = 1, 2, \ldots, N \tag{2.6}$$

δ_{kj} denotes the Kronecker-delta function.

The modal matrix Φ contains modal vectors assembled into a matrix configuration, presented thus:

$$\Phi = [\phi_1, \phi_2, \ldots, \phi_N] \in \mathbb{R}^{N \times N} \tag{2.7}$$

Under specific circumstances, it is possible to transform the matrices that represent mass, damping, and stiffness into a diagonalised form by using modal matrices as follows:

$$\tilde{M}=\Phi^T M \Phi=I_N, \quad \tilde{C}=\Phi^T C \Phi, \quad \tilde{K}=\Omega^2=\Phi^T K \Phi \equiv \mathrm{diag}([\omega_1^2, \quad \omega_2^2, \quad \cdots, \quad \omega_N^2]) \tag{2.8}$$

The notations I and Ω are used to represent the identity matrix and the matrix of the squared circular frequencies (also known as undamped eigenvalues), respectively.

The modal damping matrix becomes diagonal according to the requirements outlined in Table 2.2. This feature is known as classical damping due to its proportional relationship with mass and stiffness matrices. Additional details regarding the diagonal aspect of the modal damping matrix are available in the references [54-56].

Table 2.2 Conditions for the classical decoupling of the linear damped system using undamped modes

Classical damping conditions	**Authors**
$MK^{-1}C = CK^{-1}M$	Caughey and O'Kelly [55]
$KM^{-1}C = CM^{-1}K$, or $MK^{-1}C = CK^{-1}M$, or $MC^{-1}K = KC^{-1}M$	Adhikari and Phani [57] Adhikari [58]
$C = M\beta_1(M^{-1}K) + K\beta_2(K^{-1}M)$, or $C = \beta_3(KM^{-1})M + \beta_4(MK^{-1})K$ β_i are smooth analytic functions realted to the all eigenavalues	Adhikari and Phani [57] Adhikari [58]

Suppose none of the conditions listed in Table 2.2 are satisfied. In that case, the dynamical system is considered non-classically damped, and the eigensolutions of the system will appear in complex form [59]. Further, the forced diagonalisation method, or the lightly non-classical

damping method, is an approximation used to obtain complex eigenvalues of damped systems. It relies on the Rayleigh damping model and treats all matrices independently, transforming them into diagonal forms using undamped modes.

As engineering structures become more complicated by incorporating isolated buildings [60-62], innovative materials [63-65], and supplementary damping sources [66, 67], their damping mechanism becomes highly complex. The forced diagonalisation method has difficulties in adequately representing the behaviour of complex systems due to their non-classical damping and intricate energy dissipation characteristics. The undamped modes are unable to decouple the system matrices and achieve a diagonal form [68]. Jiang et al. [69] study the self-adjoint quadratic eigenvalue problem for N-DOF damped systems in this context. The study examines forced diagonalization, a frequently used technique for separating dynamic systems, pointing out its constraints and errors. It highlights the necessity for more precise methods in this area.

2.2.2. Non-classical modal analysis

Non-classical damping can be divided into two primary categories: lightly non-classically damped and highly non-classically damped systems. In the case of lightly non-classically damped systems, it is possible to decouple the dynamical system by using undamped modes, subject to specific perturbation conditions, as outlined by Lord [48] in his monograph.

2.2.3. Lightly non-classical damping analysis

Within the framework of non-classical linear damping, systems exhibiting light damping can be characterized as almost diagonally dominant when the subsequent criterion is met for every mode of the system under examination:

$$\sum_{\substack{i=1 \\ i\neq j}}^{N} \left|\tilde{\mathrm{C}}_{i,j}\right| \leq \left|\tilde{\mathrm{C}}_{j,j}\right|, \qquad \forall i, j = 1,2,\ldots,N \tag{2.9}$$

The requirements for diagonality and their relationship with lightly non-classical damping are extensively explored in references [1, 54, 59, 70, 71].

Table 2.3 presents a comprehensive overview of indices about the dominant diagonal nature of the damping matrix. These indices serve as tools for assessing whether a system belongs to the lightly non-classically damped category.

Table 2.3 Diagonality dominance indices

Diagonality dominance index	Author
$\rho_1\left(\hat{\mathbf{C}}\right)=\max\left(\left\|\mathrm{eig}\left(\hat{\mathbf{C}}_d{}^{-1}\hat{\mathbf{C}}_o\right)\right\|\right)\leq 1$	Graham [72]
$\rho_2\left(\hat{\mathbf{C}}\right)=\dfrac{\sum_{j=1}^{N}\left\|\hat{\mathbf{C}}_d\right\|}{\sum_{j=1}^{N}\left\|\hat{C}_o\right\|}\geq 1$	Morzfeld et al. [70]

The eigenvalue issue associated with lightly non-classically damped systems can be clarified by assuming that $\mathrm{F}(t)=0$, reconstructing the equation of motion through the modal representation of the system's matrices and considering the solution $\mathrm{q}(t)=\phi\mathrm{e}^{\lambda t}$. The resulting quadratic eigenvalue problem, stemming from Eq. (2.1), can be formulated in terms of modal system matrices as follows:

$$\left(\lambda_j^2\mathrm{I}_N+\lambda_j\tilde{\mathrm{C}}+\omega_j^2\right)\phi_j=0,\qquad \forall j=1,2,\ldots,N \tag{2.10}$$

Assuming we diagonalize the modal damping matrix and neglect its off-diagonal elements, we can proceed to determine the system's eigenvalues accordingly. Additionally, under the assumption of strictly dissipative damping, avoiding overdamping or repeated modes, it follows that the complex eigenvalues will demonstrate as conjugate pairs (λ_j,λ_j^*), and be computed as follows:

$$\lambda_j,\lambda_j^*=-\frac{\tilde{\mathrm{C}}_{jj}}{2}\pm i\sqrt{\omega_j^2-\left(\frac{\tilde{\mathrm{C}}_{jj}}{2}\right)^2} \tag{2.11}$$

As highlighted by Ibrahimbegovic and Wilson [73], the computational complexity linked to the undamped eigenvalue problem used in the forced decoupling method is of the cubic *N* order $\mathcal{O}(N^3)$.

2.2.4. State-space linearisation method

The state-space method offers a comprehensive process for exactly calculating the eigensolutions of the quadratic eigenvalue problem in Eq. (2.2). By converting the second-order linear system Eq. (2.1) comprising *N* differential equations to a first-order linear system of 2*N* equations provides an equivalent representation [74]. The equation of motion for N-degree-of-freedom (N-DOF) linear systems described in Eq. (2.1) can be transformed into its equivalent first-order representation with 2*N* equations as follows:

$$\mathrm{A}\dot{\mathrm{u}}(t) + \mathrm{B}\mathrm{u}(t) = \mathrm{g}(t) \tag{2.12}$$

The process of determining the eigensolutions involves assuming the distinctiveness of all eigenvalues and solving the linearized eigenvalue problem. This is achieved by examining the solution of the form $\mathrm{u}(t) = \mathrm{Z}e^{\lambda t}$ as described in Equation (2.12), as follows:

$$\begin{gathered}\left(\lambda_j \mathrm{A} + \mathrm{B}\right)\mathrm{Z}_j = 0,\ \mathrm{Z}_j = \begin{Bmatrix}\lambda_j \psi_j \\ \psi_j\end{Bmatrix} \\ \Rightarrow \begin{bmatrix}\mathrm{M} & \mathrm{O} \\ \mathrm{O} & -\mathrm{K}\end{bmatrix}\begin{Bmatrix}\lambda_j \psi_j \\ \psi_j\end{Bmatrix} = \lambda_j \begin{bmatrix}\mathrm{O} & \mathrm{M} \\ \mathrm{M} & \mathrm{C}\end{bmatrix}\begin{Bmatrix}\lambda_j \psi_j \\ \psi_j\end{Bmatrix}\end{gathered} \tag{2.13}$$

Note that, $\mathrm{g}(t) \in \mathbb{R}^N$ and $\mathrm{O} \in \mathbb{R}^{N\times N}$ respectively, denote the input vector and the null matrix.

$$\mathrm{A} = \begin{bmatrix}\mathrm{O} & \mathrm{M} \\ \mathrm{M} & \mathrm{C}\end{bmatrix},\quad \mathrm{B} = \begin{bmatrix}-\mathrm{M} & \mathrm{O} \\ \mathrm{O} & \mathrm{K}\end{bmatrix},\quad \mathrm{u}\left(t\right) = \begin{bmatrix}\dot{\mathrm{q}}(t) \\ \mathrm{q}(t)\end{bmatrix},\quad \mathrm{g}(t) = \begin{Bmatrix}\mathrm{O} \\ \mathrm{F}(t)\end{Bmatrix} \tag{2.14}$$

Let $\lambda_j \in \mathbb{C}$ and $\mathrm{Z}_j \in \mathbb{C}^{2N}$ respectively represent the complex eigenvalues and their corresponding complex eigenvectors. The state-space method operates under the assumption that a bi-orthogonality relationship exists between the system matrices A and B. The computational complexity associated with the state-space method is $\mathcal{O}((2N)^3) = \mathcal{O}(8N^3)$ For a more in-depth exploration of state-space linearization methodologies, it is advised to consult the research conducted by Walsh and Day [75].

Often in academic literature, state-space representations are encountered in various forms and representations. Authors and instructors may present this concept using different perspectives or notations, certain preferences, or specific applications. As in the following three distinct illustrations of state-space representations [49].

Illustration I:

This is basically from the formulation which is the most common one:

$$\begin{bmatrix} \mathrm{I}_N & -\mathrm{C} \\ -\mathrm{K} & \mathrm{O}_N \end{bmatrix} \begin{Bmatrix} \lambda\psi \\ \psi \end{Bmatrix} = \lambda \begin{bmatrix} \mathrm{O}_N & \mathrm{M} \\ \mathrm{I}_N & \mathrm{O}_N \end{bmatrix} \begin{Bmatrix} \lambda\psi \\ \psi \end{Bmatrix} \tag{2.15}$$

Illustration II:

The use of asymmetric formulation allows for suitable scaling of the problem, enabling it to be solved using specialised methods rather than generic approaches:

$$\begin{bmatrix} \mathrm{K} & \mathrm{C} \\ \mathrm{O}_N & K \end{bmatrix} \begin{Bmatrix} \lambda\psi \\ \psi \end{Bmatrix} = \lambda \begin{bmatrix} \mathrm{O}_N & -\mathrm{M} \\ \mathrm{K} & \mathrm{O}_N \end{bmatrix} \begin{Bmatrix} \lambda\psi \\ \psi \end{Bmatrix} \tag{2.16}$$

Illustration III:

Another approach can be formulated as:

$$\begin{bmatrix} \mathrm{I}_N & \mathrm{O}_N \\ \mathrm{O}_N & -K \end{bmatrix} \begin{Bmatrix} \lambda\psi \\ \psi \end{Bmatrix} = \lambda \begin{bmatrix} M & \mathrm{O}_N \\ \mathrm{I}_N & C \end{bmatrix} \begin{Bmatrix} \lambda\psi \\ \psi \end{Bmatrix} \tag{2.17}$$

The state-space method's efficacy is offset by the need to increase the size of the original problem, leading to substantial time consumption when dealing with intricate dynamic systems with many degrees of freedom. Moreover, this approach diminishes the real-world meaning of the solved system by using sub-matrices with varying attributes [76].

2.3. Approximation method in original space

To address the limitations of the forced diagonalisation method in dealing with complex engineering structures and the time complexity of the exact analytical state space [77-80], Cha [81] presented a new approach employing perturbation theory to determine the complex eigensolutions for linear viscous non-classical damping systems. Cortés and Elejabarrieta [82] have developed a technique for calculating complex eigenvalues in systems characterized by non-classical and non-viscous damping. Özgüven [83] extensively reviewed the methods employed to

decouple non-classically damped systems. This review enhanced our understanding by comprehensively analysing the approaches used before that time. Ma et al. [84] explored the differences in modal vectors observed in classical versus non-classical damped systems. Furthermore, they proposed a method based on phase synchronization for transforming non-classical analysis into a classical framework.

Adhikari [85] introduced an iterative method to find complex eigensolutions in non-classical viscous damped systems, depending entirely on the eigensolutions of the undamped case. This method successfully combines the Galerkin minimization technique with the Neumann series expansion, improving the iterative estimation of the eigensolutions. Suleiman et al. [1] explored cost-effective alternatives to the computationally demanding exact state-space method for decoupling non-classical linear damped systems in structural dynamics. Their research compared two approaches: a modal approximation method suitable for lightly damped systems and Adhikari's first-order algorithm [85], which is more efficient for systems with significant non-classical damping, using undamped eigenanalysis and optimization techniques. The study assessed these methods' effectiveness using diagonality dominance indices and proposed a new subspace algorithm that merges both approaches, offering an efficient strategy for handling various non-classical damping scenarios.

In the present work, Suleiman et al. [2] extended the Adhikari iterative method to enhance the analysis of non-classically linear damped systems, focusing on accurately determining complex eigenvalues. This Extended Adhikari Method (EAM) integrates a self-adjoint theorem and spectral localization techniques, improving stability and precision in evaluating dynamic characteristics like eigenvalues, damping ratios, and FRF responses. EAM's effectiveness was validated through comparisons with the original method and exact state-space analyses, demonstrating significant advancements in precision, particularly for systems with high and indefinite damping. This research marks a notable contribution to structural dynamics, offering a promising approach for analysing complex dynamical systems more efficiently.

Lázaro [86] introduced a mathematical model for calculating the complex eigenvalues associated with non-classical viscous damping systems. This method incorporates the use of eigensolutions from the undamped case alongside perturbation methods based on Taylor series expansions. For the computation of complex eigenvectors, Lázaro combined these complex

eigenvalues with a second-order equation previously described in research [87]. Hračov and Náprstek [88] introduced a method for approximating complex eigensolutions in classically damped systems with an added passive damper, employing a perturbation technique for calculation. In a subsequent work, Lázaro [89] suggested a fixed-point iteration method for determining complex eigensolutions within systems featuring non-classical and non-viscous damping. This innovative approach is grounded in the mathematical framework and algorithms previously outlined in references [85, 87].

Sinha [90] introduced an iterative approach based on the continuation method for deriving non-classical complex eigensolutions in scenarios involving repeated eigenvalues. Morzfeld et al. [91] developed a technique for predicting the temporal response of systems exhibiting non-classical damping when subjected to seismic forces. This method involves dissecting the quadratic eigenvalue problem inherent to such systems. Denoël and Degée [71] introduced a strategy for separating non-classically damped systems through the use of asymptotic expansions applied to the transfer functions. Lofrano et al. [92] concentrated on examining non-classically viscous damped linear systems, investigating the use of a perturbation method for structural health monitoring and detecting damage in frame structures affected by localized harm. They view damaged configurations as slight deviations from undamaged conditions, resulting in non-classical dynamics in systems with viscous damping. Through the adept application of perturbation techniques and the state-space approach, the study achieves precise identification, quantification, and localization of structural damages. Some scholars search on coordinate decoupling the QEVP using phase synchronisation [93, 94]. The following will discuss the formulation of several approximations for decoupling the original QEVP of non-classical damped systems.

2.3.1. The Iterative Adhikari method for obtain eigensolutions of non-classically linear damped systems

Adhikari [85] introduces an iterative algorithm for modal analysis of systems with non-classical linear damping, using undamped system eigensolutions as a starting point. This method employs the Neumann series for expanding the undamped eigenvectors and the Galerkin method to minimise the error in estimating complex eigenvalues, ensuring stability and solvability by assuming distinct complex conjugate eigenvalue pairs. A significant innovation is the introduction of a decoupling parameter, streamlining the computation of complex eigenvectors and facilitating

the efficient separation of coupled equations. This enhancement markedly improves the algorithm's computational efficiency and practicality. Adhikari's algorithm, characterised by iterative refinement and a convergence criterion, offers improved accuracy in complex eigensolution approximation and is particularly useful for systems with nearly diagonally dominant damping matrices [89], providing a significant contribution to structural dynamics through a combination of rigorous mathematical methods, innovative computational techniques, and practical relevance.

Adhikari's approach is based on a mathematical process that iteratively refines complex eigenvalues with each cycle. The process ends when the eigenvalue issue is resolved within its original framework as follows: convergent complex eigensolutions $\lambda_{j,Conv.}$ and $\psi_{j,Conv.}$ for the *j*-th mode are determined. Initial conditions for the first step of calculation include lightly non-classical eigenvalues and undamped eigenvectors. After every iteration, an updated complex eigenvalue $\lambda_j^{(r+1)}$ is computed.

$$(\lambda_{j,Conv.}^2 \mathrm{M} + \lambda_{j,Conv.} \mathrm{C} + \mathrm{K})\psi_{j,Conv.} = 0, \qquad \forall j = 1, 2, \ldots, N \tag{2.18}$$

The calculation of the complex eigenvalue involves determining the parameter $\eta_j(\lambda_j^{(r)})$ from the vector $\mathrm{a}_j(\lambda_j^{(r)})$. Iterations proceed until all complex eigenvalues converge, with the formulas for these calculations specified in Eq. (2.19). Following this, complex eigenvectors are computed as outlined in Eq. (2.20).

$$\begin{gathered}
\lambda_j^{(r+1)} = -\frac{\eta_j(\lambda_j^{(r)})}{2} \pm i\sqrt{\omega_j^2 - \left(\frac{\eta_j(\lambda_j^{(r)})}{2}\right)^2}, \\
\mathrm{a}_j(\lambda_j^{(r)}) = \frac{\lambda_j^{(r)} \tilde{\mathrm{C}}_{kj}}{\omega_k^2 + \lambda_j^{(r)\,2} + \lambda_j^{(r)} \tilde{\mathrm{C}}_{kk}}, \forall k \neq j, \\
\eta_j(\lambda_j^{(r)}) = \tilde{\mathrm{C}}_{jj} + \nu_j^T \mathrm{a}_j(\lambda_j^{(r)}), \\
\nu_j = [\tilde{\mathrm{C}}_{1,j} \quad \tilde{\mathrm{C}}_{2,j} \quad \cdots \quad \text{j-th terms deleted} \quad \cdots \quad \tilde{\mathrm{C}}_{N-1,j} \quad \tilde{\mathrm{C}}_{N,j}]
\end{gathered} \tag{2.19}$$

$$\psi_j(\lambda_j^{(r+1)}) = \phi_j + \sum_{\substack{k=1 \\ k\neq j}}^{N} \mathrm{a}_j(\lambda_j^{(r+1)})\phi_k, \qquad \forall k \neq j \tag{2.20}$$

Adhikari's algorithm concludes once the computed error falls at or below a pre-defined tolerance level, as described by the expression following in Eq. (2.21).

$$\epsilon_j = \left| \frac{\lambda_j^{(r+1)} - \lambda_j^{(r)}}{\lambda_j^{(r)}} \right| \leq \epsilon_{Tol.} \tag{2.21}$$

This method primarily uses undamped eigenanalysis for solving, showcasing a computational complexity denoted by $\mathcal{O}(N^3 + C_l)$, where C_l is tied to the number of iterations required to achieve each complex eigensolution.

2.3.2. Lazaro's perturbation method for calculating complex eigensolutions in non-classical linear damped systems

Lázaro [86] proposed a perturbation method for determining complex eigenvalues and eigenvectors of non-classically linear damped systems. This method, developed considering light or moderate damping, uses the Taylor series and introduces a continuous, dimensionless parameter p (ranging from 0 to 1) to model the effect of damping as a perturbation of the undamped system, considering the concept of continuous damping sensitivity.

The mathematical formulation begins with the modified eigenvalue problem:

$$\left(\lambda_j^2 \mathrm{M} + p\lambda_j \mathrm{C} + \mathrm{K}\right)\bar{\psi}_j = \mathrm{D}(\lambda_j, p)\psi_j = 0 \tag{2.22}$$

The parameter p is introduced to transition smoothly from the undamped system $\left(p = 0\right)$ to the fully damped system $\left(p = 1\right)$, enabling the study of the system's response to varying levels of damping.

The eigenvalues of this problem, as functions of p, are denoted by $\lambda_j\left(p\right)$ and the corresponding eigenvectors by $\psi_j\left(p\right)$. The sensitivity of these eigenvalues to changes p leads to

deriving an ordinary differential equation whose solution approximates the complex eigenvalues, incorporating the effects of off-diagonal damping matrix terms.

Lázaro's method culminates in a closed-form expression for the eigenvalues that accounts for the modal damping matrix's diagonal and off-diagonal terms, providing a computationally efficient solution. Hence, the expression for the complex eigenvalue λ_j is given by:

$$\begin{aligned} \lambda_j \approx i\omega_j e^{i\zeta_j + \alpha_j/2} &= i\omega_j \exp\left(\frac{i\tilde{C}_{jj}}{2} + \frac{1}{2}\sum_{\substack{k=1 \\ k\neq j}}^{N} \frac{\tilde{C}_{kj}^2}{\omega_k^2 - \omega_j^2} \right), \\ \alpha_j &= \sum_{\substack{k=1 \\ k\neq j}}^{N} \frac{\tilde{C}_{kj}^2}{\omega_k^2 - \omega_j^2} \end{aligned} \tag{2.23}$$

Where α_j captures the effect of non-classical damping through off-diagonal damping matrix elements and the separation between natural frequencies.

With the use of the approximated complex eigenvalue provided earlier, and assuming the system is fully damped $(p=1)$, Lázaro determines the corresponding complex eigenvector by employing a second-order formula, as elaborated in [87].

$$\psi_j \approx \phi_j - i\lambda_j \sum_{\substack{k=1 \\ k\neq j}}^{N} \frac{\tilde{C}_{kj}}{\omega_k^2 + \lambda_j^2 + \lambda_j \tilde{C}_{kk}} \phi_k + \lambda_j^2 \sum_{\substack{k=1 \\ k\neq j}}^{N} \sum_{\substack{l=1 \\ l\neq j\neq k}}^{N} \frac{\tilde{C}_{kl}\tilde{C}_{lj}}{\left(\omega_k^2 + \lambda_j^2 + \lambda_j \tilde{C}_{kk}\right)\left(\omega_l^2 + \lambda_j^2 + \lambda_j \tilde{C}_{ll}\right)} \tag{2.24}$$

2.3.3. Hu and Li's iterative method to find complex eigensolutions of linear damped systems

Hu and Li [95] present a method for calculating complex eigenpairs of linear damped systems, focusing on efficiency and avoiding modal truncation. They leverage undamped modes, combining the Neumann series with a reduced basis technique. This approach requires only the undamped eigenpairs of interest, simplifying the process. The sufficient condition for Neumann series convergence is derived, and the method's computational advantage over traditional state-space methods is highlighted through case studies. Their findings show that complex eigenpairs can be obtained by post-processing undamped eigenpairs, offering a practical solution for engineering applications. This method involves constituting reduced system matrices

$\mathrm{M}_R, \mathrm{C}_R$ and K_R based on the reduced subspace R_j for each complex eigenpairs. The mathematical formulations for theses reduced matrices are as follows:

$$\begin{aligned} &\Rightarrow r_0 = \omega_j^2 \phi_j, \quad r_k = \mathrm{M}^{-1} C\ r_{k-1}^{(j)} \\ &R_j = \mathrm{span}\left\{ r_0(j), r_1(j), \cdots, r_{r-1}(j) \right\} \in \mathbb{R}^{N \times r} \end{aligned} \tag{2.25}$$

The reduced system matrices $\mathrm{M}_R, \mathrm{C}_R$ and K_R are derived from the original system matrices, projected onto the reduced subspace R_j, as following:

$$\left.\begin{aligned} \mathrm{M}_R &= R_j^T \mathrm{M} R_j \\ \mathrm{C}_R &= R_j^T \mathrm{C} R_j \\ \mathrm{K}_R &= R_j^T \mathrm{K} R_j \end{aligned}\right\} \in \mathbb{R}^{r \times r} \tag{2.26}$$

Then the original eigenvalue problem is reformed as follows:

$$\left(\lambda_j^2 \mathrm{M}_R + \lambda_j \mathrm{C}_R + \mathrm{K}_R\right) \alpha_j = 0 \tag{2.27}$$

Now using the subsequently formulation anyone can obtain λ_j ,and then authors suggested to use the obtained α_j to find the corresponding complex eigenvector as follows:

$$\varphi_j \approx \sum_{k=0}^{r-1} \alpha_k^{(j)} r_k^{(j)} = R_j \alpha_j, \quad \text{where } \alpha_j = \left\{ \alpha_1^{(j)}, \alpha_2^{(j)}, \cdots, \alpha_{r-1}^{(j)} \right\}^T \tag{2.28}$$

The complicity $O(N^3 + 0.5N^2 + 2LrN^{1.5})$. Note that, as r is bigger as the result more accurate.

2.4. Exploring decoupling techniques for linear structures with non-classical damping: numerical study and evaluation

This subsection presents the mathematical framework of our study, as detailed in [1], focusing on two approximation techniques for decoupling systems with non-classical linear damping in their original space: the lightly non-classical damping approach and Adhikari's first-order algorithm. It includes advances in the decoupling process for lightly non-classical damping, utilizing the expression found in [87]. Additionally, this research introduces a mixed algorithm that combines both service methods under diagonal dominance conditions.

2.4.1. Enhancing the decoupling of lightly non-classical method

Using the lightly non-classical damping method, the complex eigenvectors can be determined through the expression in [87], as following:

$$\boldsymbol{\psi}_j = \boldsymbol{\phi}_j + \sum_{\substack{k=1 \\ k \neq j}}^{N} \frac{\lambda_j \tilde{C}_{kj}}{\omega_k^2 + \lambda_j^2 + \lambda_j \tilde{C}_{kk}} \boldsymbol{\phi}_k, \quad \boldsymbol{\psi}_j^* = \text{conj}(\boldsymbol{\psi}_j) \tag{2.29}$$

This equation calculates the complex eigenvectors linked to the complex eigenvalues identified by the lightly non-classical damping method, facilitating further separation of the undamped eigenvectors and introduce the damping effect of shaping these eigenvectors. The computation only necessitates the undamped eigensolutions and the modal damping matrix and is recommended when the system shows a clear diagonal dominance.

This technique capitalises on the uniqueness of the operation without the need for iterative processes. Lázaro [96] initially applied the second-order version of expression to compute complex eigenvectors from established complex eigenvalues. However, it's important to highlight that Lázaro's application did not specifically align with diagonal dominance conditions. Furthermore, whereas Lázaro's work involved a second-order equation, this study employs a first-order version, reducing the computational complexity.

2.4.2. Proposed subspace algorithm to decouple linear non-classically linear damped systems

In order to more precisely approximate non-classical complex eigensolutions, a novel subspace approach is presented here. Initially, the algorithm evaluates the system's diagonal dominance (see Table 2.3 for diagonal dominance indices) to determine the most suitable method, choosing between the lightly non-classical damping technique or Adhikari's first-order algorithm [85]. For the lightly non-classical damping approach, it employs a simple formula from Eq. (2.29). to improve the decoupling of modes. In contrast to the state space method, which solves for all non-classical complex eigensolutions in a larger eigenvalue problem simultaneously, this algorithm adopts a structured, sub-iterative strategy. This enables the algorithm to specifically tackle the quadratic eigenvalue problem, facilitating quick identification of solutions within designated eigensolution ranges. The algorithm's operational framework is illustrated in Figure 2.2.

Function $[\lambda, \psi] = decoupling(\Omega, \Phi, \tilde{C}, \rho_2, N, N_c, \epsilon_{Tol})$

for j $= 1 : N_c$ do

if $\rho_2\left(\tilde{C}\right) < 1$ do

$r = 0; \epsilon = 100;$

$$\nu_j = \left[\tilde{C}_{1,j} \quad \tilde{C}_{2,j} \quad \cdots \quad j\text{th terms deleted} \quad \cdots \quad \tilde{C}_{N-1,j} \quad \tilde{C}_{N,j}\right]$$

$$\lambda_j^{(r)} = -\frac{\tilde{C}_{jj}}{2} \pm i\sqrt{\omega_j^2 - \left(\frac{\tilde{C}_{jj}}{2}\right)^2},$$

while $\epsilon > \epsilon_{Tol}$ do

$$\mathbf{a}_j\left(\lambda_j^{(r)}\right) = \frac{\lambda_j^{(r)}\tilde{C}_{kj}}{\omega_k^2 + \lambda_j^{(r)2} + \lambda_j^{(r)}\tilde{C}_{kk}}$$

$$\eta_j\left(\lambda_j^{(r)}\right) = \tilde{C}_{jj} + \nu_j^T \mathbf{a}_j\left(\lambda_j^{(r)}\right),$$

$$\lambda_j^{(r+1)} = -\frac{\eta_j\left(\lambda_j^{(r)}\right)}{2} \pm i\sqrt{\omega_j^2 - \left(\frac{\eta_j\left(\lambda_j^{(r)}\right)}{2}\right)^2},$$

$$\epsilon = \left|\frac{\lambda_j^{(r+1)} - \lambda_j^{(r)}}{\lambda_j^{(r)}}\right|$$

$r = r + 1;$

end while

$$\psi_j\left(\lambda_j^{(r)}\right) = \phi_j \pm \sum_{\substack{k=1 \\ k \neq j}}^{N} \mathbf{a}_j\left(\lambda_j^{(r)}\right)\phi_k,$$

end if

$$\lambda_j = -\frac{\tilde{C}_{jj}}{2} \pm i\sqrt{\omega_j^2 - \left(\frac{\tilde{C}_{jj}}{2}\right)^2},$$

$$\psi_j = \phi_j \pm \sum_{\substack{k=1 \\ k \neq j}}^{N} \frac{\lambda_j \tilde{C}_{kj}}{\omega_k^2 + \lambda_j^2 + \lambda_j \tilde{C}_{kk}}\phi_k$$

end for

end Function

Figure 2.2 The proposed formulated subspace algorithm to decouple the non-classically linear damped systems [1]

Parameters N, N_c, and $\varepsilon_{Tol.}$ represent the size of the eigenvalue problem (calculable via Eq. (2.30)), the number of modes to compute, and the error tolerance for Adhikari's first-order algorithm, respectively.

$$N = \text{length}\left(\mathrm{M}\right) \tag{2.30}$$

The algorithm uses initial values such as the lightly non-classical complex eigenvalues from Eq. (2.11), the modal damping matrix from Eq. (2.8), and the undamped eigenvectors from Eq. (2.7).

2.5. Extending Adhikari iterative method

Based on our paper [2], we introduce a mathematical modification to the Adhikari method that uses self-adjoint theory and Adhikari's complex eigenvectors to make it more accurate in calculating complex eigenvalues.

2.5.1. Finding complex eigensolutions of linear non-classically damped system based on self-adjoint theorem

The dynamic stiffness matrix $\mathrm{D}(\lambda)$ is supposed self-adjoint if $\mathrm{D}(\lambda) = \mathrm{D}(\lambda^*)$ for all $\lambda \in \mathbb{C}$, as per reference [50]. For this matrix to be considered self-adjoint, it must be maintained that M, C, and K are real, symmetric, and Hermitian matrices. For such self-adjoint quadratic eigenvalue problems (QEVPs), 2*N* eigenrelations are established as:

$$\mathrm{D}(\lambda_j)\psi_j = 0 \quad \Leftrightarrow \quad \psi_j^* \mathrm{D}(\lambda_j^*) = 0, \qquad \forall j \in \left[1, 2, \ldots, N\right] \tag{2.31}$$

In this context, ψ_j acts as a right complex eigenvector for λ_j and as a left complex eigenvector for λ_j^*. Therefore, the sets of left and right complex eigenvectors are identical for real matrices. Addressing each decoupled right complex eigenvector, the individual mode's recursive eigenvalue challenge is expressed in Eq. (2.32), simplifying the distribution across terms from Eq. (2.2) to yield:

$$\lambda_j^2 \mathrm{M}\psi_j + \lambda_j \mathrm{C}\psi_j + \mathrm{K}\psi_j = 0 \tag{2.32}$$

Using the complex eigenvectors' orthogonality, Eq. (2.32) can be combined with the complex conjugate transpose of ψ_j, as:

$$\psi_j^H \mathrm{M}\psi_j \lambda_j^2 + \psi_j^H \mathrm{C}\psi_j \lambda_j + \psi_j^H \mathrm{K}\psi_j = 0 \tag{2.33}$$

Here, $(^H)$ signifies the Hermitian transpose. Solving Eq. (2.33) facilitates the identification of conjugate complex eigenvalue pairs, as demonstrated below in Eq. (2.34):

$$\lambda_j, \lambda_j^* = \frac{-\psi_j^H \mathrm{C}\psi_j \pm \sqrt{(\psi_j^H \mathrm{C}\psi_j)^2 - 4(\psi_j^H \mathrm{M}\psi_j)(\psi_j^H \mathrm{K}\psi_j)}}{2(\psi_j^H \mathrm{M}\psi_j)} \tag{2.34}$$

This research enhances the Adhikari method by integrating the formula presented in Eq. (2.34), enabling the use of complex eigenvectors derived via the Adhikari method for identifying their associated complex eigenvalues. Table 2.4 offers an in-depth analysis of the computational complexities of the formula in Eq. (2.34). Moreover, a detailed examination of the Adhikari algorithm and its extension is conducted. Notably, the computational complexity ranking of the original Adhikari method is maintained even with the addition of the extension.

Table 2.4 Evaluate the complexity of the given expression in Eq. (2.34)

Operation	Computational Complexity
Complex multiplication	$\mathcal{O}(N)$
Real multiplication	$\mathcal{O}(N)$
Scalar multiplication and division	Constant-time
Denominator operation	$\mathcal{O}(N)$
Numerator operations (3 multiplications, 1 division)	$\mathcal{O}(N)$
Overall expression complexity (including scalars)	$\mathcal{O}(N^3)$

N represents the size of the initial matrices. However, the computational complexity of the extended lambda expression amounts to $\mathcal{O}(N^3)$.

For an analysis of computational complexities, Table 2.4 delivers a thorough review of the computational demands associated with each eigensolver used in this research thesis for QEVP of systems with N -DOF that are damped.

Table 2.5 The computational complexity of solvers for the QEVPs

Eigenvalue solver	Computational Complexity
1. Original quadratic eigenvalue problem	$\mathcal{O}(N)^3$
2. Undamped eigenvalue problem	$\mathcal{O}(N^3)$
3. State-space representation	$\mathcal{O}(2N)^3 = \mathcal{O}(8N^3)$
4. Adhikari method	$\mathcal{O}(N^3 + C_l)$
5. Extended Adhikari method	$\mathcal{O}(N^3 + C_l)$

2.5.2. Proposed extended Adhikari algorithm

This section introduces the extended Adhikari method (EAM), which uses the formula in Eq. (2.34), (refer to Figure 2.3) for calculating complex eigenvalues in systems with N-DOF that are damped. The development of this method leverages the self-adjoint characteristics of quadratic eigenvalue problems tailored for non-classically linear damped systems.

for $j = 1 : N$ do

$r = 0;\ \epsilon = 100;\ \epsilon_{Tol.} = 1 \times 10^{-6}$

$\mathrm{v}_j = \left[\tilde{C}_{1,j}, \tilde{C}_{2,j}, \cdots j\text{th terms deleted} \cdots, \tilde{C}_{N,j} \right]$

$$\lambda_j^{(r)} = -\frac{\tilde{C}_{j,j}}{2} \pm i\sqrt{\omega_j^2 - \left(\frac{\tilde{C}_{j,j}}{2}\right)^2}$$

While $\epsilon \succ \epsilon_{Tol.}$ do

$$\mathrm{a}_j\left(\lambda_j^{(r)}\right) = \frac{\lambda_j^{(r)} \tilde{C}_{k,j}}{\omega_k^2 + \left(\lambda_j^{(r)}\right)^2 + \lambda_j^{(r)} \tilde{C}_{k,k}}$$

$$\eta_j\left(\lambda_j^{(r)}\right) = \tilde{C}_{j,j} + \mathrm{v}_j^T \mathrm{a}_j\left(\lambda_j^{(r)}\right)$$

$$\lambda_j^{(r+1)} = \frac{\eta_j\left(\lambda_j^{(r)}\right)}{2} \pm i\sqrt{\omega_j^2 - \left(\frac{\eta_j\left(\lambda_j^{(r)}\right)}{2}\right)^2}$$

$$\epsilon = \left| \frac{\lambda_j^{(r+1)} - \lambda_j^{(r)}}{\lambda_j^{(r)}} \right|$$

$r = r + 1;$

end while

$$\psi_j\left(\lambda_j^{(r)}\right) = \phi_j + \sum_{\substack{k=1 \\ k \neq j}}^{N} \mathrm{a}_j\left(\lambda_j^{(r)}\right) \phi_k$$

$$\lambda_{j,Extended}\left(\psi_j\left(\lambda_j^{(r)}\right)\right) = \frac{-\left(\left(\psi_j\left(\lambda_j^{(r)}\right)\right)^H C \psi_j\left(\lambda_j^{(r)}\right)\right) \pm \sqrt{\left(\left(\psi_j\left(\lambda_j^{(r)}\right)\right)^H C \psi_j\left(\lambda_j^{(r)}\right)\right)^2 - 4\left(\left(\psi_j\left(\lambda_j^{(r)}\right)\right)^H M \psi_j\left(\lambda_j^{(r)}\right)\right)\left(\left(\psi_j\left(\lambda_j^{(r)}\right)\right)^H K \psi_j\left(\lambda_j^{(r)}\right)\right)}}{2\left(\left(\psi_j\left(\lambda_j^{(r)}\right)\right)^H M \psi_j\left(\lambda_j^{(r)}\right)\right)}$$

end for

Figure 2.3 The extended Adhikari algorithm [2]

2.6. Exploring vibrational analysis through complex eigensolutions

This subsection illustrates the methodologies employed to determine the damped eigenvalues, modal damping ratios, damping quality factors, modal assurance criteria, and Frequency Response Function (FRF) responses.

2.6.1. The damped eigenvalues

Damped eigenvalues, also known as the natural frequencies, are crucial for analysing damped harmonic oscillators. They denote the frequencies at which a system vibrates when it encounters damping effects. The calculation of these damped eigenvalues is derived from the complex eigenvalues through the following formula, as presented by Chen et al. [68]:

$$\omega_d = \sqrt{\left(\mathrm{Re}(\lambda)\right)^2 + \left(\mathrm{Im}(\lambda)\right)^2} \equiv \omega\sqrt{\left|\zeta^2 - 1\right|} \tag{2.35}$$

To determine the absolute error in the damped eigenvalues, the subsequent formula can be applied:

$$\mathcal{E}_{\omega_d} = \frac{\left|\omega_{d,Exact} - \omega_{d,App.}\right|}{\left|\omega_{d,Exact}\right|} \times 100\% \tag{2.36}$$

2.6.2. The modal damping ratios

Modal damping ratios are critical for evaluating the behaviour of dynamic systems, especially within the fields of structural and mechanical engineering. They quantify a system's damping level relative to the critical damping threshold. The process for determining the modal damping ratio is as follows [68]:

$$\zeta = -\frac{\mathrm{Re}(\lambda_j)}{\mathrm{Im}(\lambda_j)} \times 100\% \tag{2.37}$$

To calculate the absolute error in modal damping ratios, the ensuing formula is employed:

$$\mathcal{E}_{\zeta} = \frac{\left|\zeta_{Exact} - \zeta_{App.}\right|}{\left|\zeta_{Exact}\right|} \times 100\% \tag{2.38}$$

Note that each mode of the damped system exhibits underdamped behaviour when the damping ratio (ζ) is less than 1, overdamped behaviour when ζ is larger than 1, and critically damped behaviour when ζ equals 1. Oscillatory behaviour appears when the value of ζ falls below 1. More details can be found in [97].

2.6.3. The damping quality factor

The damping quality factor is calculated as per Eq. (2.39), aimed at quantitatively evaluating the modal damping across different modes in the system. This metric is also useful for verifying the accuracy of determined complex eigenvalues.

$$Q = -\frac{\mathrm{Im}(\lambda_j)}{2\,\mathrm{Re}(\lambda_j)} \tag{2.39}$$

The damping quality factor Q, inversely relates to modal damping strength; a lower Q value signifies higher modal damping. It essentially represents the relationship between the complex mode's real and imaginary parts.

According to Lázaro [96], modes with $Q \leq 10$ are considered highly damped, whereas modes with $Q = \infty$ are viewed as undamped.

For the precise calculation of the absolute error in quality factor outcomes, the following formula is used:

$$\mathcal{E}_Q = \frac{\left|Q_{Exact} - Q_{App.}\right|}{\left|Q_{Exact}\right|} \times 100\% \tag{2.40}$$

2.6.4. The modal assurance criterion

The Modal Assurance Criterion (MAC) is a scalar value used to evaluate the similarity between a computed eigenvector and the exact eigenvector. This comparison is quantified using Eq. (2.41), which measures the consistency or alignment between the two modal vectors. The computation of the MAC follows the formula provided by Allemang [98], capturing the level of similarity between the estimated and exact modal vectors.

$$\mathrm{MAC}\left(\{\Psi_{App}\},\{\Psi_{exact}\}\right) = \frac{\left|\{\Psi App\}^H \{\Psi exact\}\right|^2}{\left(\{\Psi App.\}^H \{\Psi App.\}\right)\left(\{\Psi exact\}^H \{\Psi exact\}\right)} \tag{2.41}$$

The symbol (*H*) denotes the Hermitian conjugate. The range of the MAC spans from zero to one, indicating that a MAC value close to or exactly one suggests a high degree of alignment between the approximated and exact complex eigenvectors. For further insight into the modal assurance criterion, references [99, 100] provide comprehensive details.

To assess the error associated with the MAC, the following equation is used for calculation:

$$\mathcal{E}_{MAC} = \left|1 - \mathrm{MAC}\right| \times 100\% \tag{2.42}$$

2.6.5. Calculation of frequency response function (FRF)

The FRF is an indicator of a system's dynamic reaction to a given frequency of input excitation, detailing the interplay between input and output in the frequency domain. This analysis breaks down each FRF plot into three components: amplitude, phase response, and the discrepancy in amplitude findings across various approximation methods versus the exact calculations. Graphically, the analysis is organized with driving point FRF outcomes on the left and cross-point FRF outcomes on the right. To facilitate a thorough evaluation, the chosen excitation frequency $(\bar{\omega})$ spans all resonance frequencies relevant to the systems being studied.

2.6.5.1. Direct frequency response function analysis

Employing the Laplace transform and verifying the solution $\mathrm{X}(t)=\mathrm{X}(i\bar{\omega})e^{i\bar{\omega}t}$ within Eq. (2.1), the motion equation for an *N*-DOF system is transformed to the frequency domain as follows:

$$\left(-\bar{\omega}^2\mathrm{M}+i\bar{\omega}\mathrm{C}+\mathrm{K}\right)\mathrm{X}\left(i\bar{\omega}\right)=\mathrm{F}\left(i\bar{\omega}\right) \tag{2.43}$$

Here, $\bar{\omega}$ symbolises the frequency of excitation. Consequently, the FRF response is determinable via the equation:

$$\mathrm{H}\left(i\bar{\omega}\right)=\frac{\mathrm{X}\left(i\bar{\omega}\right)}{\mathrm{F}\left(i\bar{\omega}\right)}\Rightarrow\mathrm{H}\left(i\bar{\omega}\right)=\left(-\bar{\omega}^2\mathrm{M}+i\bar{\omega}\mathrm{C}+\mathrm{K}\right)^{-1} \tag{2.44}$$

The exact FRF responses for all the case studies in this thesis may be calculated using the given Eq. (2.44) since it yields identical FRF responses when the state-space complex eigensolutions are applied in the next Eq. (2.45).

2.6.5.2. Exploring FRF dynamics: integrating pole residuals and complex eigensolutions

Employing pole residual terms allows for the application of non-classical complex eigenvalues in computing the dynamic system's FRF, as outlined below:

$$\mathrm{H}\left(i\bar{\omega}\right)=\sum_{j=1}^{N}\left[\frac{\mu_j\psi_j\psi_j^T}{i\omega-\lambda_j}+\frac{\mu_j^*\psi_j^*\psi_j^{\mathcal{H}}}{i\omega-\lambda_j^*}\right],\qquad \mu_j=\frac{1}{\psi_j^T\left[2\lambda_j\mathrm{M}+\mathrm{C}\right]\psi_j} \tag{2.45}$$

It should be highlighted that Eq. (2.45) is applied to derive the FRF responses for AM across all cases examined in this research. A detailed analysis of modal transfer functions is documented in reference [101].

2.6.5.3. A new Frequency response function based on identified system matrices

Developing a novel FRF analysis approach introduces an advanced technique for calculating FRF by leveraging complex eigensolutions to accurately identify the system's damping and stiffness matrices, built on the identification strategy outlined in [10], the method uses these matrices to compute the FRF, offering a ground-breaking shift in FRF calculation and introducing a new angle through the strategic use of complex eigensolutions.

$$\hat{\mathrm{C}} = \mathrm{M}\left(\Psi\Lambda^2\Psi^{-1}\Psi^* - \Psi^*\Lambda^2\right)\mathrm{S}, \qquad \mathrm{S} = \left(\Psi^*\Lambda^* - \Psi\Lambda\Psi^{-1}\Psi^*\right)^{-1} \tag{2.46}$$

$$\hat{\mathrm{K}} = \mathrm{M}\left(\Psi^*\left(\Lambda^*\right)^2\mathrm{S}\Psi\Lambda\Psi^{-1} - \Psi\Lambda^2\Psi^{-1}\left(\mathrm{I}_N + \Psi^*\mathrm{S}\Psi\Lambda\Psi^{-1}\right)\right) \tag{2.47}$$

Here $\mathrm{I}_N \in \mathbb{R}^{N\times N}$ denotes the identity matrix. The abbreviation $\Lambda = diag([\lambda_1, \lambda_2, \cdots, \lambda_N])$ is used to represent the spectrum of complex eigenvectors, as well as the matrix of complex eigenvectors, which is represented by the symbol $\Psi = [\psi_1, \psi_2, \cdots, \psi_N]$.

The matrices for damping and stiffness identified through this process are marked as $\hat{\mathrm{C}}$ and $\hat{\mathrm{K}}$, respectively.

A noteworthy position is played by the matrix $\mathrm{S} \in \mathbb{C}^{N\times N}$, which is present in the identification process detailed in [10]. To obtain the FRF formula that is derived by substituting the identified damping and stiffness matrices into Eq. (2.43) using Eqs (2.46-2.47), the following expression is obtained:

$$\mathrm{H}(i\bar{\omega}) = \left(\mathrm{M}\left(-\bar{\omega}^2 + i\bar{\omega}\left(\left(\Psi\Lambda^2\Psi^{-1}\Psi^* - \Psi^*\Lambda^2\right)\mathrm{S}\right) + \left(\Psi^*\left(\Lambda^*\right)^2\mathrm{S}\Psi\Lambda\Psi^{-1} - \Psi\Lambda^2\Psi^{-1}\left(\mathrm{I}_N + \Psi^*\mathrm{S}\Psi\Lambda\Psi^{-1}\right)\right)\right)\right)^{-1} \tag{2.48}$$

Significantly, the FRF responses of the EAM across all scenarios presented in Chapter Four are derived employing the formula outlined in Eq. (2.50).

2.6.5.4. Quantifying FRF amplitudes: insights into system response magnitudes

The FRF amplitude is pivotal in quantifying the system's response magnitude to excitation at a given frequency, shedding light on the response intensity at that frequency, by using Eq. (2.49). Typically represented in decibels (dB), the amplitude measurement offers crucial insights into the system's dynamic behaviour.

$$\text{Amplutide}\left(\mathrm{H}_{i,j}(i\bar{\omega})\right) = 20\times\log_{10}\left(\left|\mathrm{H}_{i,j}(i\bar{\omega})\right|\right) \tag{2.49}$$

2.6.5.5. Evaluating variations in FRF amplitude

The discrepancy between the approximate and exact FRF amplitudes is calculated as follows: Calculating the difference between the estimated and exact FRF amplitudes is accomplished by the utilisation of the following formula:

$$\Delta\,\text{Amplutide}\left(\mathrm{H}_{i,j}(i\bar{\omega})\right) = \text{Amplutide}\left(\mathrm{H}_{i,j}(i\bar{\omega})\right)_{Exact} - \text{Amplutide}\left(\mathrm{H}_{i,j}(i\bar{\omega})\right)_{Approx.} \tag{2.50}$$

2.6.5.6. Determining FRF phase responses

The phase aspect of the FRF is verified by applying the two-argument arctangent function, enabling the determination of the phase angle pertinent to the FRF at specific frequencies. This approach allows for a detailed examination and interpretation of the phase response to the system's dynamic characteristics.

$$\text{phase}\left(\mathrm{H}_{i,j}\left(i\bar{\omega}\right)\right) = \text{atan2}\left(\text{Re}\left(\mathrm{H}_{i,j}\left(i\bar{\omega}\right)\right),\text{Im}\left(\mathrm{H}_{i,j}\left(i\bar{\omega}\right)\right)\right) \tag{2.51}$$

2.6.6. Validating eigensolutions consistency

The process of validating eigensolution consistency entails confirming that the derived eigenvectors and eigenvalues are approved solutions to the posed eigenvalue problem, a step crucial for the integrity and dependability of the analysis. Matrix $\Lambda = \text{diag}\left(\lambda_1,\lambda_2,\cdots,\lambda_N\right)$ qualifies as the set holding the proper complex eigenvalues provided it satisfies the following criterion:

$$\Lambda(\mathrm{D}) = \{\lambda\in\mathbb{C}:\det\mathrm{D}(\lambda) = 0\} \tag{2.52}$$

As $\Psi = [\psi_1, \psi_2, \cdots \psi_N]$ represents the right complex modal matrix, it becomes possible to extend Eq. (2.34) for the purpose of identifying the residual matrix through the following process:

$$\mathrm{R} = \Psi^H \mathrm{D}(\Lambda)\Psi = \Psi^H \left(\Lambda^2 \mathrm{M} + \Lambda \mathrm{C} + \mathrm{K}\right)\Psi \Leftrightarrow \mathrm{R} = \Psi^H \Lambda^2 \mathrm{M}\Psi + \Psi^H \Lambda \mathrm{C}\Psi + \Psi^H \mathrm{K}\Psi \quad (2.53)$$

According to the self-adjoint QEVP theorem, each of the several crucial conditions for the eigensolutions correspondence is that the diagonal elements of the residual matrix must be zero. $(\mathrm{diag}(\mathrm{R}) = 0)$.

2.7. Conclusion

This chapter has delved into the complicated process of decoupling linear non-classical damping structures by presenting a blend of thorough analysis and innovative thinking to tackle the quadratic eigenvalue problem (QEVP). We have covered various strategies for decoupling these systems, from the foundational principles of the lightly non-classical damping assumptions to the computationally coast exact analytical state-space method and the various approximation methods in original space. This chapter's unveiling of two pioneering decoupling methodologies in the original space marks a significant contribution to the field, offering fresh insights into complex vibrational challenges and new decoupling techniques. This chapter thorough examination of parametric dynamical verification techniques and frequency response function (FRF) analysis provides a solid basis for future research, offering a more simplified method for understanding the analysis of complex structural systems. It also serves as a good standard for checking the validity of the methods proposed in this chapter.

Chapter 3: A comparative evaluation of decoupling techniques for non-classical linear damped structures

3.1. Introduction

In this chapter, we present the findings from our in-depth research [1] into pioneering and low-coast computation approaches for decoupling non-classical linear damped systems in structural dynamics. The main goal of this research has been to replace the highly complicated exact state-space method with more straightforward yet effective alternatives. Two main methods have been the subject of our investigation: one is the diagonal approximation, a lightly non-classical damping technique based on undamped eigenanalysis; the other is the Adhikari first-order iterative method, which employs Galerkin's method to minimize errors in approximated complex eigensolutions and the Neumann series to expand undamped eigenvectors. We have examined the suitability of these techniques in dealing with a variety of non-classical linear damped systems by using metrics for measuring the dominance of diagonal elements. Furthermore, we propose an innovative subspace technique that merges the strengths of the two discussed methods to improve their combined effectiveness. Through this detailed study, we aim to pave the way for a new phase of efficiency and precision in the analysis and design of structural dynamics, potentially impacting a broad range of engineering practices.

3.2. Overview of the model and assumptions for the analysed 4-DOF system with non-classical damping

This study evaluates a frame structure characterised by four degrees-of-freedom (DOF), equipped with three distinct configurations of supplemental viscous dampers. This investigation is undertaken to explore three unique cases of non-classical damped systems as follows: Configuration (a) showcases an asymmetric placement of a single highly damped viscous damper located between the second and third storeys. For configuration (b), a highly viscous damper is asymmetrically situated between the third and fourth storeys. Meanwhile, configuration (c) arranges two dampers with moderate viscosity symmetrically between the first and second storeys, and similarly between the third and fourth storeys (these arrangements are depicted in Figure 3.1, which provides detailed information on the damper's structural parameters and configurations). The Adhikari method is applied, setting the error tolerance at $\epsilon_{Tol.} = 10^{-4}$. This study concentrates

on the effects of external viscous dashpot damping, consciously bypassing inherent damping mechanisms (i.e. Rayleigh damping), as illustrated in the damping matrices presented in Eq. (3.1). The analysis of the dynamic systems seeks to verify the accuracy of approximation approaches compared to exact solutions. This examination includes analysing various dynamic characteristics such as diagonal dominance indices, undamped and complex eigenvalues, modal assurance criterion (MAC), damping quality factor, damping ratio, damped eigenvalues, as well as the amplitude and phase responses of FRFs.

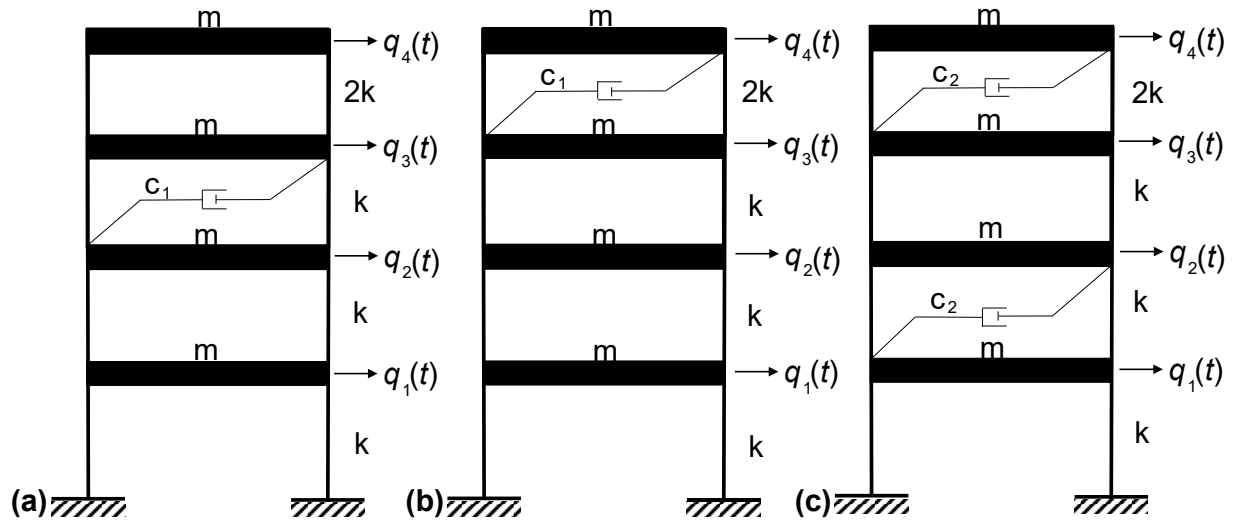

Figure 3.1 Depicts the three arrangements of the viscous dampers installation within the studied 4-DOF frame system. $m = 3\times10^3$[kg], $c_1 = 1.35\times10^3$[N.s/m], $c_2 = 6.75\times10^2$[N.s/m] and $k = 2.5\times10^3$ [N/m]

$$\mathbf{C}_a = c_1\begin{bmatrix} 0 & 0 & 0 & 0 \\ 0 & 1 & -1 & 0 \\ 0 & -1 & 1 & 0 \\ 0 & 0 & 0 & 0 \end{bmatrix},\quad \mathbf{C}_b = c_1\begin{bmatrix} 0 & 0 & 0 & 0 \\ 0 & 0 & 0 & 0 \\ 0 & 0 & 1 & -1 \\ 0 & 0 & -1 & 1 \end{bmatrix},\quad \mathbf{C}_c = c_2\begin{bmatrix} 1 & -1 & 0 & 0 \\ -1 & 1 & 0 & 0 \\ 0 & 0 & 1 & -1 \\ 0 & 0 & -1 & 1 \end{bmatrix} \tag{3.1}$$

The matrices representing mass, stiffness, and undamped eigenvectors are denoted as:

$$\mathrm{M} = m\begin{bmatrix} 1 & 0 & 0 & 0 \\ 0 & 1 & 0 & 0 \\ 0 & 0 & 1 & 0 \\ 0 & 0 & 0 & 1 \end{bmatrix},\quad \mathrm{K} = k\begin{bmatrix} 2 & -1 & 0 & 0 \\ -1 & 2 & -1 & 0 \\ 0 & -1 & 2 & -1 \\ 0 & 0 & -1 & 2 \end{bmatrix},$$

$$\mathrm{Q} = \begin{bmatrix} 0.2146 & -0.3473 & -0.3473 & -0.2146 \\ 0.3473 & -0.2146 & 0.2146 & 0.3473 \\ 0.3473 & 0.2146 & 0.2146 & -0.3473 \\ 0.2146 & 0.3473 & -0.3473 & 0.2146 \end{bmatrix} \tag{3.2}$$

The modal damping matrices for the three configurations are calculated based on the undamped eigenanalysis described in Eqs. (2.5 - 2.8) in the second chapter, and are represented as follows:

$$\mathrm{C}'_a = \begin{bmatrix} 0 & 0 & 0 & 0 \\ 0 & 0.2488 & 0 & -0.4025 \\ 0 & 0 & 0 & 0 \\ 0 & -0.4025 & 0 & 0.6512 \end{bmatrix}, \mathrm{C}'_b = \begin{bmatrix} 0.0238 & 0.0238 & 0.1006 & -0.1006 \\ -0.0238 & 0.0238 & -0.1006 & 0.1006 \\ 0.1006 & -0.1006 & 0.4262 & -0.4262 \\ -0.1006 & 0.1006 & -0.4262 & 0.4262 \end{bmatrix},$$

$$\mathrm{C}'_c = \begin{bmatrix} 0.0238 & 0 & 0.1006 & 0 \\ 0 & 0.0238 & 0 & 0.1006 \\ 0.1006 & 0 & 0.4262 & 0 \\ 0 & 0.1006 & 0 & 0.4262 \end{bmatrix} \tag{3.3}$$

3.3. Results of the dynamical analysis

The mathematical formulations in section 2.6 of the thesis are essential for all parametric dynamical studies including calculating Frequency Response Function (FRF) responses.

3.3.1. Diagonality dominance indices results

Assessing the diagonal dominance of the analysed systems involves using $\rho_1(\mathrm{C}')$ and $\rho_2(\mathrm{C}')$. Reader could refer to Table 2.3 to calculate these indices.

Nevertheless, it's noteworthy that Eq. (3.3) reveals the non-invertibility of matrix C'_a, posing a challenge in applying the $\rho_1(C')$ diagonality dominance index. Hence, this presents a novel constraint for this index when studying non-classically damped systems, which, to the author's knowledge, has yet to be explored in previous research. The outcomes of both diagonal dominance indices are outlined in Table 3.1.

Table 3.1 Diagonality dominance indices result for the modal damping matrices across the three examined configurations

Configuration	Diagonality dominance indices	
	ρ_1[-]	ρ_2[-]
a	-	1.1180
b	3.0000	0.5279
c	1.0000	2.2361

The findings from Table 3.1 reveal that configuration (a) displays nearly diagonal dominance in the modal damping matrix, whereas configuration (b) exhibits heavily non-diagonal dominance owing to the heightened damping and non-linearity resulting from the placement of the additional damper. In contrast, configuration (c) demonstrates a modal damping matrix with diagonal dominance. It's worth noting that the $\rho_1(C')$ diagonality index failed to identify the diagonal dominance due to the singularity of the matrix C'_a.

3.3.2. Complex eigenvalues results

Table 3.2 shows the finding of complex eigenvalues for the comparison between the two approximation methods, the lightly non-classical and the Adhikari method, when assessed against exact complex eigenvalue results, reveals distinct levels of accuracy and applicability across different configurations. For this specific table, we calculated the absolute relative error of the complex eigenvalues using abs (ε_{λ_j}).

In configuration (a), both methods display high accuracy, with the Adhikari method showing perfect alignment (0% error) with exact results for all modes. The lightly non-classical method also performs well, especially notable in modes 1 and 3, where it matches the exact eigenvalues perfectly. However, it encounters slight discrepancies in modes 2 and 4, with errors of 4.749% and 4.046%, respectively. These errors, while modest, highlight the method's limitations in accurately predicting eigenvalues for specific modes, especially where damping effects are more apparent.

Configuration (b) presents a more challenging scenario. Here, the lightly non-classical method struggles significantly with modes 3 and 4, where errors surge to 11.737% and 12.426%, respectively. Such high errors underscore the method's inadequacy in dealing with configurations where the damping distribution affects the system's dynamic response more substantially. Conversely, the Adhikari method maintains commendable accuracy, with the highest error being just 0.960% in mode 3. This demonstrates the algorithm's robustness and reliability, even in configurations that pose complexities for damping representation.

In configuration (c), both methods exhibit remarkable precision, with the Adhikari method achieving 0% error across all modes, underscoring its unparalleled accuracy. The lightly non-classical method, while not perfect, shows vastly improved performance with maximum errors of around 0.275%. This configuration illustrates the method's potential for high accuracy in scenarios with symmetric damping distribution, suggesting that its effectiveness may be contingent on the system's specific dynamics and damping characteristics.

Table 3.2 illustrates that the Adhikari technique is reliable for predicting complex eigenvalues due to its consistency across setups and modes. Despite its inferior accuracy, especially in intricate damping circumstances, the lightly non-classical damping method may provide sufficient estimates under certain conditions, such as symmetrically distributed damping effects. This review emphasises the need to select an approximation approach that matches the dynamic system's characteristics and needs.

Table 3.2 Presents a comparative analysis of the eigenvalues across the three examined configurations

Mode	Eigenvalues					
	Undamped	Exact	Lightly non-classical		Adhikari method	
j	ω_j (rad/s)	λ_j (rad/s)	λ_j (rad/s)	$\lvert\varepsilon_{\lambda_j}\rvert$ (%)	λ_j (rad/s)	$\lvert\varepsilon_{\lambda_j}\rvert$ (%)
Configuration (a)						
1	0.5642	-0.0000+0.5642i	-0.0000+0.5642i	0.000	-0.0000+0.5642i	0.000
2	1.0731	-0.1220+1.1193i	-0.1244+1.0659i	4.749	-0.1220+1.1193i	0.000
3	1.4771	-0.0000+1.4771i	-0.0000+1.4771i	0.000	-0.0000+1.4771i	0.000
4	1.7364	-0.3280+1.6221i	-0.3256+1.7056i	4.046	-0.3280+1.6221i	0.000
Configuration (b)						
1	0.5642	-0.0114+0.5668i	-0.0119+0.5640i	0.497	-0.0117+0.5669i	0.063
2	1.0731	-0.0083+1.0787i	-0.0119+1.0731i	0.621	-0.0093+1.0801i	0.162
3	1.4771	-0.3873+1.5220i	-0.2131+1.4616i	11.737	-0.3804+1.5354i	0.960
4	1.7364	-0.0431+1.6163i	-0.2131+1.7233i	12.426	-0.0403+1.6090i	0.478
Configuration (c)						
1	0.5642	-0.0118+0.5656i	-0.0119+0.5641i	0.271	-0.0118+0.5656i	0.000
2	1.0731	-0.0113+1.0759i	-0.0119+1.0731i	0.266	-0.0113+1.0759i	0.000
3	1.4771	-0.2132+1.4576i	-0.2131+1.4616i	0.275	-0.2132+1.4576i	0.000
4	1.7364	-0.2137+1.7186i	-0.2131+1.7233i	0.261	-0.2137+1.7186i	0.000

The complex conjugate eigenvalues' results are visually depicted in Figure 3.2 on a complex plane, offering a clear interpretation.

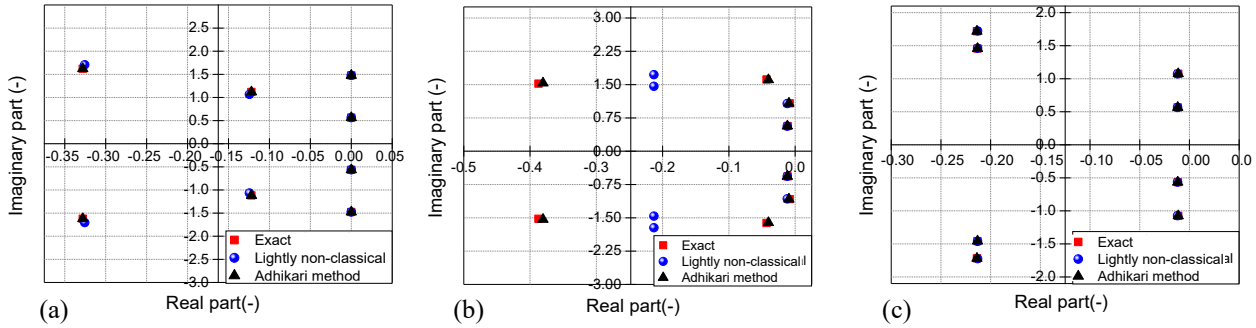

Figure 3.2 Comparative analysis of the conjugate complex eigenvalues using the complex plane

3.3.3. MAC value results

Table 3.3 shows the results of examining the MAC values across three different configurations using various approximation methods; the table offers an understand view of how these methods perform relatively to the exact eigenvectors. The analysis of the MAC values, complemented by the percentage errors (ε_{MAC}), allows for a deeper understanding of the approximation accuracy of each method.

For configuration (a), the Undamped eigenanalysis results demonstrate perfect alignment for modes 1 and 3, as indicated by MAC values of 1.000, suggesting that the undamped approximation aligns with the exact eigenvectors for these modes. However, modes 2 and 4 exhibit lower MAC values, 0.938 and 0.852, respectively, with corresponding errors of 6.2% and 14.8%, indicating a lower similarity. On the other hand, both the Lightly non-classical damping method and the Adhikari method achieve perfect MAC values for all modes. This indicates that incorporating even a light damping effect provides a more accurate approximation of the exact eigenvectors, with the Adhikari method demonstrating a particularly robust capability in accounting for damping effects across all modes in configuration (a).

In configuration (b), the limitations of the Undamped eigenanalysis become more apparent, especially for modes 3 and 4, where the MAC values drop significantly to 0.586 and 0.524, respectively. These values, coupled with substantial errors of 41.4% and 47.6%, signal a poor correlation with the exact eigenvectors, suggesting the undamped eigenanalysis inadequacy for accurately capturing the dynamics of configuration (b). The Lightly non-classical damping method shows marked improvement with MAC values of 0.827 and 0.844 for modes 3 and 4, reducing the errors to 17.3% and 15.6%, respectively. Despite this improvement, the Adhikari method excels, achieving near-perfect MAC values for all modes and demonstrating minimal errors. This underscores the method's effectiveness in accurately approximating the exact eigenvectors, especially in the more challenging aspects of configuration (b).

Configuration (c) sees all three methods performing exceptionally well for mode 1, with perfect MAC values. The Undamped method exhibits a slight decrease in MAC values for modes 2 to 4, though the errors remain minimal, indicating high accuracy. However, the Lightly non-classical damping and Adhikari methods maintain perfect MAC values across all modes, showcasing their excellent approximation of the exact eigenvectors for configuration (c).

The comparative analysis highlights the importance of considering damping effects in modal analysis. While the Undamped eigenanalysis can be effective under certain conditions, the high performance of the Lightly non-classical damping and Adhikari methods across various configurations underscores the value of incorporating damping into the approximation process. The Adhikari method, in particular, stands out for its robustness and accuracy in approximating the exact eigenvectors, demonstrating its effectiveness across a range of damping scenarios and configurations. This analysis illustrates the advances in modal approximation methods and emphasises the necessity of accurate damping modelling for precise dynamic analysis.

Table 3.3 Presents a comparative analysis of the MAC values for the three configurations under study

Mode	Modal assurance criterion					
	Undamped		Lightly non-classical		Adhikari method	
j	MAC [-]	ε_{MAC} [%]	MAC [-]	ε_{MAC} [%]	MAC [-]	ε_{MAC} [%]
Configuration (a)						
1	1.000	0.000	1.000	0.000	1.000	0.000
2	0.938	6.200	1.000	0.000	1.000	0.000
3	1.000	0.000	1.000	0.000	1.000	0.000
4	0.852	14.800	1.000	0.000	1.000	0.000
Configuration (b)						
1	0.998	0.200	1.000	0.000	1.000	0.000
2	0.989	1.100	1.000	0.000	0.999	0.100
3	0.586	41.400	0.827	17.300	0.993	0.700
4	0.524	47.600	0.844	15.600	0.991	0.900
Configuration (c)						
1	1.000	0.000	1.000	0.000	1.000	0.000
2	0.997	0.300	1.000	0.000	1.000	0.000
3	0.994	0.600	1.000	0.000	1.000	0.000
4	0.992	0.800	1.000	0.000	1.000	0.000

3.3.4. damping quality factor results

Table 3.4 presents a detailed comparative analysis of the calculation of damping quality factors across various modes and configurations, offering values derived from exact methods alongside those obtained through the lightly non-classical method and the Adhikari method. Including percentages of error (ε_Q) provides valuable insights into the discrepancies between the exact values and the approximations offered by the alternative methods.

In configuration (a), for Mode 2, both alternative methods provide relatively close estimates of the exact value. However, the lightly non-classical method exhibits a higher error of 6.576%, while the Adhikari method demonstrates a significantly lower error of 0.008%, aligning closely with the exact value. For Mode 4, the lightly non-classical method shows a higher error of 5.907%, whereas the Adhikari method aligns perfectly with the exact value, showing no error (0.000%). This highlights the higher performance of the Adhikari method in capturing the damping behaviour for Mode 4 within configuration (a).

In configuration (b), Modes 3 and 4 have the highest errors. Mode 3 exhibits a notably high error of 74.506% for the lightly non-classical method and 2.703% for the Adhikari method. Similarly, Mode 4 displays high errors of 78.459% and 6.368% for the lightly non-classical and Adhikari methods, respectively. These high errors of the lightly non-classical damping method suggest limitations in accurately capturing the damping characteristics of Mode 2 within this configuration, with similar challenges observed for Modes 3 and 4. Hence, the findings show that the Adhikari method proves significantly more effective.

In configuration (c), the modes with the highest errors are Mode 2 and 4. Mode 2 shows a relatively higher error of 5.256% for the lightly non-classical method compared to 0.001% for the Adhikari method. Similarly, Mode 4 exhibits a slightly higher error of 0.551% for the lightly non-classical method, whereas the Adhikari method aligns perfectly with the exact value. Despite these errors, configuration (c) generally demonstrates lower error percentages compared to configuration (b), indicating better agreement between the exact values and those obtained through alternative methods.

In summary, while each configuration presents different modes with varying errors, the Adhikari method consistently demonstrates superior performance in capturing damping behaviour with closer alignment to the exact values, especially for the modes with the highest errors. These findings underscore the importance of method selection in accurately predicting damping quality factors, which is crucial for practical engineering analyses and designs.

Table 3.4 Presents a comparative analysis of the damping quality factors

Mode	Damping quality factor				
	Exact	Lightly non-classical		Adhikari method	
j	$\mathcal{Q}$ [-]	$\mathcal{Q}$[-]	$\varepsilon_{\mathcal{Q}}$ [%]	$\mathcal{Q}$ [-]	$\varepsilon_{\mathcal{Q}}$ [%]
Configuration (a)					
1	∞	∞	0.000	∞	0.000
2	4.587	4.585	6.576	4.586	0.008
3	∞	∞	0.000	∞	0.000
4	2.473	2.619	5.907	2.473	0.000
Configuration (b)					
1	24.924	23.743	4.738	24.195	2.927
2	65.027	45.175	30.529	57.780	11.144
3	1.965	3.429	74.506	2.018	2.703
4	18.768	4.043	78.459	19.963	6.368
Configuration (c)					
1	24.060	23.746	1.306	24.060	0.000
2	47.680	45.175	5.256	47.681	0.001
3	3.418	3.429	0.332	3.418	0.000
4	4.021	4.043	0.551	4.021	0.000

Figure 3.3 presents the damping ratios for the three configurations under analysis. It's noteworthy that the error in estimating the damping ratio corresponds to the error in estimating the quality factor. This correlation arises from the linear relationship between the formulation for the damping ratio and the quality factor.

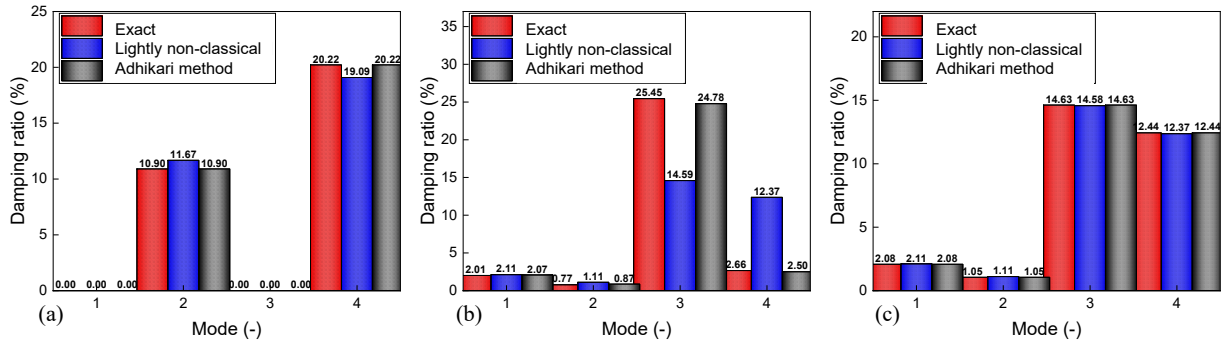

Figure 3.3. A comparison of the modal damping ratios among the studied configurations

3.3.5. Damped eigenvalue results

Table 3.5 comprehensively compares damped eigenvalues across various modes and configurations, providing insights into the accuracy of approximation methods in capturing damping effects. In each configuration, the exact values are contrasted with those obtained through the lightly non-classical method and the Adhikari method, with percentage errors ($\varepsilon_{\omega d}$) providing a measure of the discrepancies between them.

Configuration (a) showcases closely matched damped eigenvalues for all modes, with negligible percentage errors observed for both alternative methods. This suggests a high level of accuracy in approximating damping effects within this configuration, indicating the effectiveness of both the lightly non-classical method and the Adhikari method.

Moving to configuration (b), while the overall accuracy remains high, slight discrepancies are observed, particularly for Mode 3. Here, the lightly non-classical method exhibits a relatively higher error of 2.298%, while the Adhikari method demonstrates a more minor error of 0.177%. Despite these discrepancies, both methods generally provide accurate approximations of damped eigenvalues within configuration (b).

Configuration (c) mirrors the accuracy observed in configuration (a), with closely matched damped eigenvalues and minimal percentage errors for both alternative methods. Even for modes with slightly higher errors, such as Mode 3 and Mode 4, the discrepancies remain small, affirming the effectiveness of both the lightly non-classical and Adhikari methods in capturing damping behaviour within this configuration.

In summary, Table 3.5 highlights the effectiveness of the lightly non-classical method and the Adhikari method in approximating damped eigenvalues across various modes and configurations. While slight discrepancies exist, particularly in configuration (b), both methods demonstrate high accuracy overall, underscoring their utility in structural dynamics analyses and engineering designs.

Table 3.5 Provides a comparative analysis of the damped eigenvalues

Mode	Damped eigenvalues				
	Exact	Lightly non-classical		Adhikari first-order	
j	ω_d [rad/s]	ω_d [rad/s]	ε_{ω_d} [%]	ω_d [rad/s]	ε_{ω_d} [%]
Configuration (a)					
1	0.5642	0.5642	0.000	0.5642	0.000
2	1.0667	1.0658	0.088	1.0667	0.000
3	1.4771	1.4771	0.000	1.4771	0.000
4	1.7005	1.7044	0.231	1.7005	0.000
Configuration (b)					
1	0.5641	0.5641	0.002	0.5641	0.001
2	1.0731	1.0731	0.003	1.0731	0.001
3	1.4284	1.4613	2.298	1.4310	0.177
4	1.7358	1.7231	0.732	1.7358	0.004
Configuration (c)					
1	0.5641	0.5641	0.001	0.5641	0.000
2	1.0731	1.0731	0.001	1.0731	0.000
3	1.4612	1.4613	0.007	1.4612	0.000
4	1.7229	1.7231	0.009	1.7229	0.000

3.4. Convergence of Adhikari method checking

Figure 3.4 illustrates the number of iterations that are required to compute the eigensolutions while using the Adhikari method. As shown in Figure 3.4, diagonally dominating modes in configurations (a) and (c) require fewer iterations for convergence because of their low level of damping non-classicality. This is demonstrated by the fact that such modes require fewer repetitions. On the other hand, in configuration (b), the third and fourth modes exhibit a slower convergence rate due to the significant coupling between them, whilst the different modes converge at a faster pace.

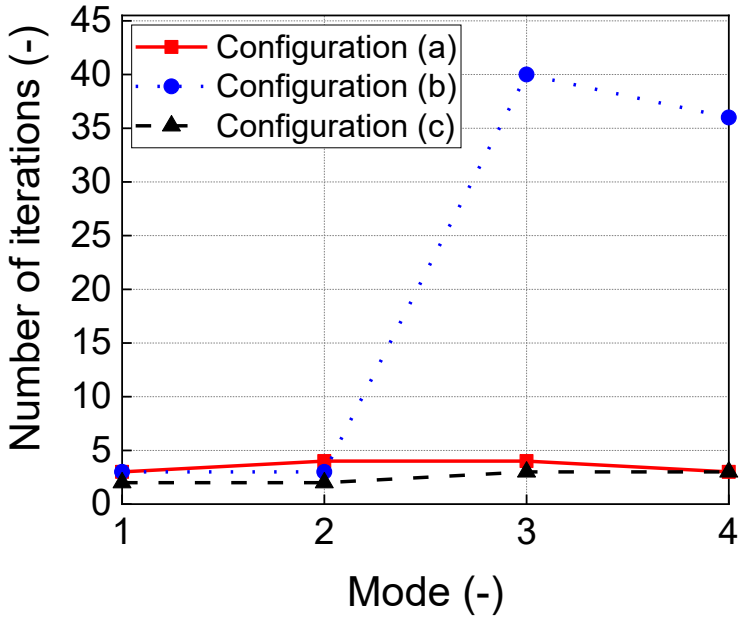

Figure 3.4 The index representing the total iterations of the Adhikari method used to find the complex eigensolutions

3.5. FRF responses results

Figures 3.5-3.7 focus on the computation of FRF responses. In Figure 3.5, it is demonstrated that in configuration (a), the first and second modes show minimal modal damping, leading to only two resonance peaks in both the driving-point-FRF and cross-FRF outcomes. Utilizing the lightly non-classical damping approach and the Adhikari method yields FRF amplitudes and phase responses that closely match the exact results, exhibiting negligible discrepancies.

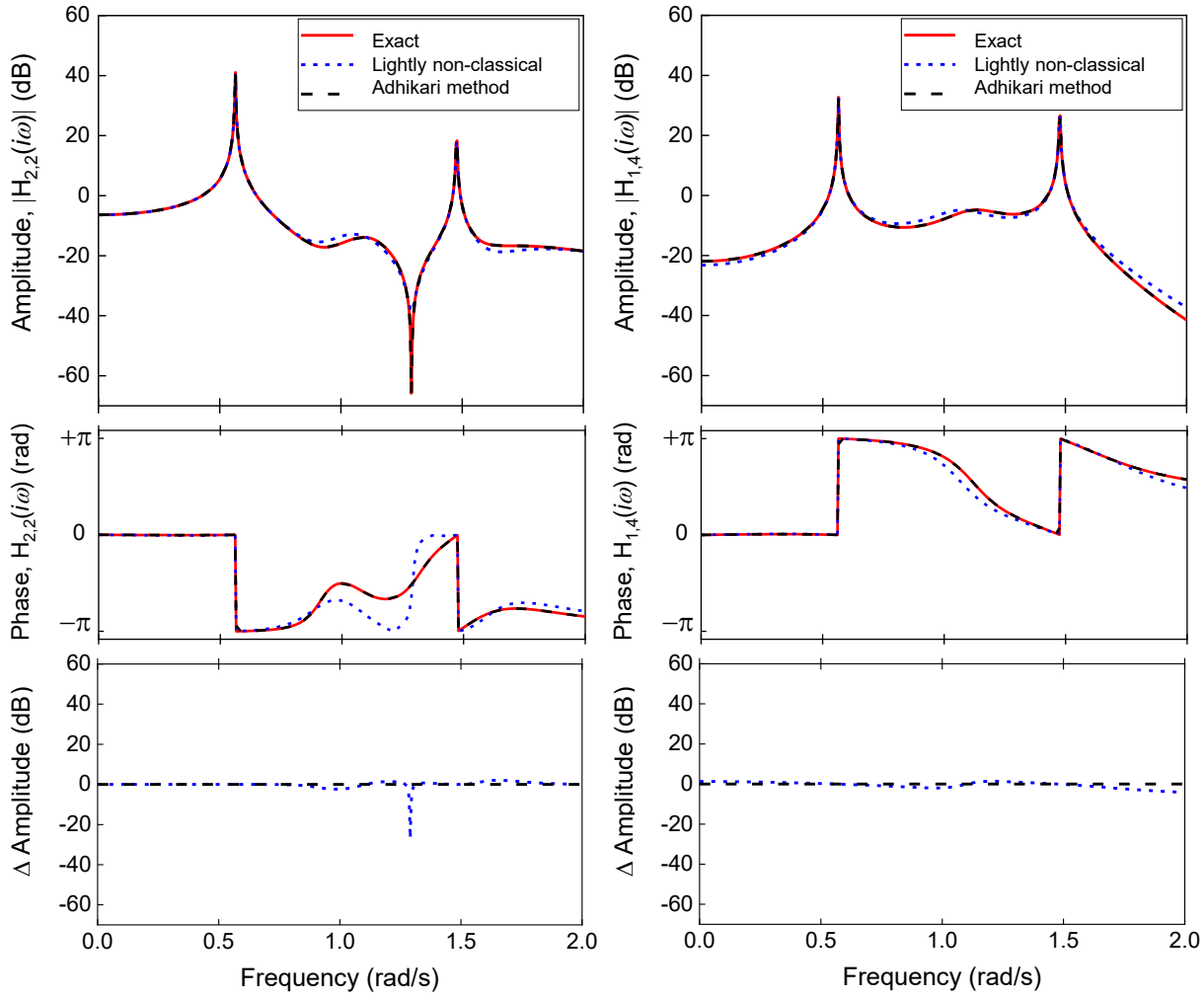

Figure 3.5 A comparison in the FRF responses of configuration (a), showcasing $\mathbf{H}(i\boldsymbol{\omega})_{2,2}$ on the left and $\mathbf{H}(i\boldsymbol{\omega})_{1,4}$ on the right

In Figure 3.6, the FRF responses of configuration (b) are depicted, where the first, second, and fourth modes demonstrate minimal modal damping, leading to the appearance of three resonance peaks in both the driving-point-FRF and the cross-FRF. However, the lightly non-classical damping method fails to accurately replicate the exact FRF responses, as indicated by the absence of the third peak. This deviation, termed fictional damping, arises when the modal coupling is notably high (for a more comprehensive elucidation of fictional damping associated with the classical damping hypothesis, please refer to [102]). Conversely, Adhikari's method effectively approximates the exact FRF amplitude and phase response outcomes.

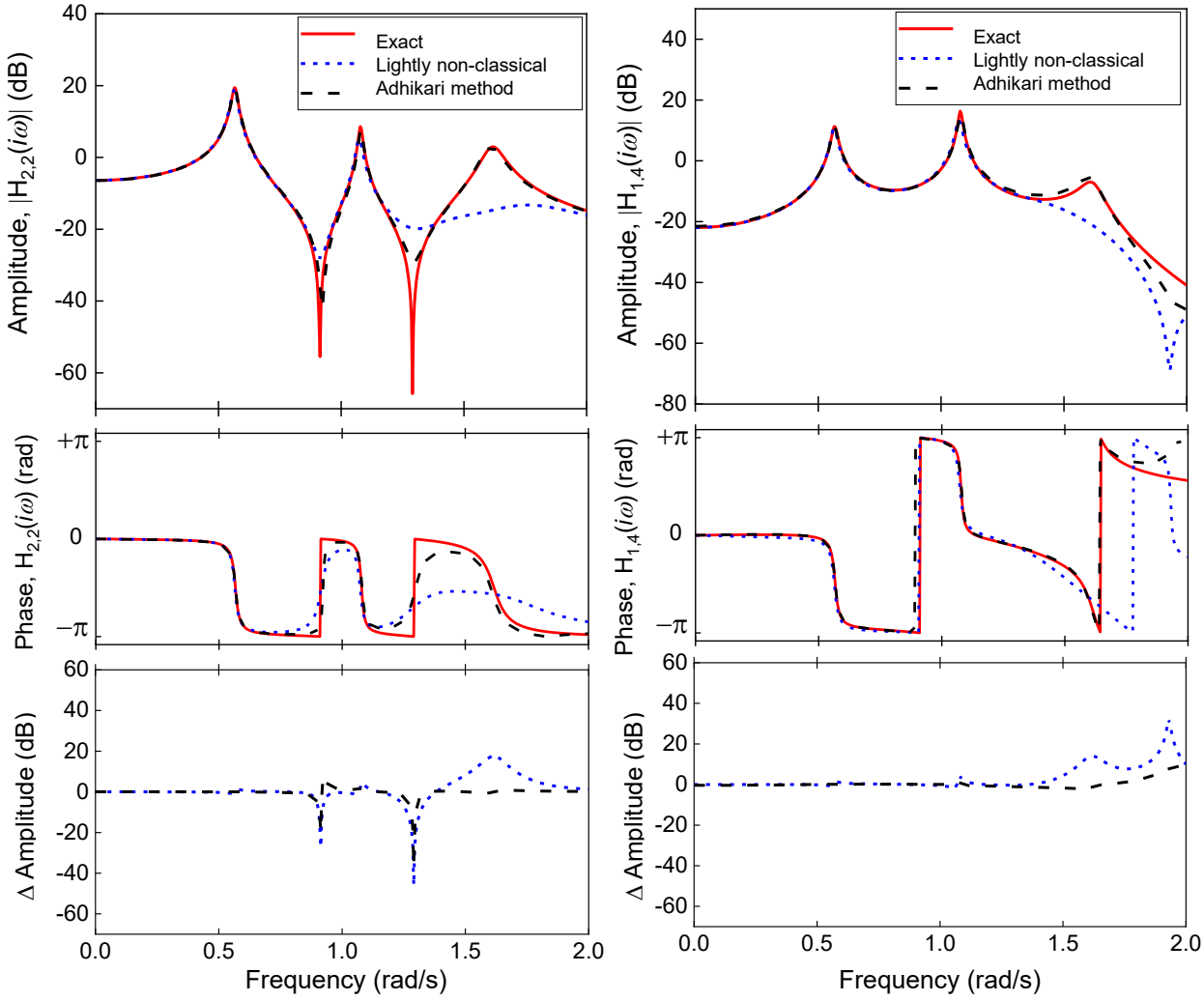

Figure 3.6 A comparison in the FRF responses of the configuration (b): for the $\mathbf{H}(i\boldsymbol{\omega})_{2,2}$ in left, for the $\mathbf{H}(i\boldsymbol{\omega})_{1,4}$ in the right

Figure 3.7 showcases the FRF responses of configuration (c), wherein the first and second modes demonstrate minimal modal damping. This leads to observing only two discernible resonance peaks in both the driving-point-FRF and the cross-FRF. Compared to the exact results, the FRF amplitude and phase responses computed using the lightly non-classical damping method and the Adhikari method closely correspond, exhibiting minimal disparities.

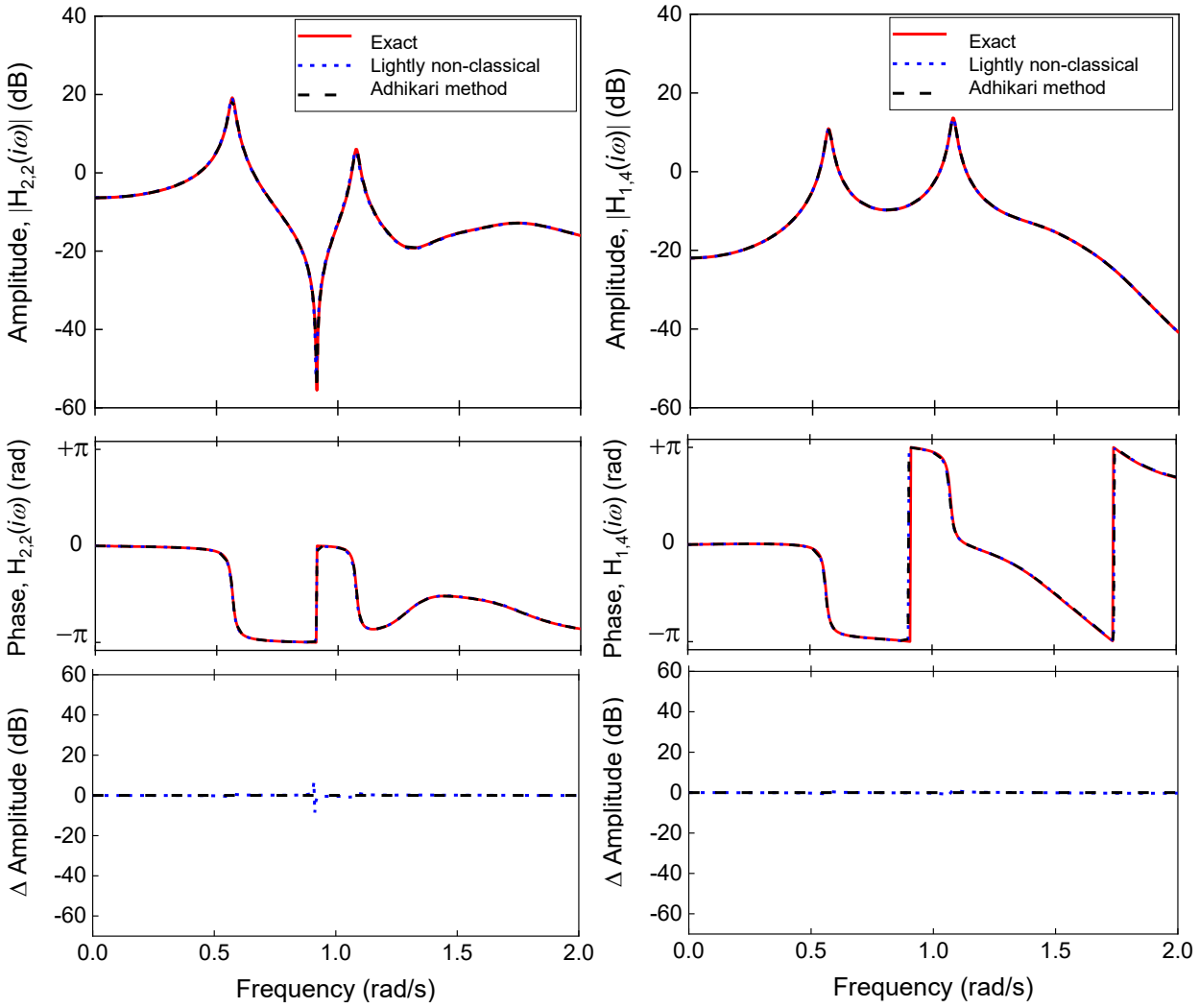

Figure 3.7 A comparison in the FRF responses of the configuration (c): for the $\mathbf{H}(i\boldsymbol{\omega})_{2,2}$ in left, for the $\mathbf{H}(i\boldsymbol{\omega})_{1,4}$ in the right

3.6. Key insights from the study

This subsection highlights a significant relationship between modal coupling and the accuracy of computing dynamical parameters and responses. Hence, Figure 3.8-a, a comparison between the diagonal dominance index ρ_2 from Table 3.1 and the minimum Modal Assurance Criterion (MAC) values from Table 3.3 reveals a direct correlation between diagonal dominance and modal decoupling of the eigenvectors. The Adhikari method consistently provides highly decoupled eigenvectors across a range of ρ_2 values, with MAC values close to one. Conversely, undamped eigenvectors exhibit significant modal coupling when ρ_2 is less than one. In contrast, the lightly non-classical damping method achieves complete eigenvector decoupling accurately using the formulation in Eq. (2.29) only when ρ_2 is more significant than one.

In Figure 3.8-b, a direct correlation is observed between the diagonal dominance index ρ_2 and the error of the computed eigenvalues (the relative absolute error in the complex eigenvalues) from Table 3.2. The Adhikari method consistently predicts complex eigenvalues accurately over a range of ρ_2 values, with typical errors averaging around 1%. However, the lightly non-classical damping method exhibits significant errors when ρ_2 is below one and more tolerable errors when the system is uncoupled (i.e., ρ_2 is greater than or equal to one).

As shown in Figure 3.8-c, the quality factor verifies the equilibrium between the real and imaginary components of the complex eigensolutions. A comparison between the diagonal dominance index and the maximum error in the computed damping quality factor from Table 3.4 indicates that for ρ_2 values smaller than one, the Adhikari method's results are deemed acceptable, with a maximum inaccuracy of approximately 11%. However, it yields extremely precise outcomes when ρ_2 is greater than or equal to one. In contrast, when ρ_2 is less than one, the lightly non-classical damping method exhibits substantial errors due to modal coupling, with an error exceeding 78%, while a reasonable allowance for error is observed after the system is decoupled (i.e., ρ_2 is greater than or equal to one).

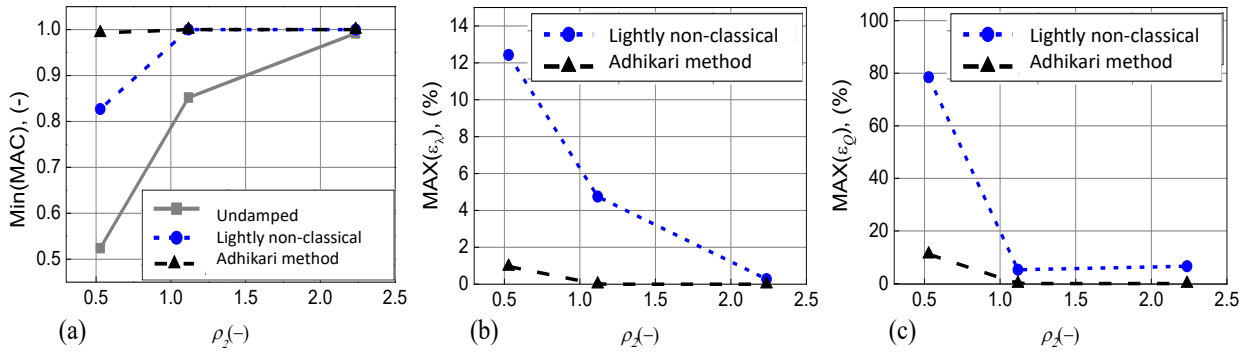

Figure 3.8 The diagonal dominance index in three different contexts: (a) with respect to the estimated eigenvectors' minimum MAC values, (b) for the complex values' maximum error, and (c) for the quality factors' maximum error

3.7. Conclusion

This chapter investigates the effects of non-classical damping on the modal decoupling of linear systems, employing two diagonality dominance indices to assess the damping's non-classicality. Through a comparative analysis of the lightly non-classical damping method and Adhikari's method applied to a 4-DOF frame system with varying external damping characteristics, the research highlights the importance of selecting the appropriate method based on the damping matrix's diagonal dominance. The study demonstrates that the lightly non-classical damping method excels in cases with dominant diagonal elements, while Adhikari's algorithm is better suited for handling non-diagonal dominance, directly influencing the accuracy of damping loss factor estimations and Frequency Response Function (FRF) predictions.

Based on these findings, the chapter introduces a novel subspace algorithm in Figure 2.1 that merges the advantages of both methods to enhance the prediction and decoupling of complex eigensolutions in non-classically damped systems. This algorithm, tailored to improve upon the limitations identified in traditional approaches, offers a practical solution for accurately approximating non-classical complex eigensolutions.

Chapter 4: Advancing Eigenanalysis in Linear Non-Classically Damped Systems: A new extended version of the Adhikari iterative method

4.1. Introduction

In this chapter, we delve into the examination of complex dynamical systems identified by highly non-classical damping and unstable behaviour, which pose significant challenges in terms of analysis and comprehension referring to our research paper [2]. The inherent complexities, stemming from non-classical damping mechanisms and the propensity for unstable dynamics, substantially complicate the accurate determination of complex eigenvalues and the analysis of dynamic characteristics. To address these challenges, we introduce a novel extension to the Adhikari method, specifically tailored to confront these intricacies. This extension, featuring advanced mathematical concepts such as a self-adjoint theorem and spectral localisation techniques, aims to effectively decouple these complex systems, ultimately enhancing the accuracy and stability of complex eigenvalue determination. This chapter sets the stage for our in-depth exploration of these complex systems and the methodologies employed to better understand their behaviour. The mathematical representation of the Adhikari method is described in section 2.3.1 of this thesis, while the mathematical representation of the suggested extended version of the Adhikari method is discussed in section 2.5.2 of this thesis.

4.2. Dynamic analysis of three distinct cases of non-classically damped systems

In this section, we showcase the effectiveness and precision of the extended Adhikari iterative method by presenting three numerical examples drawn from prior research. The calculations were performed on a PC featuring an Intel CPU i5-3230M processor, 6GB of RAM, with code development and execution carried out using MathWorks MATLAB software [103]. The mathematical formulations presented in section 2.6 of the thesis are fundamental to all parametric dynamical analyses and the computation of Frequency Response Function (FRF).

4.2.1. Three-degree-of-freedom non-classically damped system

The analysis of the dynamic system with 3-DOF and non-classical damping, as discussed in [104], is presented, with the system configuration depicted in Figure 4.1. The representation of the mass, non-classical damping, stiffness, and modal matrices described as follows in Eq. (4.1):

$$\mathrm{M}=\begin{bmatrix}1.5 & 0 & 0\\ 0 & 2 & 0\\ 0 & 0 & 1.3\end{bmatrix},\quad \mathrm{C}=\begin{bmatrix}0.1856 & 0.2290 & -0.9702\\ 0.2290 & 0.03008 & -0.0297\\ -0.9702 & -0.0297 & 0.1241\end{bmatrix},$$
$$\mathrm{K}=\begin{bmatrix}7 & -2 & 0\\ -2 & 4 & -2\\ 0 & -2 & 5\end{bmatrix},\quad \Phi=\begin{bmatrix}0.4575 & 0.3521 & 0.0090\\ 0.4264 & -0.5510 & -0.1206\\ 0.0918 & -0.1446 & 0.9852\end{bmatrix} \tag{4.1}$$

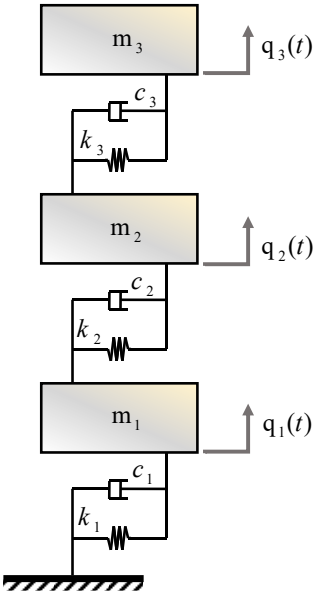

Figure 4.1 The 3-DOF non-classically damped system, as described in [104]

4.2.1.1. The complex eigenvalues for result the 3-DOF system

The comparison presented in Table 4.1 offers valuable insights into the performance of the Adhikari Iterative Method (AM) and the Extended Adhikari Iterative Method (EAM) in estimating the complex eigenvalues compared to the exact results in a dynamic system.

In the first mode, both methods produce complex eigenvalues close to the exact result. EAM demonstrates slightly higher accuracy across real and imaginary parts, with a smaller percentage of errors in real and imaginary parts than AM. Specifically, AM yields eigenvalues of approximately (-0.02578+0.85280i), whereas EAM provides (-0.02603+0.85283i). The percentage errors for AM in the real and imaginary parts are (0.988%) and (0.004%), respectively, while for EAM, they are (0.019%) and (0.006%), respectively.

This trend continues in the second mode, where EAM significantly outperforms AM, providing complex eigenvalues that more closely match the exact solution. For Mode 2, AM yields approximately (-0.02122+1.55327i) eigenvalues, while EAM provides (-0.02019+1.55287i). The percentage errors for AM in the real and imaginary parts are (4.842%) and (0.026%), respectively, while for EAM, they are (0.250%) and (0.028%).

In the third mode, AM and EAM closely approximate the exact complex eigenvalues, indicating their robustness in handling dynamic systems with non-classical damping. AM yields eigenvalues of approximately (−0.05369+3.14082i), and EAM provides (−0.05445+3.14080i), with minimal percentage errors of approximately (0.00014%) and (0.00021%) respectively.

In summary, the comparison presented in Table 4.1 highlights the strengths and limitations of the AM and the EAM in estimating eigenvalues for non-classically damped systems. While both methods offer viable solutions, EAM shows superior accuracy, particularly in Mode 2, which could have significant implications for engineering applications requiring precise eigenvalue estimation.

Table 4.1 The eigenvalues for the 3-DOF system

Mode	Eigenvalues					
	Undamped	Exact	Adhikari		Extended Adhikari	
j	ω(rad/sec)	λ(rad/sec)	λ(rad/sec)	ε_λ (%)	λ(rad/sec)	ε_λ (%)
1	0.84374	-0.02578+0.85280i	-0.02603+0.85283i	0.98770+0.00355i	-0.02578+0.85286i	0.01865+0.00626i
2	1.54164	-0.02122+1.55327i	-0.02019+1.55287i	4.84227+0.02620i	-0.02116+1.55283i	0.24951+0.02839i
3	3.20075	-0.05369+3.14082i	-0.05445+3.14080i	1.42333+0.00042i	-0.05369+3.14081i	0.00021+0.00033i

Figure 4.2 illustrates the placement of the approximated complex eigenvalues obtained using both approximation methods, in comparison to the exact results.

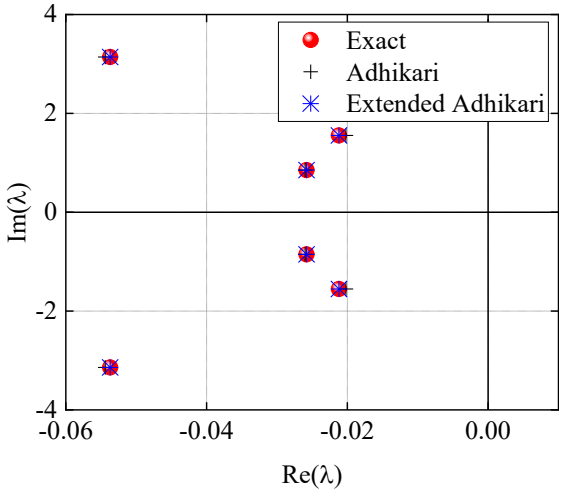

Figure 4.2 Representation of the conjugated complex eigenvalues in Gauss plane for the 3-DOF system

4.2.1.2. The damped eigenvalues result for the 3-DOF system

Table 4.2 shows the computation of the damped eigenvalues employing both AM and EAM in comparison to the exact results using state space. The outcomes are for three different modes of oscillation of the system.

Considering the additional information that the damping ratios are low and that a high tolerance of (10^{-6}) was taken into account in the calculations for both approximation methods, it's noteworthy that both methods yielded identical results to the exact values for modes 1 and 3 and a very close approximation for mode 2.

In Mode 1 and Mode 3, both AM and EAM matched the exact values of ω_d, which were (0.8532 rad/sec) and (3.1413 rad/sec), respectively. The zero-percentage error indicates that both methods are highly effective in calculating the damped eigenvalues for these modes, even with low damping.

Mode 2 presents a slightly different scenario, where the damped eigenvalue computed was (1.5534 rad/sec), and both AM and EAM approximated (1.553 rad/sec). The percentage error is minimal at (0.0257%). This minor discrepancy is well within the high tolerance level set for the computations and can be considered negligible for many practical engineering applications. The

fact that both methods yielded the same results despite the error suggests that they are consistent in their computational approach.

For the readers, it's essential to understand that in the context of dynamic systems, especially those with low damping ratios, the precision of computational methods is critical. The results demonstrate that both AM and EAM are highly precise, with the EAM not showing a significant advantage over AM in this specific case, likely due to the low damping effects not necessitating the extended capabilities of EAM.

Table 4.2 The damped eigenvalues for the 3DOF system

Mode	Damped eigenvalues				
	Exact	Adhikari		Extended Adhikari	
j	ω_d (rad/sec)	ω_d (rad/sec)	ε_{ω_d} (%)	ω_d (rad/sec)	ε_{ω_d} (%)
1	0.8532	0.8532	0.0000	0.8532	0.0000
2	1.5534	1.5530	0.0257	1.5530	0.0257
3	3.1413	3.1413	0.0000	3.1413	0.0000

4.2.1.3. The damping ratios result for the 3-DOF system

Figure 4.3 compares the damping ratios obtained through the Exact method, the AM, and EAM across three distinct modes of a dynamic system. In Mode 1, both AM and EAM methods are in very close agreement with the Exact results, indicating a high level of accuracy for damping ratio calculations. For mode 2, the AM method exhibits a noticeable increase in the percentage error, quantified at 5.0613%, suggesting a reduction in accuracy for these results. In contrast, the EAM method maintains a significantly lower error rate at 0.2218% in Mode 2, showcasing its enhanced precision in estimating damping ratios.

For Mode 3, the chart indicates that both methods revert to a close approximation of the Exact values with negligible error. Hence, this reinforces the suitability of both methods for specific modes while highlighting the efficacy of the EAM method in situations requiring greater precision, such as in calculating damping ratios.

Overall, the bar chart in Figure 4.3 concisely demonstrates the comparative statically accuracy of the AM and EAM methods. EAM is the more precise method for computing damping ratios in dynamic systems.

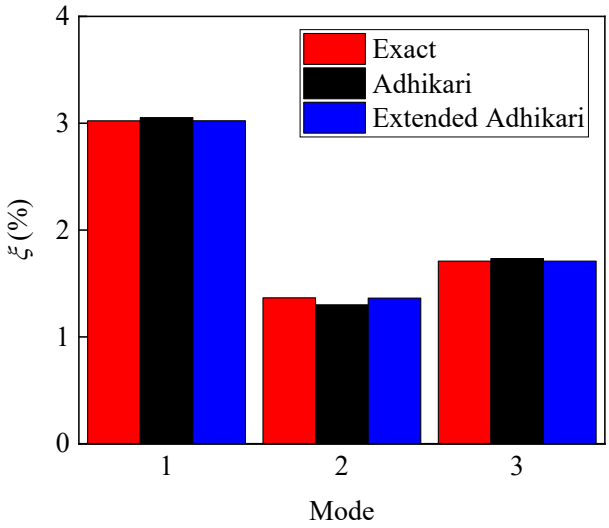

Figure 4.3 A comparison in the damping ratios for the 3-DOF system

4.2.1.4. The damping quality factor result for the 3-DOF system

The analysis of Table 4.3 reveals insights into the damping quality factor of a 3-DOF system calculated by AM and EAM methods compared to the exact state-space method. For Mode 1, the AM displays a percentage error of 0.9751%, which indicates a slight deviation from the exact value. In contrast, the EAM demonstrates a significantly lower percentage error of 0.0127%. This minimal error suggests that the EAM closely approximates the exact value, making it a more precise method for Mode 1.

Moving to Mode 2, the AM's accuracy decreases, with a percentage error of 5.0613%, a considerable deviation that signals the method's noticeable inaccuracy in this mode. However, the EAM shows substantial improvement with a percentage error of only 0.2218%. Despite being higher than the error for Mode 1, it is markedly lower than the AM for Mode 2. This improvement underscores the EAM's enhanced performance and suitability for higher modes.

For Mode 3, the AM's performance slightly improves, with a percentage error of 1.4038%, suggesting a modest deviation from the exact value. On the other hand, the EAM achieves an exceptional accuracy level with a remarkably 0.0003% percentage error. This near-perfect estimation implies that the EAM is extremely accurate for Mode 3, indicating a precision almost equivalent to the exact method.

Considering the errors across all modes, the EAM consistently outperforms the AM in capturing the exact damping quality factor. The EAM's errors are notably minimal; for Mode 3, the error is almost negligible. This consistent accuracy suggests that the EAM should be the preferred method for applications requiring high precision in estimating the damping quality factor. The notable improvement from the AM to the EAM, particularly the over twentyfold error reduction seen in Mode 2, suggests that the EAM includes specific modifications or enhancements that greatly benefit the accuracy in higher modes of a 3-DOF system.

Table 4.3 The quality factor results for the 3-DOF system

Mode	Damping quality factor				
	Exact	Adhikari		Extended Adhikari	
j	Q(-)	Q(-)	ε_Q (%)	Q(-)	ε_Q (%)
1	16.5420	16.3807	0.9751	16.5399	0.0127
2	36.6051	38.4578	5.0613	36.6863	0.2218
3	29.2497	28.8391	1.4038	29.2496	0.0003

4.2.1.5. Verifying the convergence of the Adhikari method for the 3-DOF system

Figure 4.4 presents a graphical comparison of the number of iterations required for converging complex eigensolutions across three modes, comparing the Adhikari and the Extended Adhikari methods. The convergence criterion for both methods was set at an error tolerance of $\epsilon_{Tol.} = 10^{-6}$. The graph displays a horizontal trend for both methods, with data points consistently at or around four iterations for all modes. This indicates that, regardless of the mode considered, both the Adhikari and Extended Adhikari methods required the same number of iterations to reach the desired level of accuracy in the solutions. The uniformity of iterations across the modes suggests that the complexity of the eigensolutions does not significantly affect the computational effort needed for convergence within these methods.

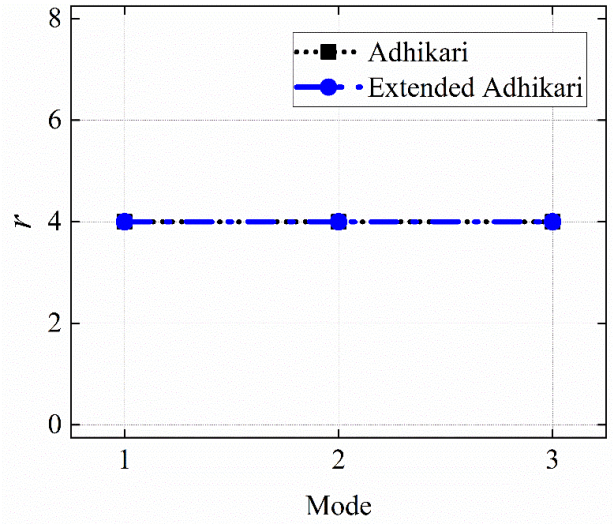

Figure 4.4 The convergence iterations between the Adhikari and the Extended Adhikari method across the three modes for the 3-DOF system

4.2.1.6. Confirming the modal decoupling with MAC Analysis for the 3-DOF System

Figure 4.5 shows the finding of the modal assurance criterion (MAC) Matrix of approximated and exact complex eigenvectors. This matrix plot displays the MAC values, which quantify the correlation between the approximated eigenvectors obtained from the AM and EAM methods and the exact state-space complex eigenvectors for a 3-DOF system. The colour coding from green to red corresponds to MAC values ranging from 0 to 1. A MAC value close to 1 indicates a strong correlation, signifying that the mode shapes are almost identical. The diagonal entries, representing the correlation of each mode with itself, are nearly 1, indicating full decoupling and high fidelity of the approximated eigenvectors with the exact ones. Hence, both AM and EAM methods provide a reliable approximation of the mode shapes, as the approximated complex eigenvectors for both methods are identical.

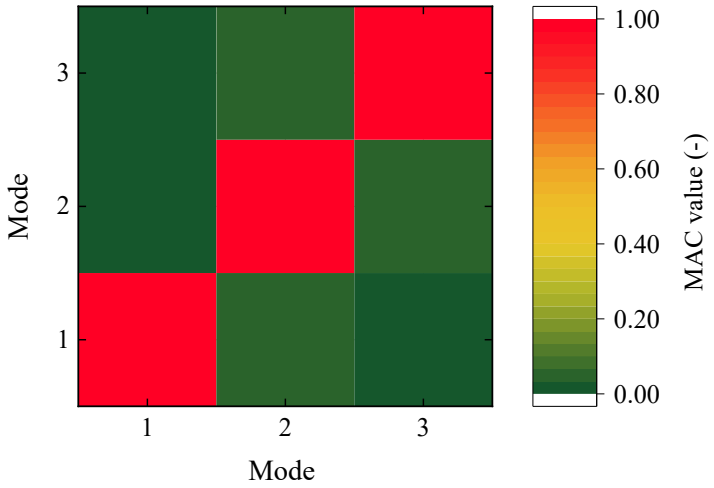

Figure 4.5 MAC results between Adhikari and exact complex eigenvectors for the 3-DOF system

4.2.1.7. Assessing the conformity of the predicted complex eigenvalues with their corresponding eigenvectors for the 3-DOF System

Figure 4.6 shows that the correspondence between complex eigenvalues and their associated eigenvectors can be effectively assessed using Eq. (2.53). Subfigure (a) displays the expected ideal results for the exact state-space complex eigensolutions, where the map should ideally show zeros across all elements, indicating a perfect match.

Subfigure (b) illustrates the results for the AM, where ideally, zero values would be seen along the diagonal of the matrix map. Hence, each mode's eigenvalue and eigenvector correspond correctly. However, it exhibits small non-zero values on the diagonal and off-diagonal, indicating a less precise correspondence.

Subfigure (c) presents the results for the EAM, where a zero value along the diagonal would indicate an accurate match between the eigenvalues and eigenvectors for each mode. The EAM achieves this zero-diagonal, which signifies precise correspondence between the eigenvalues and eigenvectors. The clear diagonal in subfigure (c) attributed to the EAM reflects its superior performance in accurately matching eigenvalues to their respective complex eigenvectors when compared to the AM, as evidenced by the non-zero values in subfigure (b). Hence, this denotes that the EAM is more adept at pairing the correct eigenvalue with its corresponding complex eigenvector for each mode.

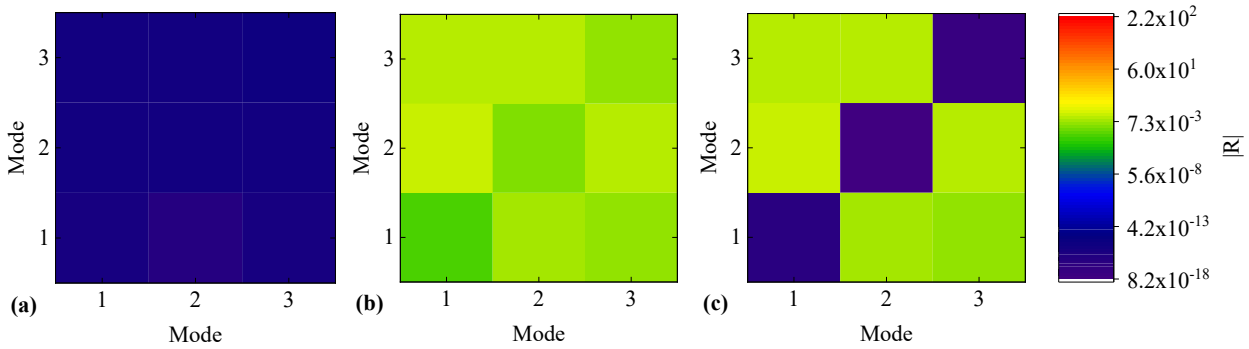

Figure 4.6 The residual map for the 3-DOF system: a) using the exact complex eigensolutions, b) using the Adhikari complex eigensolutions, and c) using the extended complex eigenvalues and Adhikari complex eigenvectors

4.2.1.8. The FRF analysis of the 3-DOF system

Figure 4.7 depicts the Frequency Response Function (FRF) for the 3-DOF system, comparing the Exact method with two approximation methods: AM and EAM. The graphs are divided into two main comparisons: the left side shows the FRF results for $H_{3,3}$, and the right side for $H_{3,1}$.

In both cases, the top graphs represent the amplitude of the FRF; the middle graphs show the phase of the FRF, and the bottom graphs display the dispersing in amplitude, all as a function of frequency in radians per second. The exact method is depicted with a solid red line, the AM with a dotted black line, and the EAM with a dash-dot blue line. The amplitude plots reveal that both the AM and EAM closely follow the trend of the Exact method, with the EAM showing a marginally closer fit, especially noticeable in the response peaks. The phase plots demonstrate a similar accuracy, with all methods exhibiting nearly coincident phase angles across the frequency range.

The figure suggests that while the AM and EAM can accurately capture the system's FRF, the EAM slightly improves precision. This improvement could be attributed to a more refined approximation of the complex eigenvalues, particularly in non-classically damped systems.

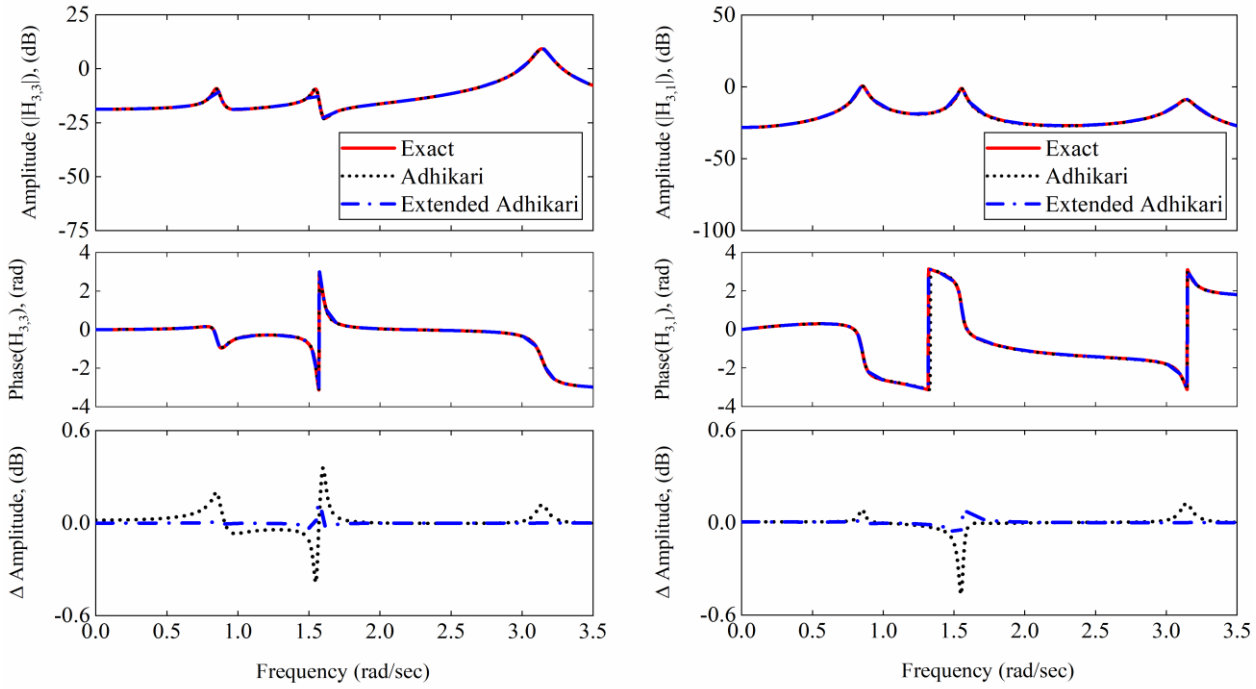

Figure 4.7 A comparison in the FRF responses for the 3DOF system: $H_{3,3}$ in left, and for $H_{3,1}$ In the right

4.2.2. Four-degrees-of-freedom non-classically damped system

This section discusses analysing a system with 4-DOF and non-classically damping properties, as outlined in reference [92]. (The configuration of this system is visualised in Figure 4.8). For this study, the mass $m = 1\,\text{kg}$, and the stiffness $k = 1{,}800\,\text{N/m}$. The system's damping attribute is a combination, integrating the proportional Rayleigh damping model, defined by coefficients $(a_0 = 0.31501\,\text{sec}^{-1}$ and $a_1 = 0.0003\,\text{sec})$. An additional external damping component is introduced by attaching a dashpot with a viscous damping coefficient $(c_d = 25\,\text{N/m})$ to the third stage. This arrangement introduces an advanced damping matrix to the system's structure. Damping and the stiffness matrices undergo adjustments by the parameter γ, as illustrated in [92]. The analysis is oriented towards the most challenging scenario by setting $\gamma = 0.5$, aiming to rigorously test the efficiency of the EAM method. This selection is strategic and intended to assess the method's efficiency exhaustively. The equations representing the system's mass, damping, stiffness, and modal matrices are depicted in Eq. (4.2).

$$\mathrm{M} = m\left[\mathrm{I}_4\right],\quad \mathrm{C} = \begin{bmatrix} 2c_p & -c_p & 0 & 0 \\ -c_p & 2c_p+\gamma c_d & -\left(c_p+\gamma c_d\right) & 0 \\ 0 & -\left(c_p+\gamma c_d\right) & 2c_p+\gamma c_d & -c_p \\ 0 & 0 & -c_p & c_p \end{bmatrix},$$
$$\mathrm{K} = \begin{bmatrix} 2k & -k & 0 & 0 \\ -k & k\left(2-\gamma\right) & -k\left(1-\gamma\right) & 0 \\ 0 & -k\left(1-\gamma\right) & k\left(2-\gamma\right) & -k \\ 0 & 0 & -k & k \end{bmatrix},\ \Phi = \begin{bmatrix} -0.1852 & -0.5659 & -0.4239 & -0.6824 \\ 0.3516 & 0.6999 & 0.1004 & 0.6135 \\ 0.6135 & 0.1004 & 0.6999 & -0.3516 \\ 0.6824 & 0.4239 & -0.5659 & 0.1852 \end{bmatrix} \tag{4.2}$$

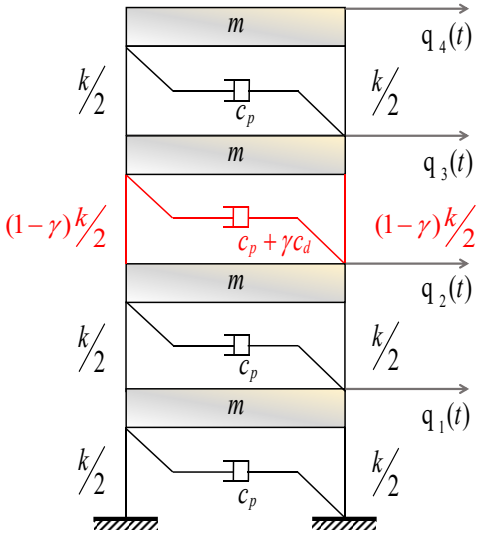

Figure 4.8 The 4-DOF non-classically damped system [92]

4.2.2.1. The complex eigenvalues for result the 4-DOF system

Table 4.4 reveals the superior performance of the EAM in estimating both the real and imaginary components of complex eigenvalues against the AM when comparing the results to those obtained by the exact state space method. The AM records a significant absolute maximum error of 37.79228% in the real component of the complex eigenvalue for the third mode. Conversely, the EAM improves upon this with a notably lower maximum absolute error of 4.61415% in the complex eigenvalues' real component for the fourth mode, reducing maximum relative error by 33.1995%. This marked decrease in error underscores the EAM's improved effectiveness and precision in capturing the real components of complex eigenvalues, clearly outperforming the AM's capabilities.

Similarly, when evaluating the imaginary components, the AM demonstrates a maximum error of 0.61563% in the third mode's complex eigenvalue compared to the exact state space calculation. The EAM further refines this accuracy, presenting a reduced maximum error of 0.24124% in the same mode, which translates to a decrease in absolute error of 0.37439%. This comparative analysis highlights the EAM's adeptness at more accurately estimating the imaginary parts of complex eigenvalues relative to the AM.

Therefore, the comprehensive evaluation of complex eigenvalues' real and imaginary parts distinctly showcases the EAM's advancement and its superior accuracy over the AM concerning the exact state space method.

The findings from Table 4.4 indicate that the dynamic system exhibits instability, characterised by a distinct positive real part in its complex eigenvalues. For further details on the stability aspects of dynamical systems, references [105, 106] offer comprehensive insights. These sources delve into the criteria and methodologies for assessing the stability of dynamic systems.

Table 4.4 The complex eigenvalues for the 4-DOf system

Mode	Eigenvalues					
	Undamped	Exact	Adhikari		Extended Adhikari	
j	ω(rad/sec)	λ(rad/sec)	λ(rad/sec)	ε_λ (%)	λ(rad/sec)	ε_λ (%)
1	13.48557	0.22947+13.53983i	0.23330+13.54028i	1.66873+0.00338i	0.22943+13.54014i	0.01967+0.00231i
2	37.06396	3.67672+37.49236i	3.69656+37.47522i	0.53953+0.04571i	3.67795+37.49145i	0.03328+0.00242i
3	63.45284	1.34933+64.65697i	0.83939+64.25892i	37.79228+0.61563i	1.37710+64.50099i	2.05782+0.24124i
4	72.23669	4.72445+69.28131i	5.47639+69.55212i	15.91592+0.39089i	4.94245+69.13026i	4.61415+0.21803i

Figure 10 shows the placement of the approximated complex eigenvalues using both approximation methods in comparison to the exact results.

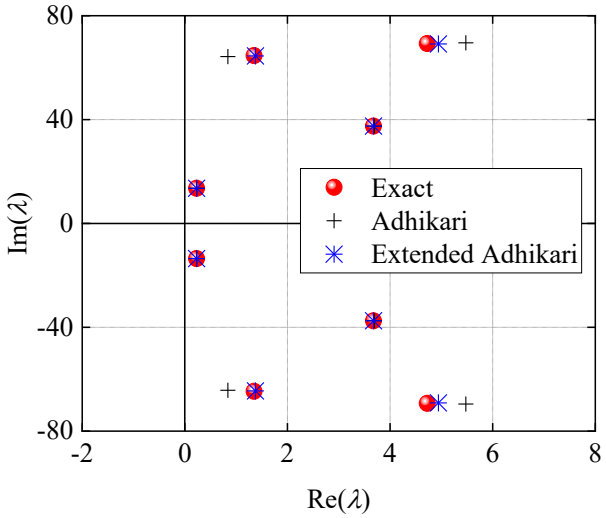

Figure 4.9 Representation of the conjugated complex eigenvalues in Gauss plane for the 4-DOF system

4.2.2.2. The damped eigenvalues result for the 4-DOF system

Table 4.5 presents the result of the damped eigenvalues for the studied 4-DOF system and compares the results obtained through the exact method with those approximated by the AM and EAM. In Mode 1, the eigenvalue obtained by AM is very close to the exact value, with an error of only 0.0037%, and the EAM is even more precise, reducing the error to 0.0022%. Hence, this demonstrates a high level of accuracy in the eigenvalue approximation for the first mode for both methods, with the EAM showing a slight improvement.

For Mode 2, the AM shows a slightly larger error of 0.0401%, indicating a small deviation from the exact value. However, the EAM greatly improves on this with an error of only 0.0021%, which is almost negligible and suggests that the EAM is particularly effective for this mode.

Mode 3 reveals a notable discrepancy in the AM's approximation, with a more significant error of 0.6287%. The EAM, while still showing an error, reduces it considerably to 0.2401%. Hence, this suggests that the EAM offers a substantial improvement over the AM in approximating the damped eigenvalues for this mode, although there is room for further accuracy enhancements.

In Mode 4, the AM's error is 0.4683%, which is less than that in Mode 3 but still significant. The EAM reduces this error to 0.1951%, demonstrating better accuracy than the AM but not as precise as in the previous modes.

Overall, the EAM consistently offers more accurate approximations of the damped eigenvalues across all modes when compared to the AM. The reduced percentage errors in the EAM results reflect its enhanced ability to closely match the exact damped eigenvalues of the system closely, thus affirming its utility in dynamic analysis of systems where precise eigenvalue calculation is critical for assessing stability and response characteristics.

Table 4.5 The damped eigenvalues for the 4-DOF system

Mode	Damped eigenvalues				
	Exact	Adhikari		Extended Adhikari	
j	ω_d (rad/sec)	ω_d (rad/sec)	ε_{ω_d} (%)	ω_d (rad/sec)	ε_{ω_d} (%)
1	13.5418	13.5423	0.0037	13.5421	0.0022
2	37.6722	37.6571	0.0401	37.6714	0.0021
3	64.6710	64.2644	0.6287	64.5157	0.2401
4	69.4422	69.7674	0.4683	69.3067	0.1951

4.2.2.3. The damping ratios result for the 4-DOF system

Figure 4.10 shows that the AM has a high peak relative error in estimating damping ratios, especially in the third mode, with an error of 59.7619%. On the other hand, the EAM significantly reduces this error to just 4.6194% in the fourth mode, demonstrating its superior accuracy and making it a more reliable choice for calculating damping ratios.

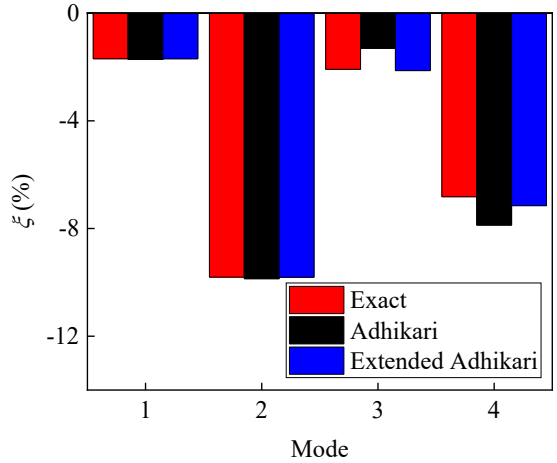

Figure 4.10 A comparison in the damping ratios for the 4-DOF system

It is important to mention that in figure 4.10, all modes of the dynamical system are undamped and have negative signals due to their instability.

4.2.2.4. The damping quality factor result for the 4-DOF system

The data in Table 4.6 compares the damping quality factors for a 4-DOF system using two methods against the exact values. The AM shows a significant error in the third mode, with a 59.7619% deviation from the exact calculation. Hence, this indicates that the AM may not provide reliable results for practical applications for this mode.

On the other hand, the EAM greatly improves the accuracy across all modes, with the highest error reduced to 4.6194% in the fourth mode. Hence, this is a substantial improvement and suggests that the EAM is considerably more precise, with the maximum error being more than 55% lower than that of the standard AM.

The results reflect that the EAM is a more accurate and reliable tool for calculating the damping quality factors of non-classically damped systems compared to the AM.

Table 4.6 The quality factor results for the 4-DOF system

Mode	Damping quality factor				
	Exact	Adhikari		Extended Adhikari	
j	Q(-)	Q(-)	ε_Q (%)	Q(-)	ε_Q (%)
1	-29.5021	-29.0189	1.6378	-29.5086	0.0220
2	-5.0986	-5.0689	0.5825	-5.0968	0.0353
3	-23.9589	-38.2772	59.7619	-23.4192	2.2526
4	-7.3322	-6.3502	13.3930	-6.9935	4.6194

4.2.2.5. Verifying the convergence of the Adhikari method for the 4-DOF system

Figure 4.11 displays the number of iterations needed for each mode to achieve convergence of the complex eigensolutions found using both AM and EAM, with an error tolerance of $\epsilon_{Tol.} = 10^{-6}$. Note, the both approaches can only handle iterations up to 9, as seen in the Figure 4.11.

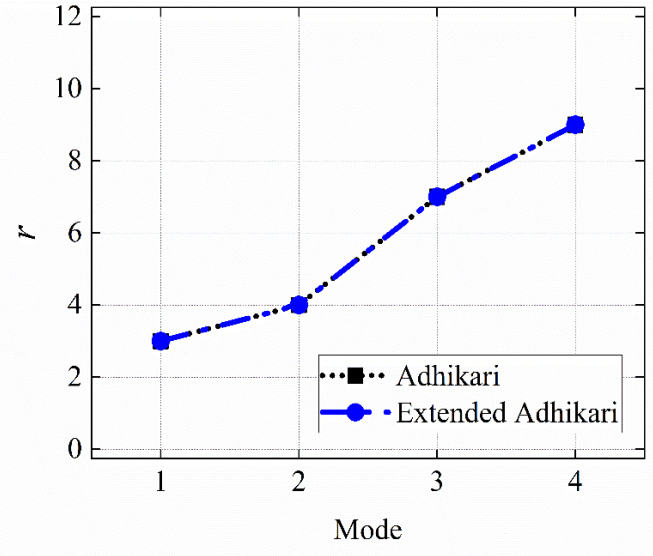

Figure 4.11 Convergence of Adhikari iterative method for the 4-DOF system

4.2.2.6. Confirming the modal decoupling with MAC Analysis for the 4-DOF System

Figure 4.12 displays the MAC matrix that quantifies the correlation between the approximated and exact complex eigenvectors, as determined by the Adhikari method, and the exact state-space eigenvectors for a given system. The MAC values range from 0 to 1, with 1 indicating perfect correlation.

The matrix shows high MAC values along the diagonal, suggesting that the modes are well-decoupled and the approximated eigenvectors closely correlate with the exact eigenvectors for each corresponding mode.

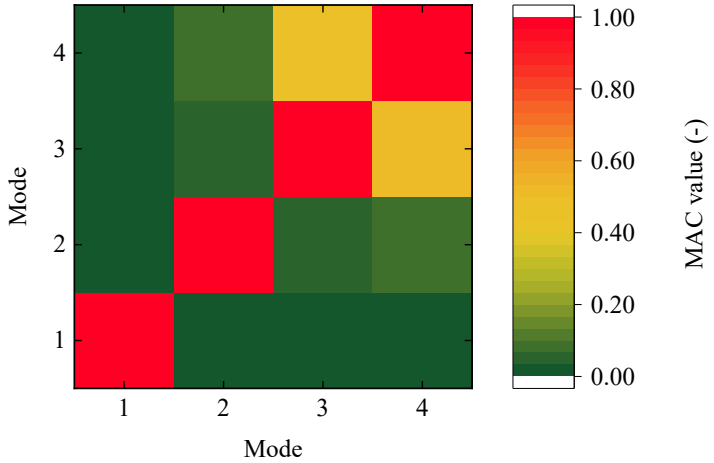

Figure 4.12 Modal Assurance Criterion (MAC) between Adhikari and exact complex eigenvectors for the 4-DOF system

4.2.2.7. Assessing the conformity of the predicted complex eigenvalues with their corresponding eigenvectors for the 4-DOF System

Figure 4.13 appears to represent three residual matrices for the 4-DOF system using Eq. (2.53), corresponding to different methods of eigenvalue and eigenvector calculation:

In subfigure (a), This matrix likely corresponds to the residuals obtained using the exact state-space eigensolutions. The uniform blue colouration suggests that all off-diagonal residuals are negligible or zero, indicating a perfect match between each complex eigenvalue and its corresponding eigenvector.

In subfigure (b), The second matrix, with varying colours, illustrates the residuals using the Adhikari method's eigensolutions. Colours other than blue, especially red and yellow, indicate higher residual values. Hence, this means that while the AM approximates the correct eigenpairs, there is a notable deviation from the exact solutions along the diagonal and off-diagonal elements.

In subfigure (c), The third matrix shows the residuals using the EAM for eigensolutions. The colour variation here is less extreme than in matrix (b), with more blues and greens, suggesting lower residual values than the Adhikari method. The diagonal of this matrix shows perfect zeros. However, the finding indicated a better approximation than the standard Adhikari method.

Overall, these residual matrices visually demonstrate the accuracy of each method in pairing eigenvalues with eigenvectors. The EAM exhibits improved accuracy over the AM but still shows some degree of error when compared to the exact state-space solutions. The colour scale on the right references the residual values, with the blue end representing lower errors and the red end representing higher errors.

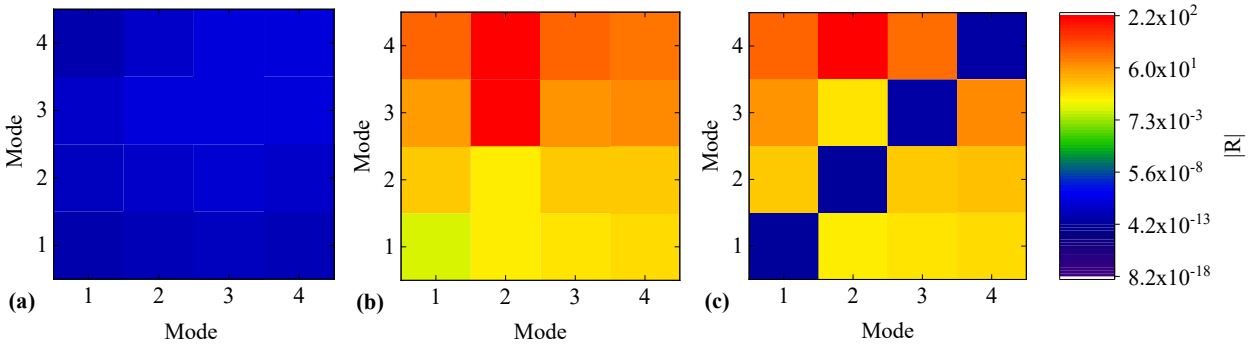

Figure 4.13 Representing the residual matrix for the 4-DOF system: a) represent the residual of using the exact complex eigensolutions, b) represent the residual of using the Adhikari complex eigensolutions, and c) represent the residual using the extended complex eigenvalues and Adhikari complex eigenvectors

4.2.2.8. The FRF analysis of the 4-DOF system

Figure 4.14 showcases the Frequency Response Function (FRF) for two different response points, $H_{4,4}$ on the left and $H_{4,1}$ on the right, comparing the exact state-space method against the Adhikari method and the Extended Adhikari method.

In both sets of results, the AM and EAM are seen to follow the exact FRF closely. The amplitude plots at the top of each side indicate that both approximation methods effectively capture the peak responses, with the EAM displaying a slightly tighter fit to the exact solution, particularly noticeable in the $H_{4,4}$ plot.

The phase plots, shown in the middle of each side, further confirm the accuracy of both methods, with phase angles being nearly indistinguishable from the exact solution. Again, the EAM shows an improved alignment, suggesting a more accurate phase approximation.

The bottom plots represent the coherence function $A_{mplitude}$, which measures the degree to which the approximate methods deviate from the exact FRF. A value of 0 dB across all frequencies would indicate perfect coherence. Here, the EAM generally maintains a closer coherence to the exact solution, especially in the lower frequency ranges, indicating a more consistent and accurate approximation.

Overall, the EAM shows a modest yet consistent improvement over the standard AM across the amplitude, phase, and coherence metrics. This improved performance implies that the EAM is more reliable for predicting the dynamic behaviour of non-classically damped systems.

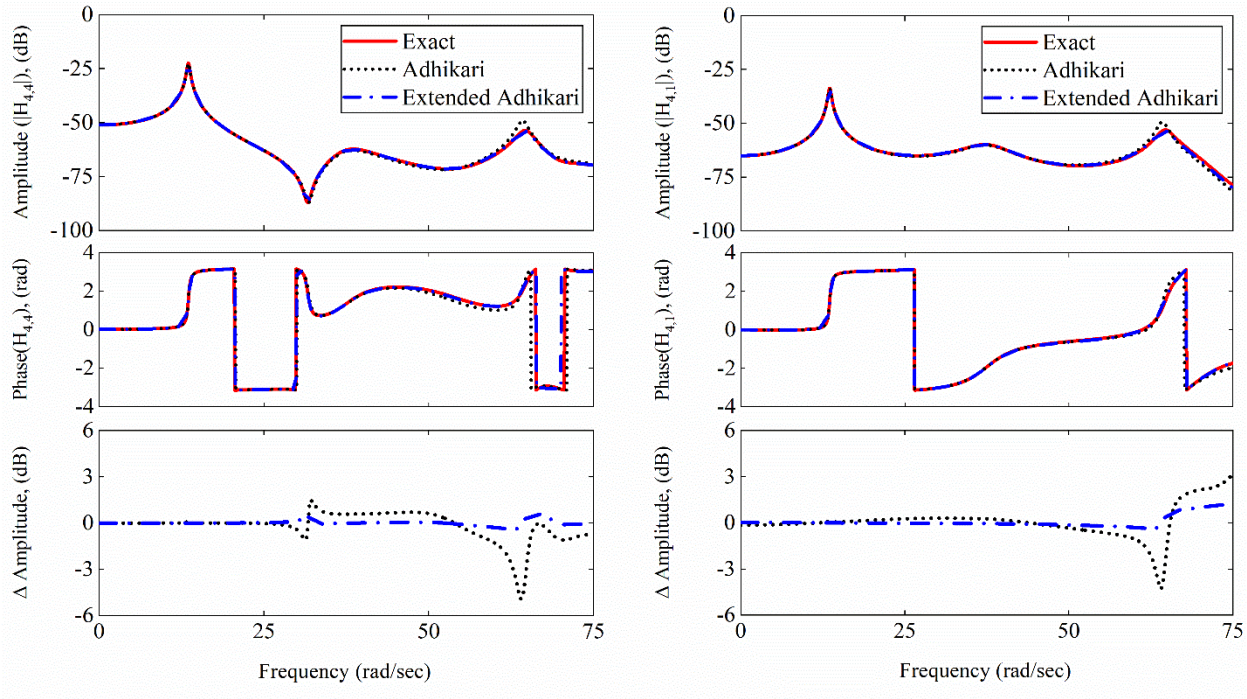

Figure 4.14 A comparison in the FRF responses for the 4-DOF system: $H_{4,4}$ in left, and for $H_{4,1}$ In the right

4.2.3. Six-degrees-of-freedom non-classically damped system

In this study, calculations were conducted on a system with six degrees of freedom, as illustrated in Figure 4.15 and referenced in [79, 86]. This system features six masses, each with a mass of $m = 10,000\,\text{kg}$, linked by springs that have a stiffness coefficient of $k = 100,000\,\text{N/m}$. It also includes two viscous dashpot dampers, each with a damping coefficient set as $c_1 = c_2 = 2m\omega_0\xi$. The reference frequency, ω_0 is determined by the square root of the stiffness-to-mass ratio, calculated as $(\omega_0 = \sqrt{k/m} = 10\,\text{rad/sec})$. The system's mass matrix is denoted by $\mathrm{M} = m[\mathrm{I}_6]$, and its damping, stiffness, and modal matrices are described in Eq. (4.3).

$$\mathrm{C}=\begin{bmatrix} 0 & 0 & 0 & 0 & 0 & 0 \\ 0 & c_2 & 0 & 0 & 0 & 0 \\ 0 & 0 & 0 & 0 & 0 & 0 \\ 0 & 0 & 0 & c_1 & -c_1 & 0 \\ 0 & 0 & 0 & -c_1 & c_1 & 0 \\ 0 & 0 & 0 & 0 & 0 & 0 \end{bmatrix}, \quad \mathrm{K}=k\begin{bmatrix} 2 & -1 & 0 & 0 & 0 & 0 \\ -1 & 2 & -1 & 0 & 0 & 0 \\ 0 & -1 & 2 & -1 & 0 & 0 \\ 0 & 0 & -1 & 2 & -1 & 0 \\ 0 & 0 & 0 & -1 & 2 & -1 \\ 0 & 0 & 0 & 0 & -1 & 2 \end{bmatrix},$$

$$\Phi=\begin{bmatrix} 0.2319 & -0.4179 & -0.5211 & 0.5211 & 0.4179 & 0.2319 \\ 0.4179 & -0.5211 & -0.2319 & -0.2319 & -0.5211 & -0.4179 \\ 0.5211 & -0.2319 & 0.4179 & -0.4179 & 0.2319 & 0.5211 \\ 0.5211 & 0.2319 & 0.4179 & 0.4179 & 0.2319 & -0.5211 \\ 0.4179 & 0.5211 & -0.2319 & 0.2319 & -0.5211 & 0.4179 \\ 0.2319 & 0.4179 & -0.5211 & -0.5211 & 0.4179 & -0.2319 \end{bmatrix} \tag{4.3}$$

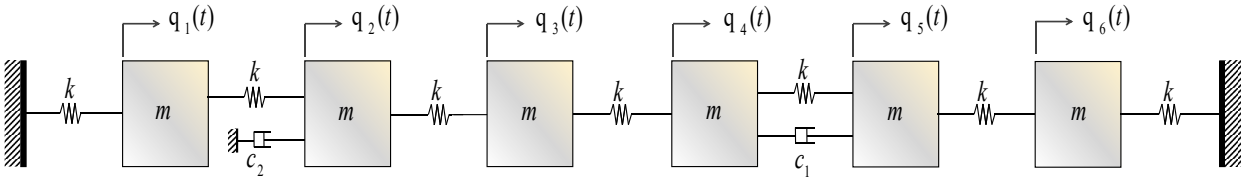

Figure 4.15 The studied 6-DOF lumped-mass dynamical system with viscous dampers [86]

4.2.3.1. The complex eigenvalues for result the 6-DOF system

Table 4.7 assesses two distinct methods for estimating complex eigenvalues under different damping scenarios, focusing on the AM and the EAM. For the lightly damped case (LD), the data indicates that the AM yields a maximum relative error of 0.08010% in the real part of the eigenvalues and an even smaller error of 0.0001% in the imaginary part. In comparison, the EAM demonstrates a remarkable improvement in precision, with a maximum relative error of just 0.00005% in the real part and 0.00001% in the imaginary part, showcasing its exceptional accuracy for lightly damped systems.

An obvious contrast in performance is observed for the highly damped case (HD). The AM method's relative error increases considerably, with the real part of the eigenvalues showing a maximum relative error of 13.94354% and the imaginary part exhibiting an error of 0.18050%. These figures suggest that the AM's effectiveness decreases with increased damping.

Conversely, the EAM's performance under high damping conditions demonstrates its robustness, achieving a maximum relative error of 4.23511% in the real part and 0.14024% in the imaginary part of the eigenvalues. While the errors are larger than those in the lightly damped case, they are significantly lower than those in the AM. Hence, this indicates that the EAM is more adept at handling the complexities introduced by higher damping.

Table 4.7 shows the EAM's superior performance over the AM in both lightly and highly damped cases. This consistency in precision across varying levels of damping suggests that the EAM is a more reliable method for estimating complex eigenvalues. For engineers and practitioners in fields where accurate eigenvalue estimation is crucial, the EAM offers a significant advantage, potentially leading to better-informed decisions in the design and analysis of dynamic systems. The representation of the conjugated complex eigenvalues in the Gauss plane for the 6-DOF system is shown in Figure 4.16, which presents the comparison between the exact outcomes and the arrangement of the approximated complex eigenvalues acquired by both approximation methods in two cases: (a) for the lightly damped case and (b) for the highly damped case.

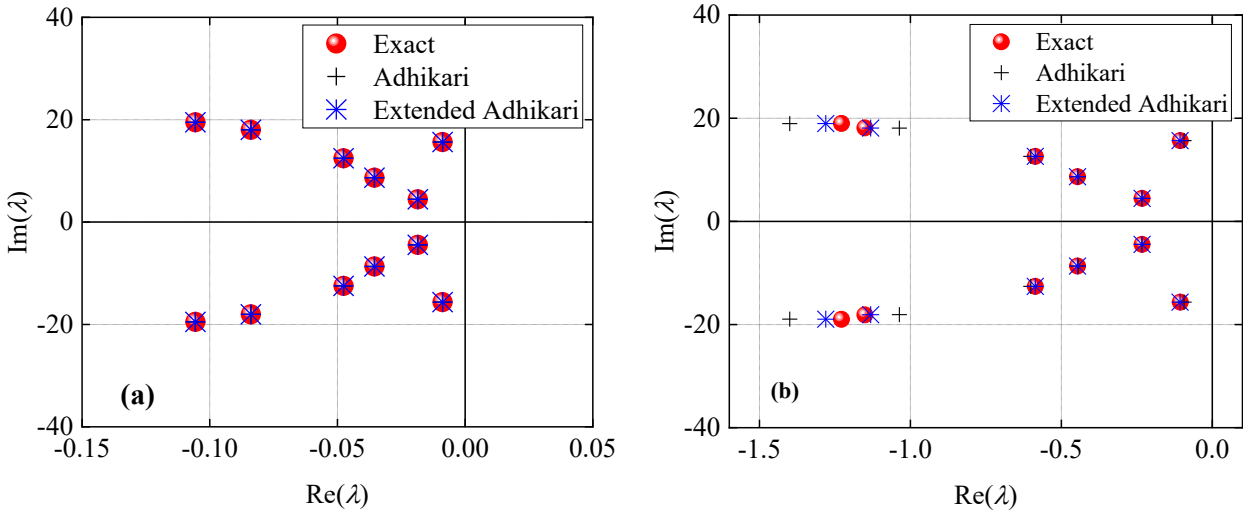

Figure 4.16 Representation of the conjugated complex eigenvalues in Gauss plane for the 6-DOF system: a) for lightly damped case, and b) for highly damped case

Table 4.7 The complex eigenvalues for the 6-DOF system

Mode	Eigenvalues					
	Undamped	Exact[86]	Adhikari		Extended Adhikari	
j	ω(rad/sec)	λ(rad/sec)	λ(rad/sec)	ε_λ (%)	λ(rad/sec)	ε_λ (%)
LD						
1	4.45042	-0.01853+4.45051i	-0.01853+ 4.45051i	0.00140+0.00000i	-0.01853+ 4.45051i	0.00000+0.00000i
2	8.67767	-0.03552+8.67756i	-0.03552+ 8.67756i	0.00302+0.00000i	-0.03552+ 8.67756i	0.00000+0.00000i
3	12.46980	-0.04760+12.47062i	-0.04761+12.47062i	0.01441+0.00000i	-0.04760+12.47062i	0.00000+0.00000i
4	15.63663	-0.00884+15.63678i	-0.00883+15.63678i	0.08010+0.00000i	-0.00884+15.63678i	0.00005+0.00000i
5	18.01938	-0.08390+18.01961i	-0.08386+18.01961i	0.04433+0.00001i	-0.08390+18.01961i	0.00002+0.00000i
6	19.49856	-0.10561+19.49573i	-0.10565+19.49573i	0.03623+0.00000i	-0.10561+19.49573i	0.00000+0.00001i
HD						
1	4.45042	-0.23254+4.46417i	-0.23306+ 4.46414i	0.22346+0.00058i	-0.23254+ 4.46419i	0.00078+0.00055i
2	8.67767	-0.44641+8.65975i	-0.44427+ 8.66010i	0.47828+0.00411i	-0.44639+ 8.66002i	0.00279+0.00312i
3	12.46980	-0.58619+12.60314i	-0.60128+12.60353i	2.57378+0.00309i	-0.58626+12.60474i	0.01192+0.01266i
4	15.63663	-0.10576+15.66004i	-0.09336+15.65650i	11.72023+0.02258i	-0.10685+15.65739i	1.03256+0.01693i
5	18.01938	-1.15068+18.12225i	-1.03665+18.07636i	9.90985+0.25326i	-1.13168+18.09684i	1.65116+0.14024i
6	19.49856	-1.22843+18.98432i	-1.39972+18.95005i	13.94354+0.18050i	-1.28046+18.96227i	4.23511+0.11614i

4.2.3.2. The damped eigenvalues result for the 6-DOF system

Table 4.8 showcases the calculated damped eigenvalues for systems with varying damping conditions, specifically light damping (LD) and high damping (HD) cases. The table compares the exact eigenvalues against those estimated using the Adhikari and Extended Adhikari methods and the relative error percentages for a more detailed analysis.

In the LD scenario, it is evident from the table that both the AM and the EAM perform exceptionally well, as they both exhibit a perfect relative error of 0%. Hence, this implies that both methods can estimate the damped eigenvalues with remarkable precision for lightly damped systems, mirroring the exact values with no discernible deviation.

Upon examining the LD case, there is a noticeable difference in performance between the two methods. The AM method's accuracy slightly diminishes, with the relative error for the damped eigenvalues reaching a maximum of 0.2901%. On the other hand, the EAM maintains a higher accuracy level, as indicated by a lower maximum relative error of 0.1462%. While both methods exhibit errors, the EAM's lower relative errors underscore its improved accuracy in estimating the damped eigenvalues under conditions of higher damping.

Overall, Table 4.8 provides clear insights into the comparative accuracy of the Adhikari and Extended Adhikari methods under different damping conditions. While both methods yield impeccable results in the LD case, the EAM's superior performance in the highly damped scenario suggests its more reliable applicability when damping effects are more pronounced. The data suggests that the Extended Adhikari method may be more suitable for practical applications requiring precision in dynamic systems analysis, especially those with significant damping.

Table 4.8 The damped eigenvalues for the 6-DOF system

Mode	Damped eigenvalues				
	Exact	Adhikari		Extended Adhikari	
j	ω_d (rad/sec)	ω_d (rad/sec)	ε_{ω_d} (%)	ω_d (rad/sec)	ε_{ω_d} (%)
LD					
1	4.4506	4.4506	0.0000	4.4506	0.0000
2	8.6776	8.6776	0.0000	8.6776	0.0000
3	12.4707	12.4707	0.0000	12.4707	0.0000
4	15.6368	15.6368	0.0000	15.6368	0.0000
5	18.0198	18.0198	0.0000	18.0198	0.0000
6	19.4960	19.4960	0.0000	19.4960	0.0000
HD					
1	4.4702	4.4702	0.0000	4.4702	0.0004
2	8.6713	8.6715	0.0028	8.6715	0.0031
3	12.6168	12.6179	0.0087	12.6184	0.0128
4	15.6604	15.6568	0.0231	15.6578	0.0169
5	18.1587	18.1061	0.2901	18.1322	0.1462
6	19.0240	19.0017	0.1175	19.0055	0.0976

4.2.3.3. The damping ratios result for the 6-DOF system

Damping ratios are displayed in Figure 4.17. Both AM and EAM produce reliable outcomes that match the exact values in the scenario with low damping. On the other hand, when it comes to the highly damped circumstance, AM shows a peak relative error of 12.3966% in the sixth mode, but EAM shows a maximum relative error of 4.1749% in the same mode. The remarkable accuracy of EAM's damping ratio calculations further proves its dependability.

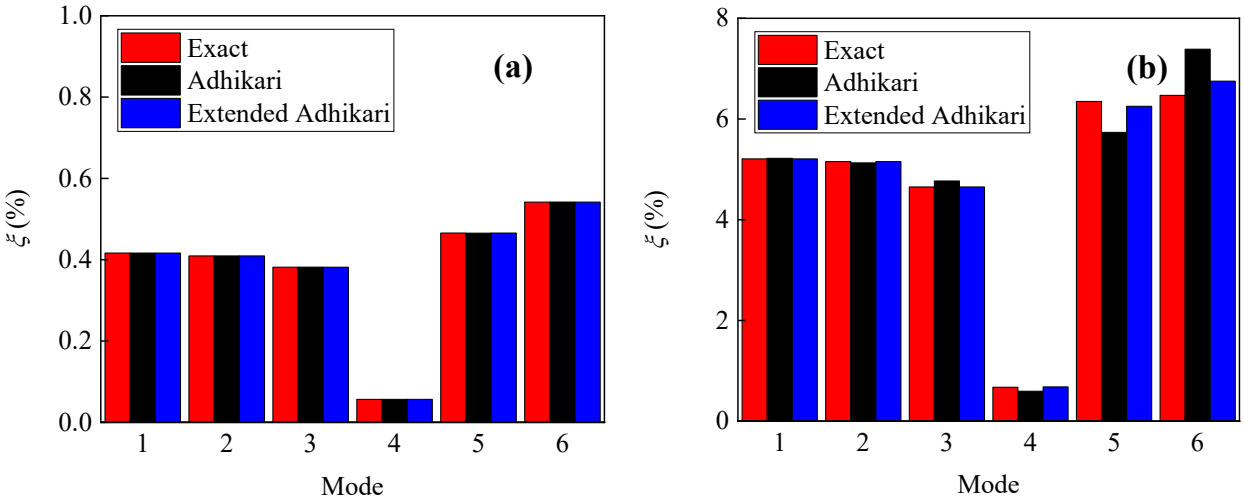

Figure 4.17 A comparison in the damping ratios for the 6-DOF system: a) for lightly damped case, and b) for highly damped case

4.2.3.4. The damping quality factor result for the 6-DOF system

Table 4.9 delineates the damping quality factors for the 6-DOF system, presenting exact values alongside those computed via the AM and the EAM. The table provides a clear representation of each mode, facilitating the comparison of the precision of these two methods under different damping conditions.

In the case of LD, the table indicates that both the AM and EAM methods align perfectly with the exact solutions, boasting a relative error of around 0%. Hence, both methods are highly effective for systems experiencing light damping and deliver exceptionally accurate results for the damping quality factor, a crucial parameter in analysing vibrational characteristics.

Conversely, the HD case reveals a disparity in the performance of the two methods. The AM method shows a maximum relative error of 12.3966%, indicating a notable deviation from the exact values as the damping increases. In contrast, the EAM method significantly reduces the relative error, with a maximum of 4.1749%. This reduced error margin in the EAM method underlines its enhanced capability to approximate the damping quality factor more accurately in systems subject to higher levels of damping.

Overall, Table 4.9 suggests that while the AM and EAM methods provide equally precise results in lightly damped systems, the EAM method is more accurate for highly damped systems. For engineering applications that require accurate damping assessments, especially in conditions of high damping, the Extended Adhikari method emerges as the more reliable computational approach, ensuring that the damping quality factors are estimated with a closer adherence to the exact values.

Table 4.9 The outcomes of damping quality factor for the 6-DOF system

Mode	Damping quality factor				
	Exact	Adhikari		Extended Adhikari	
j	Q(-)	Q(-)	ε_Q (%)	Q(-)	ε_Q (%)
LD					
1	120.0893	120.0893	0.0000	120.0893	0.0000
2	122.1503	122.1503	0.0000	122.1503	0.0000
3	130.9939	130.9664	0.0210	130.9939	0.0000
4	884.4333	885.4349	0.1132	884.4333	0.0000
5	107.3874	107.4386	0.0477	107.3874	0.0000
6	92.3006	92.2656	0.0379	92.3006	0.0000
HD					
1	9.5987	9.5772	0.2240	9.5988	0.0010
2	9.6993	9.7464	0.4856	9.7001	0.0082
3	10.7500	10.4806	2.5060	10.7501	0.0009
4	74.0357	83.8501	13.2563	73.2681	1.0368
5	7.8746	8.7186	10.7180	7.9956	1.5366
6	7.7271	6.7692	12.3966	7.4045	4.1749

4.2.3.5. Verifying the convergence of the Adhikari method for the 6-DOF system

With an error tolerance $\epsilon_{Tol.} = 10^{-6}$, Figure 4.18 displays the number of iterations needed for each mode to converge the complex eigensolutions for both AM and the EAM. Both approaches can handle cases with a maximum of 2 iterations for the LD case and 11 for the HD case, as shown in the figure.

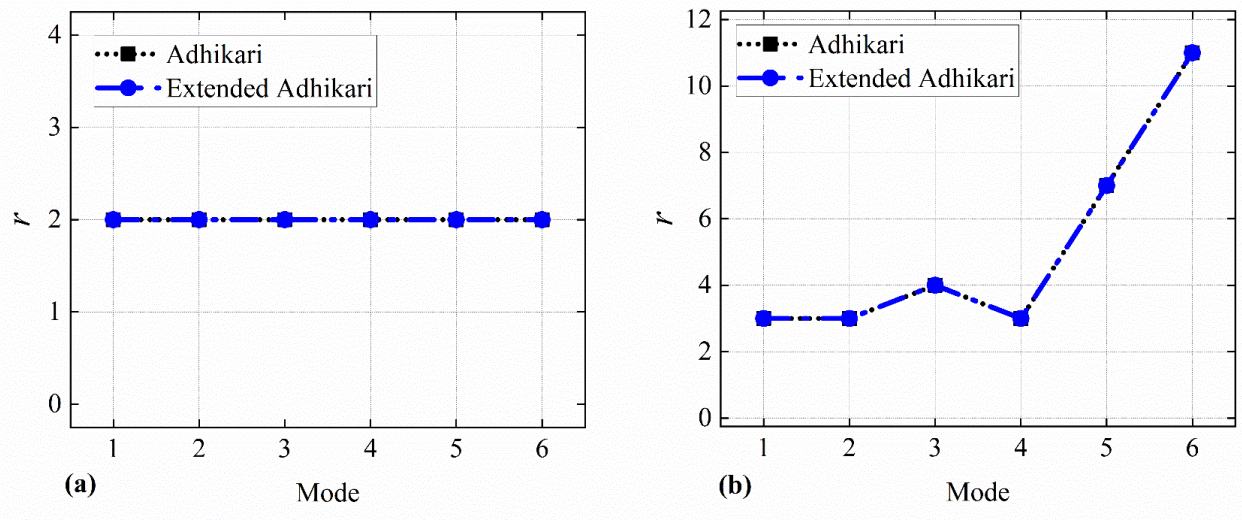

Figure 4.18 Convergence of Adhikari iterative method for the 6-DOF system: a) for lightly damped case, and b) for highly damped case

4.2.3.6. Confirming the modal decoupling with MAC Analysis for the 6-DOF System

Figure 4.19 shows the Modal Assurance Criterion (MAC) results between the approximated Adhikari and the exact state-space complex eigenvectors. The results show full decoupled modes as the diagonal of the map in the figure are so near to the value of one. Note that the approximated complex eigenvectors are the same for both AM and EAM.

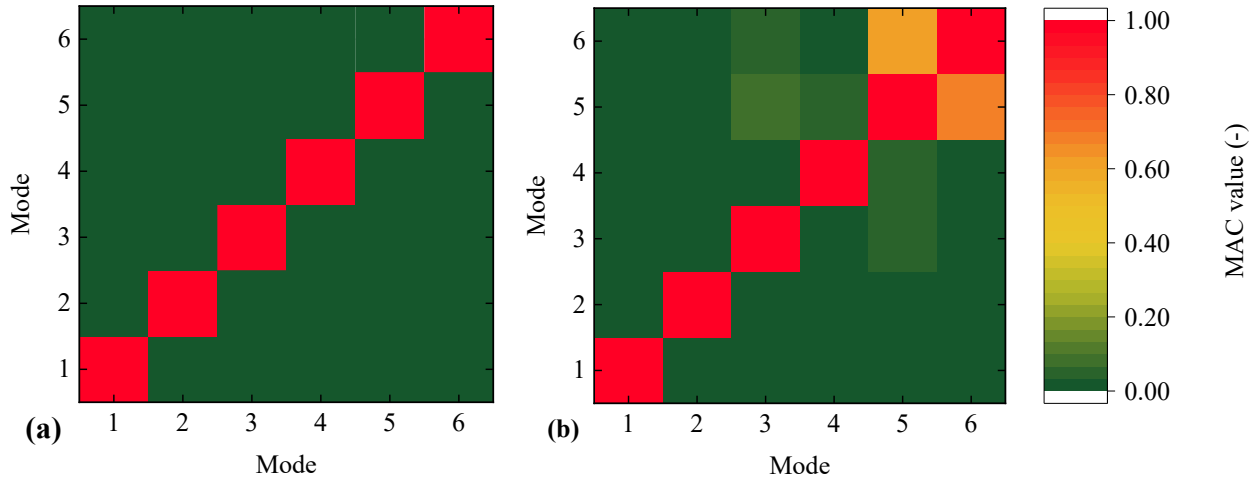

Figure 4.19 Modal Assurance Criterion (MAC) between Adhikari and exact complex eigenvectors for the 6-DOF system: a) for lightly damped case, and b) for highly damped case

4.2.3.7. Assessing the conformity of the predicted complex eigenvalues with their corresponding eigenvectors for the 6-DOF System

Figure 4.20 provides a graphical representation of the alignment between complex eigenvalues and their corresponding eigenvectors for a lightly damped case of the studied 6-DOF system. It is a key tool for verifying the accuracy of eigensolutions obtained from different approximation methods.

Subfigure (a) establishes the benchmark with a completely blue map, indicating the precision of the exact state-space complex eigensolutions with zero values. Hence, this demonstrates a perfect correspondence between eigenvalues and eigenvectors, as expected from the exact mathematical model.

Subfigure (b) presents the results from the AM displays non-zero values along the diagonal and off-diagonal elements, although these values are small. Hence, this indicates that while the AM approximates the correspondence between the eigenvalues and eigenvectors, it does so with less accuracy, as evidenced by the non-zero elements within the matrix.

Subfigure (c), attributed to the EAM, shows a zero-diagonal map indicated by the blue colour, suggesting a near-perfect correspondence between each mode and its eigenvector, similar to the exact solution. The lack of significant colour variation, especially off-diagonal, indicates that the EAM is highly accurate in matching eigenvalues with the correct eigenvectors.

However, Figure 4.20, with the correct assignment of methods to subfigures, shows that the EAM provides an enhanced accuracy in identifying the correspondence between eigenvalues and eigenvectors compared to the AM. The EAM's ability to produce a zero-diagonal map suggests that it is more precise in capturing the dynamics of the lightly damped system. Thus, it is a more reliable method for applications where high adherence to modal analysis is crucial.

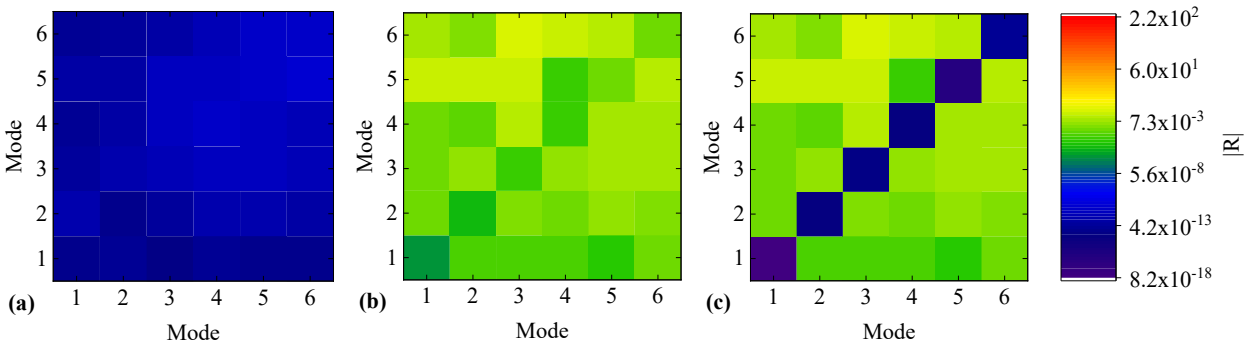

Figure 4.20 Representing the pole residual for the lightly damped case in the 6-DOF system: a) represent the residual of using the exact complex eigensolutions, b) represent the residual of using the Adhikari complex eigensolutions, and c) represent the residual using the extended complex eigenvalues and Adhikari complex eigenvectors.

Figure 4.21 presents a visualization for verifying the correspondence between complex eigenvalues and their associated eigenvectors in a highly damped 6-DOF system. The analysis is carried out using Eq. (2.53), designed to test state-space solutions' accuracy in matching eigenvalues to eigenvectors. This figure comprises three subfigures, each representing a different computational approach to solving the system: the exact method, the AM, and the EAM.

Subfigure (a) is the baseline representation, showing the results from the exact state-space solutions. In this subfigure, all elements in the matrix map are zeros, which signifies a perfect match between the complex eigenvalues and their corresponding eigenvectors. These zero matrices is the standard against which the other methods are compared, indicating the ideal outcome where each mode is precisely paired with its correct eigensolutions.

Subfigure (b) depicts the results obtained using the AM. Contrary to the exact solution, this method does not produce a matrix with zeros across all elements. Instead, small but non-zero values are scattered throughout the matrix, both along the diagonal and off-diagonal positions. Hence, this indicates a less-than-perfect correspondence between the modes and their eigensolutions, suggesting inaccuracies in the AM regarding precisely matching eigenvalues to their eigenvectors.

In subfigure (c), remarkably, the EAM produces a map with zeros along the diagonal, which implies that for each mode, the eigensolutions are correctly matched to the eigenvalues. The presence of non-zero elements is restricted to off-diagonal positions, which is a significant

improvement over the AM, indicating that the EAM has a higher fidelity in representing the true behaviour of the system.

The comparative analysis of the three methods, as presented in Figure 4.21, indicates that the EAM substantially improves matching eigenvalues to their respective eigenvectors over the AM, especially for the highly damped case of the 6-DOF system. While the AM presents a certain level of approximation, the EAM's performance is much closer to the exact solution, as evidenced by its zero-diagonal matrix map. Hence, this suggests that the Extended Adhikari method provides a more accurate and reliable approach for identifying the correct eigenvalue-eigenvector pairs in such complex systems, enhancing the precision of dynamic analyses.

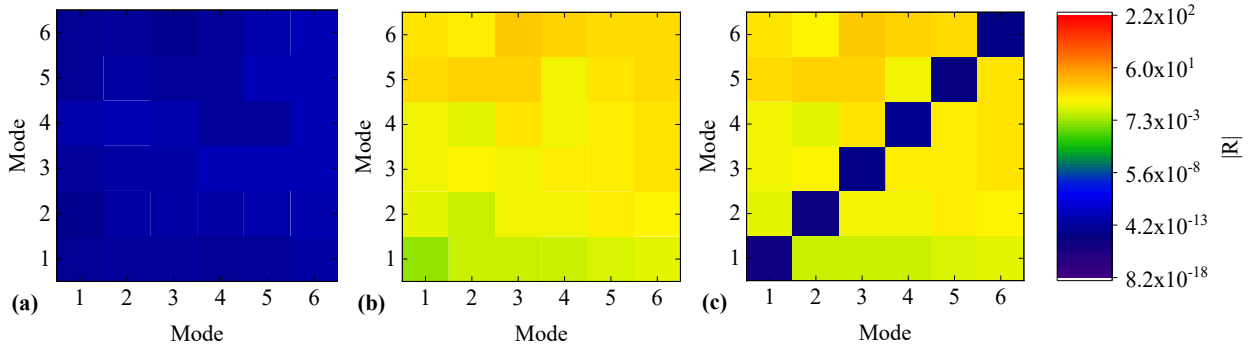

Figure 4.21 Pole residual for the highly damped case in the 6-DOF system: a) represent the residual of using the exact complex eigensolutions, b) represent the residual of using the Adhikari complex eigensolutions, and c) represent the residual using the extended complex eigenvalues and Adhikari complex eigenvectors

4.2.3.8. The FRF analysis of the 6-DOF system

Figure 4.22 is pivotal for understanding the FRF responses in the lightly damped case of the studied 6-DOF system. It showcases the amplitude and phase of the FRF at two distinct points: $H_{4,4}$ and $H_{4,1}$. These points represent the response at the fourth point due to excitation at the fourth and first points, respectively. By comparing the results from two methodologies, AM and the EAM, against the exact solutions, the figure provides insights into the accuracy of these approximation methods for analysing vibrational characteristics in engineering systems. The left side of Figure 4.22, the $H_{4,4}$ results are depicted. The red line, representing the exact FRF responses, is a benchmark for accuracy. The dotted line for AM and the dashed line for EAM

overlay closely with the exact solution, indicating high precision in capturing the system's dynamics. Hence, both methods are robust in estimating the FRF at this point of the system.

The right side of Figure 4.22 presents the $H_{4,1}$ result. Similar to the $H_{4,4}$ results, there is a remarkable correlation between the exact FRF and the results obtained from both AM and EAM. This consistency across different points of the system reaffirms the reliability of these methods in the context of lightly damped systems. Even with the overall accuracy, there is a noticeable difference in the error magnitude when comparing the two methods. The EAM, marked by the dashed line, demonstrates smaller discrepancies from the exact solution than the dotted line of AM. Hence, this suggests that the EAM has an edge in precision due to its refined approach to approximating the complex eigenvalues characteristic of non-classically damped systems.

The implications of the findings in Figure 4.22 are significant for the field of structural dynamics and vibration analysis. The EAM's superior performance in error minimisation points towards its potential for more accurate predictive modelling in engineering applications. The data suggest that EAM could provide a more reliable method for engineers dealing with complex vibrational analysis, particularly in systems where a precise understanding of the damping effects is crucial. Overall, the figure is evidence of the advancements in computational methods for dynamical systems and their practical applications in engineering design and analysis.

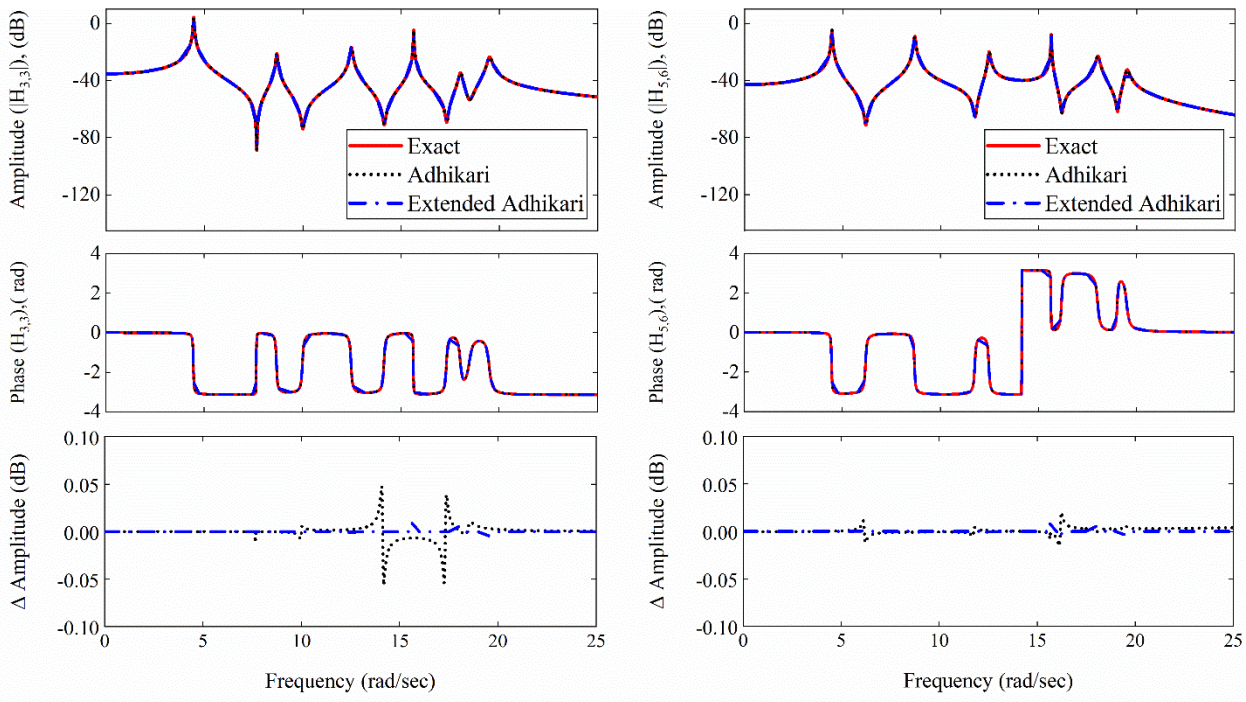

Figure 4.22 A comparison in the FRF responses for the lightly case in the 6-DOF system: $\mathbf{H_{3,3}}$ in left, and for $\mathbf{H_{5,6}}$ In the right

For the highly damped case of the 6-DOF example, Figure 4.23 provides a comparative illustration of the FRF responses. It delineates the accuracy of two approximation methods against the exact solutions. On the left, the $H_{3,3}$ results are represented, showcasing the response at a particular point and direction in the system. Similarly, the right side elucidates the $H_{5,6}$ results, indicative of a response that may represent a different point or direction, perhaps coupling effects between different vibration modes.

The top subplots of each side detail the amplitude responses over a frequency spectrum. These plots reveal that both methods are in close agreement with the exact solution, with the EAM showing consistently tighter conformance across the frequency range, suggesting its enhanced robustness in capturing the amplitude characteristics of the system's response.

Moving to the middle subplots, the phase angle responses are depicted, providing insights into the timing or delay of the system's response relative to the input across the frequency span. The methods continue to track closely with the exact solution, maintaining minimal phase

discrepancy, which is crucial for ensuring the dynamic fidelity of the system's behaviour in practical scenarios.

The bottom subplots are particularly telling, as they quantify the amplitude errors of the AM and EAM methods relative to the exact solution. The EAM's errors are notably smaller, especially at certain critical frequency points, implying a superior performance in approximating the actual system dynamics. This higher precision of the EAM is likely attributable to its refined computation of the complex eigenvalues, essential in representing the inherent damping characteristics of non-classically damped systems.

Comprehensive, Figure 4.23 underscores the effectiveness of the EAM in providing a closer match to the exact FRF, especially in the context of a highly damped case of the studied 6-DOF system. Hence, this suggests the potential for the EAM's application in more accurately modelling complex systems where non-classical damping plays a significant role, enhancing the predictive power of engineering analyses and simulations.

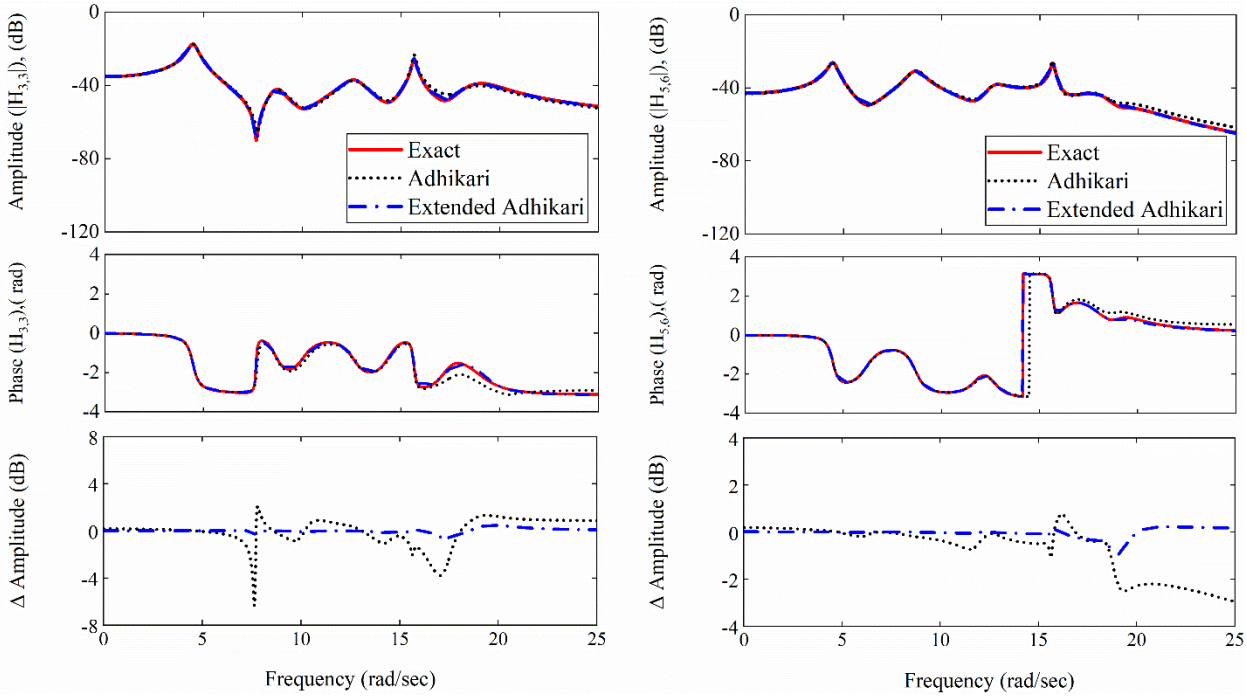

Figure 4.23 A comparison in the FRF responses for the highly damped case in the 6-DOF system: $\mathbf{H_{3,3}}$ in left, and for $\mathbf{H_{5,6}}$ In the right

4.3. Conclusion

The findings in this chapter demonstrate that our proposed extended version of the Adhikari method highlights the progress made in decoupling non-classically linear damping systems. Using the self-adjoint theorem and spectral localisation, this improvement makes the method more stable and accurate at finding complex eigenvalues. The method demonstrates its efficiency with steady convergence rates and yields complex eigenvectors similar to the original Adhikari method. It also presents a new technique for calculating Frequency Response Function (FRF), demonstrating its practical use in analysing dynamic systems. The effective implementation of these techniques on three non-classically damped system models showcases their significance and promise for future investigation and application in various scientific and technical fields.

GENERAL CONCLUSION

In conclusion, our research on decoupling linear non-classically damped systems has yielded significant advances, particularly with the introduction of our extended version of the Adhikari method. This enhanced method, incorporating the self-adjoint theorem and spectral localization, has demonstrated improved stability and accuracy in identifying complex eigenvalues for highly and indefinite damped structures. The study showcases its efficiency through steady convergence rates and the generation of complex eigenvectors similar to the original Adhikari method.

Moreover, the research introduces a novel subspace algorithm that amalgamates the strengths of the lightly non-classical damping method and Adhikari's method, addressing the limitations identified in traditional approaches. This algorithm proves to be a practical solution for enhancing the prediction and decoupling of complex eigensolutions in non-classically damped systems.

The findings of our research decorate the path towards understanding how to decouple non-classically damped systems. Our study was specifically focused on applying these decoupling techniques to linearly viscous damped systems. For these systems, the dominance of diagonal indices plays a crucial role in determining the most suitable decoupling method. The lightly non-classical damping method proves adequate for systems characterized by light and definite damping scenarios. Additionally, systems with high or indefinite damping present significant challenges and cannot be handled easily by unstable decoupling approximation techniques.

Looking forward, our future perspectives involve applying the extended version of the Adhikari method to address systems with non-linear and non-viscous damping. Additionally, we plan to implement the introduced algorithms for the time history analysis of these non-classically damped systems. These advances represent the significance and promise of our research for future investigations and applications in various scientific and technical fields.

REFERENCES

1. Suleiman, H., Afra H., Abdeddaim M., and Bouzerd H., *Exploring Decoupling Techniques For Linear Structures With Non-Classical Damping: A Numerical Study And Evaluation.* Periodico di Mineralogia, 2023. **92**(4): p. 1-25.
2. Suleiman, H., Afra H., Abdeddaim M., and Bouzerd H., *An extension to Adhikari iterative method: A novel approach for obtaining complex eigensolutions in linear non-classically damped systems.* Structures, 2024. **60**: p. 105832.
3. Bajad, M.N., *Analytical approach for damping model.* Asian Journal of Civil Engineering, 2023. **24**(1): p. 109-119.
4. Crandall, S.H., *The role of damping in vibration theory.* Journal of sound vibration, 1970. **11**(1): p. 3-IN1.
5. Jeary, A., *Damping in structures.* Journal of wind engineering industrial aerodynamics, 1997. **72**: p. 345-355.
6. Adhikari, S., *Structural dynamic analysis with generalized damping models: analysis*. 2013: John Wiley & Sons.
7. Adhikari, S., *Damping models for structural vibration*. 2001, University of Cambridge.
8. Baz, A.M., *Active and passive vibration damping*. 2019: John Wiley & Sons.
9. Prandina, M., *Spatial damping identification*. 2009: The University of Liverpool (United Kingdom).
10. Bajrić, A. and Høgsberg J., *Identification of damping and complex modes in structural vibrations.* Journal of Sound and Vibration, 2018. **431**: p. 367-389.
11. Lu, G. and Yu T., *Energy absorption of structures and materials*. 2003: Elsevier.
12. Stepinski, T., Uhl T., and Staszewski W., *Advanced structural damage detection: from theory to engineering applications.* 2013.
13. Hao, H., Bi K., Chen W., Pham T.M., and Li J., *Towards next generation design of sustainable, durable, multi-hazard resistant, resilient, and smart civil engineering structures.* J Engineering Structures, 2023. **277**: p. 115477.
14. Yenidogan, C., *Earthquake-resilient design of seismically isolated buildings: A review of technology.* J Vibration, 2021. **4**(3): p. 602-647.
15. Fu, B., Jiang H., and Wu T., *Comparative studies of vibration control effects between structures with particle dampers and tuned liquid dampers using substructure shake table testing methods.* J Soil Dynamics Earthquake Engineering, 2019. **121**: p. 421-435.
16. Saaed, T.E., Nikolakopoulos G., Jonasson J.-E., and Hedlund H., *A state-of-the-art review of structural control systems.* Journal of Vibration Control, 2015. **21**(5): p. 919-937.
17. Mrad, C., Titirla M.D., and Larbi W., *Comparison of strengthening solutions with optimized passive energy dissipation systems in symmetric buildings.* J Applied Sciences, 2021. **11**(21): p. 10103.
18. Edrees, T., *Structural control and identification of civil engineering structures*. 2015, Luleå tekniska universitet.
19. Xu, Z.-D., Guo Y.-Q., Zhu J.-T., and Xu F.-H., *Intelligent vibration control in civil engineering structures*. 2016: Academic Press.
20. Cheng, F.Y., Jiang H., and Lou K., *Smart structures: innovative systems for seismic response control*. 2008: CRC press.
21. Constantinou, M.C., Soong T.T., and Dargush G.F., *Passive energy dissipation systems for structural design and retrofit.* 1998.
22. Castaldo, P., *Integrated seismic design of structure and control systems*. 2014: Springer.
23. Kelly, J.M., Skinner R., and Heine A., *Mechanisms of energy absorption in special devices for use in earthquake resistant structures.* J Bulletin of the New Zealand Society for Earthquake Engineering, 1972. **5**(3): p. 63-88.

24. Alehashem, S.M.S., Keyhani A., and Pourmohammad H. *Behavior and performance of structures equipped with ADAS & TADAS dampers (a comparison with conventional structures)*. in *The 14th World Conference on Earthquake Engineering*. 2008.
25. Aguiar, R., Mora D., and Rodríguez M., *CEINCI-LAB. A free software to find the seismic capacity curve of frames with ADAS or TADAS dissipators.* J Revista Ingeniería de Construcción, 2016. **31**(1): p. 37-53.
26. Zhou, C. and Han J. *Study on the seismic performance of X-added damping and stiffness energy dissipation device*. in *15th world conference on earthquake engineering, Lisbon, Portugal*. 2012.
27. Zemp, R., Urrutia R.C., Rendel M., Cavalla G., and Llera Martin J.C.D.L. *Design, testing and implementation of TADAS devices in three RC buildings with shear walls and coupling beams*. in *World Conference on Earthquake Engineering (16th: 2017: Santiago, Chile)*. 2017.
28. Javanmardi, A., Ibrahim Z., Ghaedi K., Benisi Ghadim H., and Hanif M.U., *State-of-the-art review of metallic dampers: testing, development and implementation.* J Archives of Computational Methods in Engineering, 2020. **27**: p. 455-478.
29. Shu, Z., You R., and Zhou Y., *Viscoelastic materials for structural dampers: A review.* Construction and Building Materials, 2022. **342**: p. 127955.
30. Parulekar, Y., Reddy G., Vaze K., Guha S., Gupta C., Muthumani K., and Sreekala R., *Seismic response attenuation of structures using shape memory alloy dampers.* J Structural control health monitoring, 2012. **19**(1): p. 102-119.
31. Sadek, F., Mohraz B., Taylor A.W., and Chung R.M., *A method of estimating the parameters of tuned mass dampers for seismic applications.* Earthquake Engineering Structural Dynamics, 1997. **26**(6): p. 617-635.
32. Den Hartog and Pieter J., *Mechanical vibrations*. 1985: Courier Corporation.
33. Kwok, K. and Samali B., *Performance of tuned mass dampers under wind loads.* Engineering structures, 1995. **17**(9): p. 655-667.
34. Thenozhi, S. and Yu W., *Advances in modeling and vibration control of building structures.* Annual Reviews in Control, 2013. **37**(2): p. 346-364.
35. Konar, T. and Ghosh A., *A review on various configurations of the passive tuned liquid damper.* Journal of Vibration Control, 2023. **29**(9-10): p. 1945-1980.
36. Zafar, A. and Andrawes B., *Seismic behavior of SMA–FRP reinforced concrete frames under sequential seismic hazard.* J Engineering Structures, 2015. **98**: p. 163-173.
37. Hojatirad, A. and Naderpour H., *Seismic assessment of RC structures having shape memory alloys rebar and strengthened using CFRP sheets in terms of fragility curves.* J Bulletin of Earthquake Engineering, 2021. **19**: p. 5087-5112.
38. Gangil, N., Siddiquee A.N., and Maheshwari S., *Towards applications, processing and advancements in shape memory alloy and its composites.* Journal of Manufacturing Processes, 2020. **59**: p. 205-222.
39. Li, L., Hu Y., and Wang X., *STRUCTURAL MODAL REANALYSIS FOR NON-CLASSICALLY DAMPED SYSTEMS.*
40. Lei, X., Wu C., and Wu H., *A novel composite vibration control method using double-decked floating raft isolation system and particle damper.* Journal of Vibration Control, 2018. **24**(19): p. 4407-4418.
41. Yang, L., Gao W., Yang J., Zhao B., and Liu L., *A Novel Active Control Strategy with Decentralized Decoupling and Wavelet Packet Transformation: Design and Verification.* J Applied Sciences, 2021. **11**(8): p. 3554.
42. Sigdel, L.D., Al-Qarawi A., Leo C.J., Liyanapathirana S., and Hu P., *Geotechnical design practices and soil–structure interaction effects of an integral bridge system: A review.* Applied Sciences, 2021. **11**(15): p. 7131.

43. Tongaonkar, N. and Jangid R., *Seismic response of isolated bridges with soil–structure interaction.* Soil Dynamics Earthquake Engineering, 2003. **23**(4): p. 287-302.
44. Javanmardi, A., Ghaedi K., Huang F., Hanif M.U., and Tabrizikahou A., *Application of structural control systems for the cables of cable-stayed bridges: state-of-the-art and state-of-the-practice.* Archives of Computational Methods in Engineering, 2022. **29**(3): p. 1611-1641.
45. Billah, A.M., Rahman J., and Zhang Q. *Shape memory alloys (SMAs) for resilient bridges: A state-of-the-art review*. in *Structures*. 2022. Elsevier.
46. Wen, J., Han Q., Xie Y., Du X., and Zhang J., *Performance-based seismic design and optimization of damper devices for cable-stayed bridge.* Engineering Structures, 2021. **237**: p. 112043.
47. Ewins, D.J., *Modal testing: theory, practice and application*. 2009: John Wiley & Sons.
48. Lord, R., *The theory of sound (two volumes)*. reissued 1945, second edition ed. 1887: Dover Publications, New York.
49. Ali, A.H., *Modifying Some Iterative Methods for Solving Quadratic Eigenvalue Problems.* 2017.
50. Tisseur, F. and Meerbergen K., *The quadratic eigenvalue problem.* SIAM review, 2001. **43**(2): p. 235-286.
51. Woodhouse, J., *Linear damping models for structural vibration.* Journal of Sound and Vibration, 1998. **215**(3): p. 547-569.
52. Meirovitch, L., *Analytical Methods in Vibrations, Macmillan, New York, 1967.*
53. Benaroya, H., Nagurka M., and Han S., *Mechanical vibration: analysis, uncertainties, and control*. 2017: CRC Press.
54. Morzfeld, M., Ajavakom N., and Ma F., *Diagonal dominance of damping and the decoupling approximation in linear vibratory systems.* Journal of Sound and Vibration, 2009. **320**(1-2): p. 406-420.
55. Caughey, T. and O'Kelly M.E., *Classical normal modes in damped linear dynamic systems.* ASME Journal of Applied Mechanics, 1965. **32**: p. 583-588.
56. Kawano, D.T., Morzfeld M., and Ma F., *The decoupling of second-order linear systems with a singular mass matrix.* Journal of Sound and Vibration, 2013. **332**(25): p. 6829-6846.
57. Adhikari, S. and Phani A.S. *Rayleigh's classical damping revisited*. in *International Conference on Civil Engineering in the New Millennium: Opportunities and Challenges*. 2007.
58. Adhikari, S., *Damping modelling using generalized proportional damping.* Journal of Sound and Vibration, 2006. **293**(1-2): p. 156-170.
59. Suleiman, H., Jaradat O., Benmalek H., Khattab M., and Afra H., *Analysing modal coupling in non-classically damped systems: beyond Rayleigh's damping hypothesis—a comparative study.* Asian Journal of Civil Engineering, 2024.
60. Behnamfar, F. and Alibabaei H., *Classical and non-classical time history and spectrum analysis of soil-structure interaction systems.* Bulletin of Earthquake Engineering, 2017. **15**: p. 931-965.
61. Cruz, C. and Miranda E., *Evaluation of soil-structure interaction effects on the damping ratios of buildings subjected to earthquakes.* Soil Dynamics and Earthquake Engineering, 2017. **100**: p. 183-195.
62. Zhang, Z., Wei H., and Qin X., *Experimental study on damping characteristics of soil-structure interaction system based on shaking table test.* Soil Dynamics and Earthquake Engineering, 2017. **98**: p. 183-190.
63. Li, L., Hu Y., and Wang X., *Harmonic response calculation of viscoelastic structures using classical normal modes: An iterative method.* Computers & Structures, 2014. **133**: p. 39-50.
64. Ding, Z., Li L., and Hu Y., *A modified precise integration method for transient dynamic analysis in structural systems with multiple damping models.* Mechanical Systems and Signal Processing, 2018. **98**: p. 613-633.

65. Gao, Y., Zhang S., Zhao G., and Schmidt R., *Numerical modeling for cantilever sandwich smart structures with partially covered constrained viscoelastic layer.* Composite Structures, 2022. **281**: p. 114981.
66. De Domenico, D., Falsone G., and Ricciardi G., *Improved response-spectrum analysis of base-isolated buildings: a substructure-based response spectrum method.* Engineering structures, 2018. **162**: p. 198-212.
67. Nasr, A., Mrad C., and Nasri R., *Explicit Formulas for Optimal Parameters of Friction Dynamic Vibration Absorber Attached to a Damped System Under Various Excitations.* Journal of Vibration Engineering & Technologies, 2023. **11**(1): p. 85-97.
68. Chen, H., Tan P., and Zhou F., *An improved response spectrum method for non-classically damped systems.* Bulletin of Earthquake Engineering, 2017. **15**(10): p. 4375-4397.
69. Jiang, N., Chu M.T., Shen J.J.J.o.S., and Vibration, *Structure-preserving isospectral transformation for total or partial decoupling of self-adjoint quadratic pencils.* 2019. **449**: p. 157-171.
70. Morzfeld, M., Ma F., and Ajavakom N., *On the decoupling approximation in damped linear systems.* Journal of Vibration and Control, 2008. **14**(12): p. 1869-1884.
71. Denoël, V. and Degée H., *Asymptotic expansion of slightly coupled modal dynamic transfer functions.* Journal of Sound and Vibration, 2009. **328**(1-2): p. 1-8.
72. Graham, A., *Nonnegative Matrices and Applicable Topics in Linear Algebra*. 1987: Halsted Press, New York.
73. Ibrahimbegovic, A. and Wilson E.L., *Simple numerical algorithms for the mode superposition analysis of linear structural systems with non-proportional damping.* Computers & Structures, 1989. **33**(2): p. 523-531.
74. Foss, K.A., *Co-ordinates which uncouple the equations of motion of damped linear dynamic systems.* J. Appl. Mech., 1958. **25**: p. 361-364.
75. Walsh, T.F. and Day D.M., *Quadratic eigenvalue problems*. 2007, *Sandia National Laboratories (SNL),* Albuquerque, United States of America.
76. Li, L., Hu Y., and Wang X., *Accurate method for harmonic responses of non-classically damped systems in the middle frequency range.* Journal of Vibration and Control, 2016. **22**(2): p. 426-441.
77. Fischer, P., *Eigensolution of nonclassically damped structures by complex subspace iteration.* Computer methods in applied mechanics and engineering, 2000. **189**(1): p. 149-166.
78. Holz, U.B., Golub G.H., and Law K.H., *A subspace approximation method for the quadratic eigenvalue problem.* SIAM journal on matrix analysis and applications, 2004. **26**(2): p. 498-521.
79. Łasecka-Plura, M. and Lewandowski R., *The subspace iteration method for nonlinear eigenvalue problems occurring in the dynamics of structures with viscoelastic elements.* Computers & Structures, 2021. **254**: p. 106571.
80. Rajakumar, C., *Lanczos algorithm for the quadratic eigenvalue problem in engineering applications.* Computer methods in applied mechanics and engineering, 1993. **105**(1): p. 1-22.
81. Cha, P.D., *Approximate eigensolutions for arbitrarily damped nearly proportional systems.* Journal of Sound and Vibration, 2005. **288**(4-5): p. 813-827.
82. Cortés, F. and Elejabarrieta M.J., *Computational methods for complex eigenproblems in finite element analysis of structural systems with viscoelastic damping treatments.* Computer methods in applied mechanics and engineering, 2006. **195**(44-47): p. 6448-6462.
83. Özgüven, H.N., *Twenty years of computational methods for harmonic response analysis of non-proportionally damped systems*, in *International Modal Analysis Conference IMAC XX*. 2002: California, United State of America. p. 390-396.
84. Ma, F., Morzfeld M., and Imam A., *The decoupling of damped linear systems in free or forced vibration.* Journal of Sound and Vibration, 2010. **329**(15): p. 3182-3202.

85. Adhikari, S., *An iterative approach for nonproportionally damped systems.* Mechanics Research Communications, 2011. **38**(3): p. 226-230.
86. Lázaro, M., *Eigensolutions of non-proportionally damped systems based on continuous damping sensitivity.* Journal of Sound and Vibration, 2016. **363**: p. 532-544.
87. Adhikari, S., *Modal analysis of linear asymmetric nonconservative systems.* Journal of Engineering Mechanics, 1999. **125**(12): p. 1372-1379.
88. Hračov, S. and Náprstek J., *Approximate complex eigensolution of proportionally damped linear systems supplemented with a passive damper.* Procedia engineering, 2017. **199**: p. 1677-1682.
89. Lázaro, M., *Eigensolutions of nonviscously damped systems based on the fixed-point iteration.* Journal of Sound and Vibration, 2018. **418**: p. 100-121.
90. Sinha, A., *Computing eigenvalues, eigenvectors and frequency responses of structures with non-proportional damping.* Journal of Sound and Vibration, 2020. **489**: p. 115681.
91. Morzfeld, M., Ma F., and Parlett B.N., *The transformation of second-order linear systems into independent equations.* SIAM Journal on Applied Mathematics, 2011. **71**(4): p. 1026-1043.
92. Lofrano, E., Paolone A., Ruta G., and Monitoring H., *Dynamic damage identification using complex mode shapes.* Structural Control and Health Monitoring, 2020. **27**(12): p. e2632.
93. Kawano, D.T., *The decoupling of linear dynamical systems*. 2011, UC Berkeley.
94. Junior, R.G.S., *Advances in the Theory of Linear Dynamical Systems Through Coordinate Decoupling*. 2019: eScholarship, University of California.
95. Hu, Y. and Li L., *Complex modal analysis using undamped modes*, in *ICCM2014*. 2014: Cambridge, England.
96. Lázaro, M., *Nonviscous modes of nonproportionally damped viscoelastic systems.* Journal of Applied Mechanics, 2015. **82**(12): p. 121011.
97. Goncalves Salsa Junior, R., *Advances in the Theory of Linear Dynamical Systems Through Coordinate Decoupling*. 2019, UC Berkeley.
98. Allemang, R.J., *The modal assurance criterion–twenty years of use and abuse.* Sound and vibration, 2003. **37**(8): p. 14-23.
99. Pastor, M., Binda M., and Harčarik T., *Modal assurance criterion.* Procedia engineering, 2012. **48**: p. 543-548.
100. Li, L., Hu Y., and Wang X., *Direct way of computing the variability of modal assurance criteria.* Mechanics Research Communications, 2014. **55**: p. 53-58.
101. Balmès, E., *Frequency domain identification of structural dynamics using the pole/residue parametrization*, in *Proceedings of the International Modal Analysis Conference*. 1996: Michigan, United State of America. p. 540–546.
102. Anajafi, H., Medina R.A., and Santini-Bell E., *Effects of the improper modeling of viscous damping on the first-mode and higher-mode dominated responses of base-isolated buildings.* Earthquake engineering & structural dynamics, 2020. **49**(1): p. 51-73.
103. Higham, D.J. and Higham N.J., *MATLAB guide*. 2016: SIAM.
104. Panda, S., Das S., Bhowmik B., and Hazra B., *Mastering Complex Modes: A New Method for Real-Time Modal Identification of Vibrating Systems.* arXiv preprint arXiv:, 2023. **17349**(2023).
105. Khamsi, M.A. and Kirk W.A., *An introduction to metric spaces and fixed point theory*. 2011: John Wiley & Sons.
106. Burton, T.A., *Stability by fixed point theory for functional differential equations*. 2013: Courier Corporation.